Journal of Chemistry

Conversion of Lignocellulosic Biomass and Derivatives into Value-Added Heteroatom-Containing Compounds

Lead Guest Editor: Hu Li
Guest Editors: Yaqiong Su and Zhichao Jin

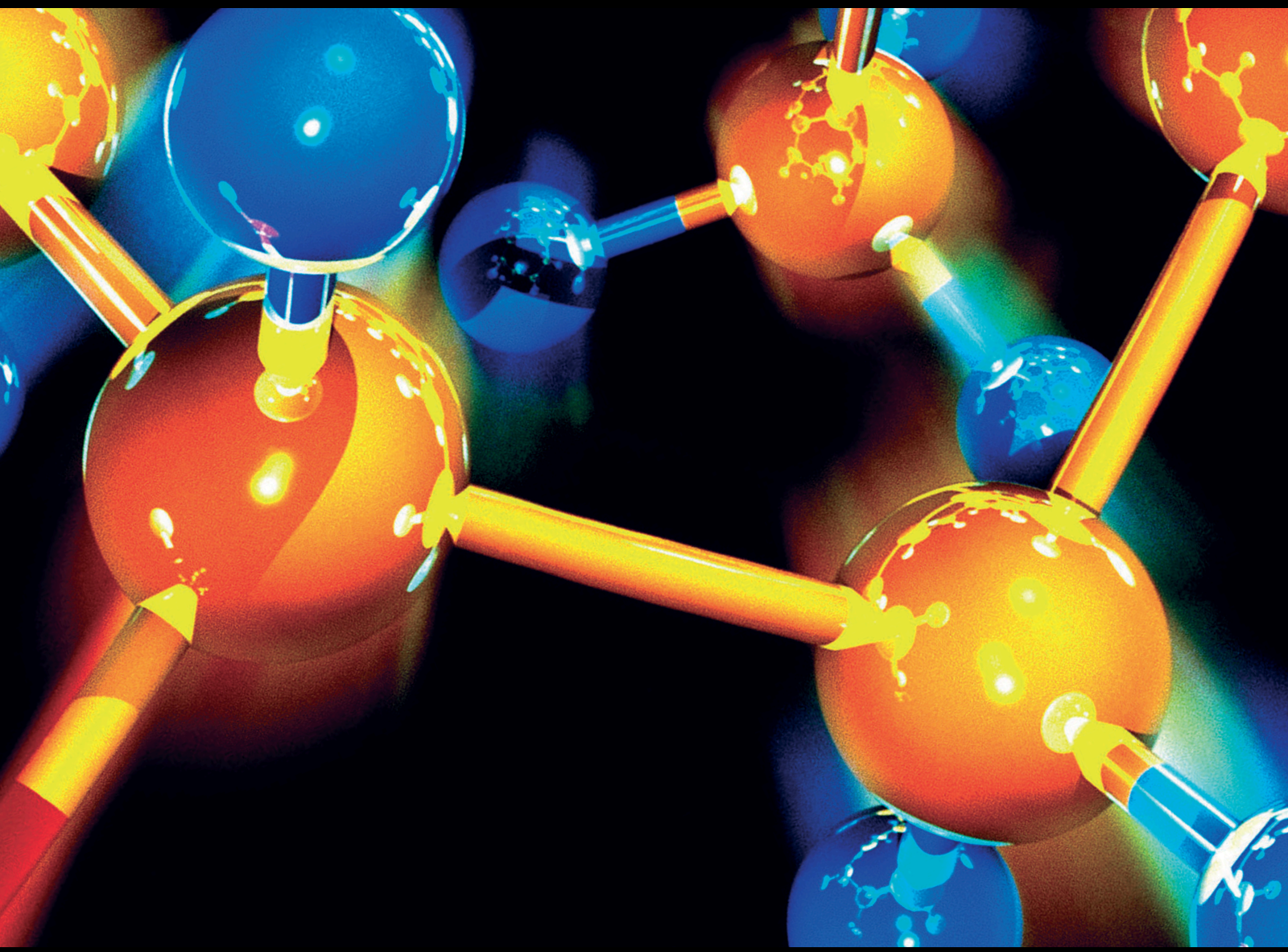

Conversion of Lignocellulosic Biomass and Derivatives into Value-Added Heteroatom-Containing Compounds

Journal of Chemistry

Conversion of Lignocellulosic Biomass and Derivatives into Value-Added Heteroatom-Containing Compounds

Lead Guest Editor: Hu Li
Guest Editors: Yaqiong Su and Zhichao Jin

Editorial Board

Contents

Conversion of Lignocellulosic Biomass and Derivatives into Value-Added Heteroatom-Containing Compounds
Hu Li, Yaqiong Su, and Zhichao Jin
Editorial (2 pages), Article ID 9153201, Volume 2020 (2020)

Highly Selective Reduction of Bio-Based Furfural to Furfuryl Alcohol Catalyzed by Supported KF with Polymethylhydrosiloxane (PMHS)
Zhaozhuo Yu, Weibo Wu, Hu Li, and Song Yang
Research Article (10 pages), Article ID 4809127, Volume 2020 (2020)

High CO2 Adsorption Enthalpy Enabled by Uncoordinated N-Heteroatom Sites of a 3D Metal-Organic Framework
Yongting Zhao and Yiming Xie
Research Article (5 pages), Article ID 4712807, Volume 2019 (2019)

Solid-Phase Preparation of Al-TiO2 for Efficient Separation of Bioderived Product Danshensu
Fei Chang, Zhong Bing He, and Quan Zhou
Research Article (7 pages), Article ID 8579528, Volume 2019 (2019)

Formaldehyde Use and Alternative Biobased Binders for Particleboard Formulation: A Review
Stephen Warui Kariuki, Jackson Wachira, Millien Kawira, and Genson Murithi
Review Article (12 pages), Article ID 5256897, Volume 2019 (2019)

Kinetic Study of Biodangerous Methylmercury Degradation under Various Light Conditions
Yutao Zhang, Xia Chen, Qixia Jiang, Xiaojuan Zhang, and Qiuyun Zhang
Research Article (5 pages), Article ID 9585140, Volume 2019 (2019)

Hindawi
Journal of Chemistry
Volume 2020, Article ID 9153201, 2 pages
https://doi.org/10.1155/2020/9153201

Editorial

Conversion of Lignocellulosic Biomass and Derivatives into Value-Added Heteroatom-Containing Compounds

Hu Li,[1,2] **Yaqiong Su**,[3] **and Zhichao Jin**[2]

[1]*College of Engineering, Nanjing Agricultural University, Nanjing 210031, China*
[2]*State-Local Joint Engineering Lab for Comprehensive Utilization of Biomass, Guizhou University, Guiyang 550025, China*
[3]*Laboratory of Inorganic Materials & Catalysis, Schuit Institute of Catalysis, Eindhoven University of Technology, P.O. Box 513, 5600 MB, Eindhoven, Netherlands*

Correspondence should be addressed to Hu Li; hli13@gzu.edu.cn

Received 30 March 2020; Accepted 30 March 2020; Published 15 April 2020

Lignocellulosic biomass has been developed as a sustainable and promising feedstock for production of various value-added chemicals and biofuels [1–3]. Due to the oxygen-rich features of biomass sources, the yielded products are typically functionalized with oxygen-containing species, remarkably enriching the product variety [4–7]. Moreover, functionalization of biomass derivatives with nitrogen, sulphur, phosphorus, and silicon atoms can also be achieved via specific reaction routes or catalytic pathways [8, 9]. Those heteroatom-containing compounds are crucial core scaffolds or key intermediates in a wide range of bioactive molecules and functional materials and can also be directly used as solvents, surfactants, and so on [10–12].

This special issue intends to highlight current advances in the development and optimization of catalytic systems and processes for the selective transformation of lignocellulosic biomass and derivatives to value-added products, especially heteroatom-containing compounds. The papers selected are on the development of green technologies to upgrade biomass and waste resources, and those with topics on the design of appropriate catalytic materials/molecules with controllable functionalities or the establishment of fitting catalytic processes to boost conversion processes are also considered. Hereby, we are pleased to share six exciting papers on biomass valorization with the readers.

In the paper entitled "Hydrothermal Catalytic Conversion of Glucose to Lactic Acid with Acidic MIL-101(Fe)," X. Liu et al. explore MIL-101(Fe) as a heterogeneous acid catalyst for direct conversion of glucose to lactic acid, with a moderate yield of 25.4% in water at a reaction temperature of 190°C after 2 h. The unique catalyst structure properties and appropriate acid strength are demonstrated to be responsible for the superior activity of MIL-101(Fe) in the synthesis of lactic acid from glucose. After four consecutive recycles, glucose conversion decreases from 70.8% to 54.9%, and LA yield is dropped from an initial value of 25.4% to 18.5%, possibly due to the partial deposition of oligomeric byproducts in the catalyst pores that lead to the blocking of the active sites and partial ingredient changes in the catalyst.

In the paper entitled "Highly Selective Reduction of Bio-Based Furfural to Furfuryl Alcohol Catalyzed by Supported KF with Polymethylhydrosiloxane (PMHS)," Z. Yu et al. present an economical and benign catalytic system, containing an easily prepared and reusable catalyst 5 wt.% KF/ZrO_2 and a low-cost hydrogen source PMHS, which is efficient for hydrogenation of furfural (FUR) to high-value furfuryl alcohol (FFA) under mild reaction conditions. A high FFA yield (97%) and FUR conversion (99%) can be obtained over KF/ZrO_2 at 25°C in just 0.5 h, which is superior to those attained with other tested catalysts. It is found that the performance of KF/ZrO_2 is remarkably affected by acid-base properties of the ZrO_2 support and KF loading doge. In addition, the KF/ZrO_2 catalyst can be recycled at least five times, with the FFA yield decreasing from 97% to 71%, which is attributed to the catalyst pores covered by the PMHS-based resin.

In the paper entitled "Formaldehyde Use and Alternative Biobased Binders for Particleboard Formulation: A Review," S. W. Kariuki et al. overview the application of starch as an alternative binder to formaldehyde in formulation of

particleboard. The use of the modified starch is illustrated to show increased particleboard performance. The authors point out that mechanical strength, such as modulus of rupture, modulus of elasticity, and internal bonding in particleboards, however, remains to be a challenge.

In the paper entitled "Solid-Phase Preparation of Al-TiO_2 for Efficient Separation of Bioderived Product Danshensu," F. Chang et al. prepare four Al-TiO_2 solid samples with different Ti/Al ratios of 1 : 0.1, 1 : 0.09, 1 : 0.07, and 1 : 0.05 synthesized by a solid-phase synthesis method, which are characterized by XRD, SEM, EDS, BET, and other techniques. These Al-TiO_2 samples were tested to have good adsorption and desorption ability, in which the solid Al-TiO_2 with a Ti/Al ratio of 1 : 0.05 is more suitable for the separation of Danshensu. A high adsorption of 77.70% is attained after 2 h adsorption time with a pH value of 3, and a high desorption rate of 70.29% was received at the sample concentration of 3.0 mg/mL with 80% ethanol eluent.

In the paper entitled "Kinetic Study of Biodangerous Methylmercury Degradation under Various Light Conditions," Y. Zhang et al. investigate the kinetics and mechanism of methylmercury (MeHg) degradation under UVB, UVA, natural light, and dark and disclose that light radiation can enhance MeHg degradation but has no significant influence on the final balance between MeHg and inorganic Mercury (Hg^{2+}) in pure water. This balance can be used as a key fundamental to estimate MeHg cycling in other complicated aquatic environments.

In the paper entitled "High CO_2 Adsorption Enthalpy Enabled by Uncoordinated N-Heteroatom Sites of a 3D Metal-Organic Framework," Y. Zhao et al. examine the CO_2 adsorption properties of a prepared 3D metal-organic framework, $Mn_2L_2(H_2O)_2 \cdot (DMF)$, with uncoordinated N-heteroatom sites. The uncoordinated nitrogen heteroatom sites are uncovered to markedly increase the reciprocity between host frame and CO_2 at room temperature, therefore showing high adsorption enthalpy of CO_2.

Conflicts of Interest

The editors declare that they have no conflicts of interest regarding the publication of this Special Issue.

Acknowledgments

The guest editors would like to thank all the authors who contributed to this issue and the reviewers for their timely and constructive feedback. The editors also wish to thank the editorial staff of *Journal of Chemistry* for their help to organize this issue. The editors hope that the topics presented in this issue would be helpful to further explore catalytic strategies for sustainable production of heteroatom-containing compounds from biomass.

Hu Li
Yaqiong Su
Zhichao Jin

References

[1] J. He, H. Li, S. Saravanamurugan, and S. Yang, "Catalytic upgrading of biomass-derived sugars with acidic nanoporous materials: structural role in carbon-chain length variation," *ChemSusChem*, vol. 12, no. 2, pp. 347–378, 2019.

[2] H. Li, Y. Li, Z. Fang, and R. L. Smith Jr., "Efficient catalytic transfer hydrogenation of biomass-based furfural to furfuryl alcohol with recycable Hf-phenylphosphonate nanohybrids," *Catalysis Today*, vol. 319, pp. 84–92, 2019.

[3] H. Pan, H. Li, H. Zhang, A. Wang, D. Jin, and S. Yang, "Effective production of biodiesel from non-edible oil using facile synthesis of imidazolium salts-based Brønsted-Lewis solid acid and co-solvent," *Energy Conversion and Management*, vol. 166, pp. 534–544, 2018.

[4] H. Li, C. Wang, Y. Xu et al., "Heterogeneous (de)chlorination-enabled control of reactivity in the liquid-phase synthesis of furanic biofuel from cellulosic feedstock," *Green Chemistry*, vol. 22, no. 3, pp. 637–645, 2020.

[5] H. Zhang, H. Li, H. Pan et al., "Magnetically recyclable acidic polymeric ionic liquids decorated with hydrophobic regulators as highly efficient and stable catalysts for biodiesel production," *Applied Energy*, vol. 223, pp. 416–429, 2018.

[6] T. Yang, W. Zhao, H. Li, S. Saravanamurugan, and S. Yang, "Porous Zr-bibenzyldiphosphonate nanohybrid with extra hydroxy species for enhancive upgrading of biomass-based levulinates," *ChemistrySelect*, vol. 3, no. 16, pp. 4252–4261, 2018.

[7] H. Li and R. L. Smith Jr., "Solvents take control," *Nature Catalysis*, vol. 1, no. 3, pp. 176-177, 2018.

[8] M. J. Hülsey, H. Yang, and N. Yan, "Sustainable routes for the synthesis of renewable heteroatom-containing chemicals," *ACS Sustainable Chemistry & Engineering*, vol. 6, no. 5, pp. 5694–5707, 2018.

[9] H. Li, H. Guo, Z. Fang, T. M. Aida, and R. L. Smith Jr., "Cycloamination strategies for renewable N-heterocycles," *Green Chemistry*, vol. 22, no. 3, pp. 582–611, 2020.

[10] Y. Wang, S. Furukawa, X. Fu, and N. Yan, "Organonitrogen chemicals from oxygen-containing feedstock over heterogeneous catalysts," *ACS Catalysis*, vol. 10, no. 1, pp. 311–335, 2020.

[11] H. Li, H. Guo, Y. Su et al., "N-formyl-stabilizing quasi-catalytic species afford rapid and selective solvent-free amination of biomass-derived feedstocks," *Nature Communications*, vol. 10, p. 699, 2019.

[12] H. Wu, Z. Yu, Y. Li, Y. Xu, H. Li, and S. Yang, "Hot water-promoted catalyst-free reductive cycloamination of (bio-)keto acids with HCOONH4 toward cyclic amides," *The Journal of Supercritical Fluids*, vol. 157, p. 104698, 2020.

Hindawi
Journal of Chemistry
Volume 2020, Article ID 4809127, 10 pages
https://doi.org/10.1155/2020/4809127

Research Article

Highly Selective Reduction of Bio-Based Furfural to Furfuryl Alcohol Catalyzed by Supported KF with Polymethylhydrosiloxane (PMHS)

Zhaozhuo Yu, Weibo Wu, Hu Li, and Song Yang

State Key Laboratory Breeding Base of Green Pesticide & Agricultural Bioengineering, Key Laboratory of Green Pesticide & Agricultural Bioengineering, Ministry of Education, State-Local Joint Laboratory for Comprehensive Utilization of Biomass, Center for Research & Development of Fine Chemicals, Guizhou University, Guiyang, Guizhou 550025, China

Correspondence should be addressed to Hu Li; hli13@gzu.edu.cn and Song Yang; jhzx.msm@gmail.com

Received 13 August 2019; Revised 26 November 2019; Accepted 11 December 2019; Published 28 January 2020

Academic Editor: Antonio De Lucas-Consuegra

Hydrogenation of bio-based furfural (FUR) to furfuryl alcohol (FFA) is tremendously expanding the application of biomass in many industries such as resins, biofuels, and pharmaceuticals. However, mass manufacture of FFA from FUR is restrained by strict requirements of reaction conditions and expensive catalysts. In this work, an economical and benign catalytic system, containing an easily prepared and reusable catalyst 5 wt.% KF/ZrO_2 and a low-cost hydrogen source polymethylhydrosiloxane (PMHS), was developed to be efficient for the hydrogenation of FUR to high-value FFA under mild conditions. The catalyst reactivity was found to be remarkably influenced by the support acid-base properties and KF loading doge. In the presence of 5 wt.% KF/ZrO_2, a high FFA yield of 97% and FUR conversion of 99% could be obtained at 25°C in just 0.5 h, which was superior to those attained with other tested catalysts. The KF/ZrO_2 catalyst could be recycled at least five times, with the FFA yield slightly decreasing from 97% to 71%. The spare decrease in FFA yield is possibly attributed to the catalyst pore blocking, as clarified by SEM, BET, XPS, and ICP-MS measurements of the fresh and reused catalysts.

1. Introduction

Diversiform sustainable clean energies have been developed to get rid of the dependence of nonrenewable fossil energy and relieve environmental deterioration caused by combustion of fossil fuel in past decades [1–3]. In particular, biomass containing abundant carbon source is considered as the best source to replace fossil fuels, for the production of various biofuels such as biodiesel, ethanol, and 2,5-dimethylfuran [4–8]. In addition, through a series of chemical reactions including hydrolysis, dehydration, oxidation, hydrogenation, and hydrogenolysis, lignocellulosic biomass can be transformed into numerous value-added oxygen-containing heterocyclic compounds [9–17].

Furfural (FUR) is an important biomass-derived compound, which is mainly obtained from the xylose which is one of the main hydrolyzates of hemicellulose [18, 19]. Through the partial reduction of FUR, furfuryl alcohol (FFA) can be prepared. FFA is indispensable feedstock for the synthesis of diverse downstream compounds including ethyl furfuryl ether, tetrahydrofurfuryl alcohol, γ-valerolactone, levulinic acid, and so on, all of which have wide applications in fuels, pharmaceuticals, and food and chemical industries (Figure 1) [20–29]. Up to now, artificial synthesis of FUR and FFA is of high cost and needs a complex conversion process, indicating that the hydrogenation of FUR not only enlarges the application of biomass but also sharply decreases the synthesis cost of various downstream compounds [30, 31].

The H-donor for the hydrogenation of FUR to FFA is classified as gas- and liquid-phase reaction processes, all of which have corresponding advantages and shortages.

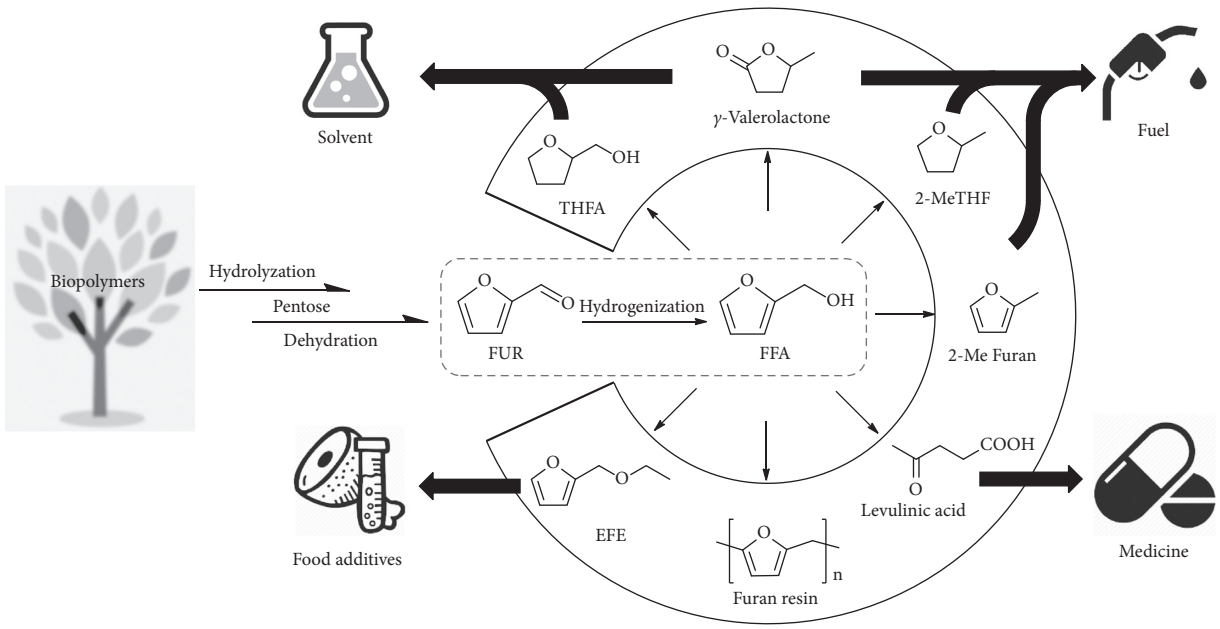

Figure 1: Biomass valorization by the hydrogenation of FUR to FFA. FUR: furfural; FFA: furfuryl alcohol; EFE: 2-(ethoxymethyl) furan; THFA: tetrahydrofurfuryl alcohol; 2-Me THF: 2-methyltetrahydrofuran; 2-MeFuran: 2-methylfuran.

Hydrogen gas as a gaseous H-donor has superiority in the product separation and thus is broadly applied in the diverse hydrogen reactions [32]. At room temperature, hydrogen gas is hard to react with other compounds until the reaction conditions change. High temperature and metal catalysts are effective for the activation of hydrogen gas. Thus, in industrial manufacture, the production of FFA from FUR and molecular hydrogen is completed at high temperatures catalyzed by noble metals (e.g., Au, Ru, Pd, and Pt) [33–36], nonnoble metals (e.g., Co, Cu, and Fe) [19, 37–40], and metallic oxides (e.g., $CrCuO_3$) [41]. However, due to the high activity of metal catalysts, aldehyde group and furan ring can be both reduced in this reaction system, resulting in that most catalysts used in the hydrogenation of FUR to FFA are still applied in the laboratory scale. In addition, with the reaction temperature exceeding the boiling point of FUR (167°C), FFA can be efficiently prepared from gas state FUR and hydrogen gas in atmospheric pressure, which indicates that the hydrogenation of FUR can react in both vapor state and liquid state. At the relatively low temperature, hydrosilane, alcohol, acid, and similar liquid compounds with free hydrogen atoms are good H-donor for hydrogenation of FUR to FFA in the liquid phase. The Meerwein–Ponndorf–Verley (MPV) reduction which is used alcohol as liquid H-donor has been largely applied in the reduction of biomass platform molecules, which can simultaneously produce two useful compounds and thus attracts the attention of numerous researchers focusing on biomass valorization [42–44]. Generally, the catalysts performing high catalytic activity for the MPV reduction of FUR to FFA include acid-base bifunctional catalysts (e.g., Pd/HZSM-5 and MgO-Al_2O_3) [45, 46] and Lewis acid catalysts (e.g., Al-, Zr-zeolites, and Zr-, Al-, Hf-based catalysts) [47–49]. It is noteworthy that the drawbacks of the MPV reaction system such as difficult separation of products and relatively harsh conditions still trouble researchers in this research field. Besides gas-phase H-donor hydrogen gas and alcohol H-donor, increasing reports about the hydrogenation of FUR to FFA by another liquid H-donor hydrosilane have been presented in the past decade [50, 51]. In this reaction system, FFA is obtained from FUR in high selectivity under mild conditions (atmospheric pressure, <80°C), which makes up the imperfection of the reaction system when hydrogen and alcohol are used as H-donor.

For hydrosilane, polymethylhydrosiloxane (PMHS) as the cheapest hydrosilane agent and the by-product of the silicon industry is an ideal H-donor for the hydrogenation of FUR to FFA [8, 52, 53]. At the same time, PMHS is a green agent as it is nontoxic and having great chemical stability for water and atmosphere [54, 55].

Recently, a series of fluoride salts were reported for the conversion of aldehyde to corresponding alcohol by PMHS in highly selective and effective environment [56, 57]. However, the fluoride salts as homogeneous catalysts are not suitable for economically manufacturing FFA from FUR, for which a novel and recyclable catalyst KF/support is reported in this article. The catalyst prepared by the impregnation method provides a suitable carrier for KF to attach, which is favorable for the contract of the substrate with KF and preventing KF from the erosion of solvent and substrate [32, 58]. Through the impregnation method, the obtained solid catalyst that combines the high efficiency of KF and the heterogeneous property of support was developed to catalyze the hydrogenation of FUR to FFA at a lower cost.

2. Results and Discussions

2.1. Effect of Different Supports. For the impregnation method, the loading amount of active sites on the solid support is generally decided by the support porosity and

chemical property [59]. Therefore, the influence of different porous supports on the catalytic behavior of KF was initially investigated (Figure 2). The loading rate of all support catalysts is 3 wt.%.

The results listed in Figure 2 show that KF supported on acidic montmorillonite K-10 (K-10) and alkaline hydroxyapatite microspheres (HAP) and nanomagnesium oxide (MgO) performed poor reactivity in this reaction system, which could be attributed to the ion exchange between the support with KF [60] or the competing reaction of fluoride ion and hydroxide released from the support [61], remarkably weakening the nucleophilic attack ability of KF. In connection with this, nanotitanium dioxide (TiO_2) and zirconium oxide nanopowder (ZrO_2) with both moderate acid and base sites supported KF showed relatively good catalytic activity for the conversion of FUR to FFA. In addition, due to the relatively high surface area of ZrO_2, the catalyst using ZrO_2 (75% FFA yield) as support had better catalytic reactivity than TiO_2 (55% FFA yield). Therefore, ZrO_2 which has both moderate acid and base sites and the relatively high surface area is the optimum support for catalyst KF/support.

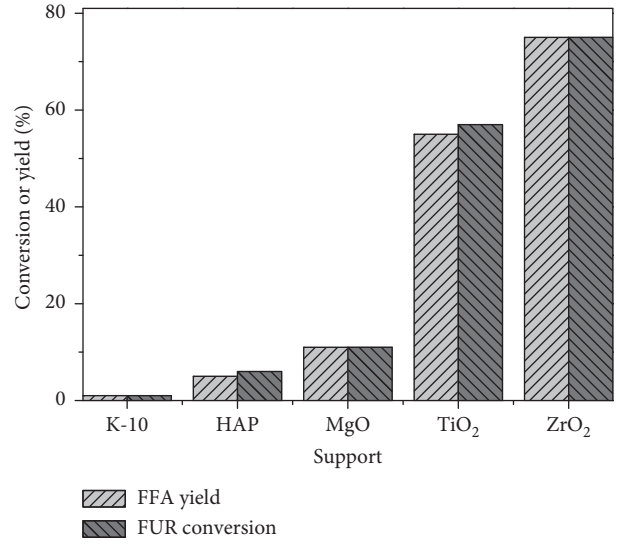

Figure 2: Effect of different supports on the synthesis of FFA from FUR. Reaction conditions: 0.5 mmol FUR, 25 mg catalyst, 2.5 equiv. H^- of PMHS, 2 mL DMF, 25°C, and 30 min. K-10: montmorillonite K-10; HAP: hydroxyapatite microspheres; MgO: nanomagnesium oxide; TiO_2: nanotitanium dioxide; ZrO_2: zirconium oxide nanopowder.

2.2. Effect of the Loading Rate of KF. Apart from the support, the loading rate of KF is another important factor for the catalyst preparation via impregnation [62]. The KF/ZrO_2 catalysts with different KF loading rates (1–15 wt.%) were prepared by the impregnation method for the test of catalytic activity (Figure 3). It was shown that 5 wt.% was the best loading rate of KF/ZrO_2 catalyst and increasing the loading rate of KF gave rise to the slight reduction of the catalyst activity of KF/support catalyst. For the decrease of catalytic activity of 15 wt.% KF/ZrO_2, this phenomenon could be attributed to the reduction of pore diameter which is caused by the excess of KF. To prove the inference, N_2 adsorption-desorption isotherms of KF/support in different loading rates are presented in Figure S3. The hysteresis loop appearing in the N_2 adsorption-desorption isotherms of 5 wt.% and 15 wt.% KF/ZrO_2 (Figure S3) is the phenomenon of decrease in pore diameter of 5 wt.% and 15 wt.% KF/ZrO_2 catalysts, proving the inference why the catalytic activity of 15 wt.% KF/ZrO_2 catalyst is declined.

Through the optimization of the support type and the loading content of KF, 5 wt.% KF/ZrO_2 shows the best catalytic activity for the hydrogenation of FUR to FFA. In addition, comparison of the results obtained in this work with those of previous studies for the conversion of FUR to FFA is presented in Table 1, which shows that 5 wt.% KF/ZrO_2 is a more efficient catalyst for the selective hydrogenation of FUR to FFA.

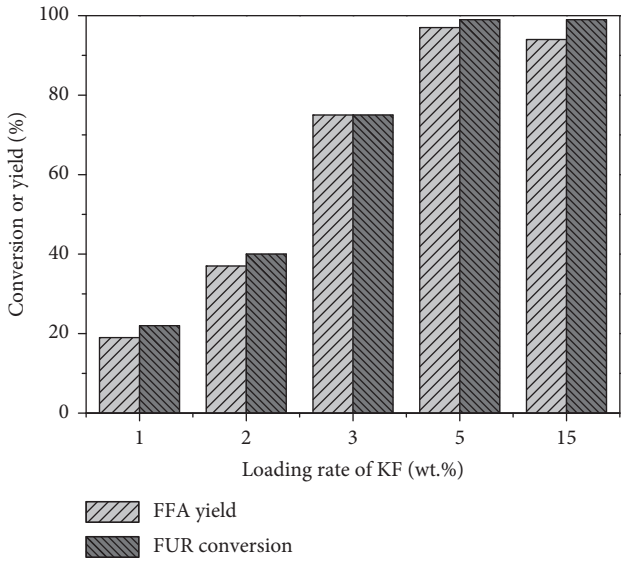

Figure 3: Effect of KF loading rate of KF/ZrO_2 on the reduction of FUR to FFA. Reaction conditions: 0.5 mmol FUR, 25 mg KF/ZrO_2, 2.5 equiv. H^- of PMHS, 2 mL DMF, 25°C, and 30 min.

2.3. Catalyst Characterization. The successful preparation of KF/ZrO_2 by the impregnation method commonly keeps the original configuration of support and makes the active substrate KF uniformly distributed in the internal surface of ZrO_2. According to the XRD patterns of KF/ZrO_2 catalysts with different KF loading rates (1–15 wt.%) (Figure 4), it can be seen that the crystal structure of ZrO_2 does not change significantly. The crystal faces of ZrO_2 including (1, 1, 0), (−1, 1, 1), (1, 1, 1), (1, 0, 2), (−2, 2, 1), (1, 3, 0), and (1, 3, 1) are attributed to the diffraction peaks at 24.1°, 27.9°, 31.4°, 34.1°, 40.8°, 50.4°, 55.3°, and 59.6°, respectively. As can be seen from the XPS spectra of 5 wt.% KF/ZrO_2 (Figure 5), the peaks of 690 eV and 290 eV that, respectively, correspond to the fluorine and potassium are detected, indicating that KF is successfully distributed in the external surface of the support. In the XRD pattern of KF/ZrO_2, the diffraction peak at 39.5° can be observed, manifesting the formation of the

Table 1: Catalytic results collected for the hydrogenation of FUR to FFA.

Catalyst	Temperature (°C)	Time (h)	H-donor	Yield (%)	Selectivity (%)	Reuse times (yield)	Ref.
Fe-L1/C-800	160	15	2-Butanol	75.87	82.9	5 (60.1%)	[44]
γ-Fe_2O_3@HAP	180	3	*iso*-Propanol	59.5	91.6	6 (57.2%)	[63]
Co/SBA-15	150	1.5	2 MPa H_2	87.6	95.6	11 (50.5%)	[64]
5 wt.% Ni/CN	200	4	1 MPa H_2	91.4	95.0	4 (91.4%)	[65]
CuCo0.4/C-873	140	1	3 MPa H_2	28.5	93.4	4 (17.4%)	[66]
5 wt.% KF/ZrO_2	25	0.5	PMHS	97.0	98.0	5 (71%)	This work

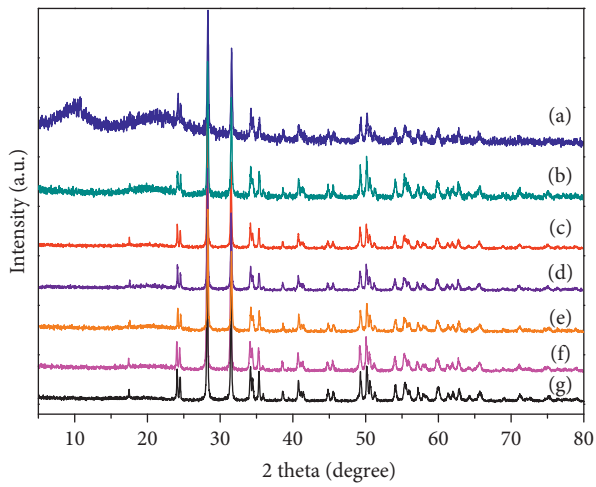

Figure 4: XRD patterns of (a) 5 wt.% KF/ZrO_2 (after recycling 5 times), (b) 15 wt.% KF/ZrO_2, (c) 5 wt.% KF/ZrO_2, (d) 3 wt.% KF/ZrO_2, (e) 2 wt.% KF/ZrO_2, (f) 1 wt.% KF/ZrO_2, and (g) ZrO_2.

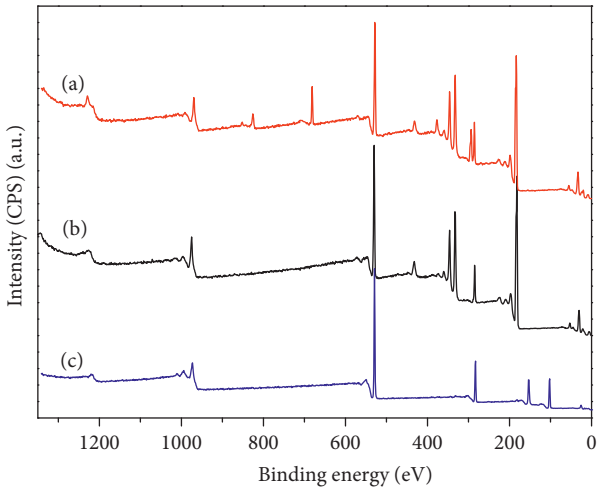

Figure 5: XPS profiles of (a) 5 wt.% KF/ZrO_2, (b) ZrO_2, and (c) 5 wt.% KF/ZrO_2 (after recycling 5 times).

alkaline active species ($K_3Zr_2F_{11}$) by the chemical combination of K^+ and oxygen species [67]. The results show that KF is immobilized on ZrO_2 which is realized by both physical adsorption and chemical interaction. It is known that ZrO_2 as a porous material has a relatively large surface area (ca. 80–110 m^2/g), most of which is provided by the internal surface [68, 69]. Through comparison of the detection results obtained by XPS and ICP-MS analysis (Table 2), a relatively high K content of KF/ZrO_2 detected by ICP indicated that KF is successfully distributed in both the external and internal surface of ZrO_2. In addition, the thermostability of catalysts was detected by TG analysis, and the results show that the quality of KF/ZrO_2 is very stable, in which the catalyst weight is slightly decreased when the calcination temperature increases from 25 to 600°C.

2.4. Effect of Different Solvents. Five kinds of solvents were chosen for comparing the effect of different solvents on the reduction of FUR to FFA (Figure 6). For the protic solvent, methanol (MeOH) or *n*-butanol (*n*-BuOH) used as solvent showed relatively low reactivity (6% or 43% FFA yield and 11% or 44% FUR conversion, respectively). It was proposed that alcohol could react with PMHS to produce hydrogen gas [70], significantly decreasing the amount of PMHS for the reduction of FUR, which thus afforded lower FFA yield and FUR conversion. For the aprotic solvent, the order of reactivity is correlated with the order of the solvent polarity: *N*,*N*-dimethylformamide (DMF) > ethyl acetate (EA) > 2-methylfuran (2-MeTHF) (Figure 6). DMF as the relatively high polarity solvent shows the best FFA yield (97%) and FUR conversion (99%), for which DMF was considered as the optimum solvent for this reaction system.

2.5. Effect of PMHS Dosage and Hydrosilane Type. Effect of PMHS dosage was investigated from 0.5 to 4 equiv. at intervals of 0.5 equiv. (Figure 7). It was obvious that the low dosage of PMHS could not provide enough H-donor to complete the reduction of FUR to FFA and the excess dosage of PMHS against the dissociation between FFA and PMHS, thus reducing the yield of FFA [71]. PMHS with 2.5 equiv. H^- was found to be the optimum dosage of PMHS, which is in favor of the FUR to FFA hydrogenation in an economical and efficient way.

After confirming the optimum dosage of PMHS, there are eight kinds of hydrosilanes that are used for the study of hydrosilane type effect (Table 3). For the hydrosilanes containing phenyl species, phenylsilane (PS) and diphenylsilane (DPS) showed very good activity in the reduction of FUR to FFA, giving FFA yield in >99% or 99.0%, respectively. For the hydrosilanes not containing phenyl species, 99% FFA yield could be obtained using PMHS as H-donor, which is the highest FFA yield (1–75%) among the hydrosilanes not containing phenyl groups. From the point of economy, although using hydrosilanes containing phenyl groups as H-donor achieved high FFA yields, the price of PS and DPS is 72 and 38 times higher than that of PMHS,

Table 2: Composition of the fresh and reused catalysts detected by XPS and ICP analysis.

Entry	Detection method	Sample	K (mol%)	F (mol%)
1	ICP	5 wt.% KF/ZrO_2	3.58	—
2	ICP	Reused 5 wt.% KF/ZrO_2	3.02	—
3	XPS	5 wt.% KF/ZrO_2	2.99	3.79
4	XPS	Reused 5 wt.% KF/ZrO_2	0.01	0.01

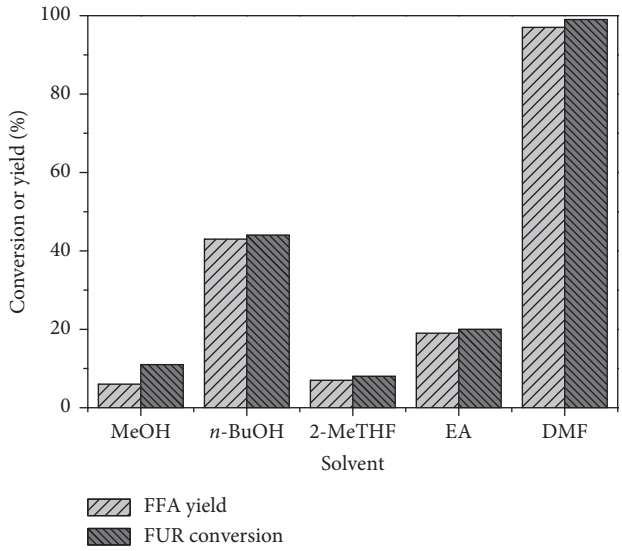

Figure 6: Influence of solvent type on the hydrogenation of FUR to FFA. Reaction conditions: 0.5 mmol FUR, 25 mg 5 wt.% KF/ZrO_2, 2.5 equiv. H^- of PMHS, 2 mL solvent, 25°C, and 30 min. DMF: *N*,*N*-dimethylformamide; EA: ethyl acetate; 2-MeTHF: 2-methylfuran; MeOH: methanol; *n*-BuOH: *n*-butanol.

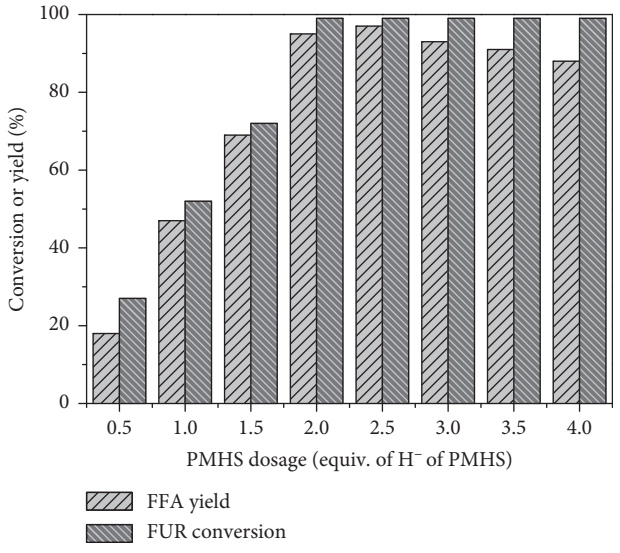

Figure 7: Effect of PMHS dosage on the reduction of FUR to FFA. Reaction conditions: 0.5 mmol FUR, 25 mg 5 wt.% KF/ZrO_2, 2 mL DMF, 25°C, and 30 min.

respectively [50], which is too expensive to carry out for practical application. As the cheapest hydrosilane, PMHS performed relatively high FFA yield (99%) as well, for which PMHS is considered as the optimum hydrosilane from the examined hydrosilanes.

2.6. Catalyst Recycling Study. The reusability of 5 wt.% KF/ZrO_2 was also investigated, and the obtained results are shown in Figure 8. After five consecutive runs, the FFA yield marginally decreased from 97% to 71%.

From the XRD pattern of reused 5 wt.% KF/ZrO_2 catalyst, it was revealed that the crystallization of the catalyst was decreased after recycles (Figure 4). Thus, the reason why the catalyst activity is slightly decreased could be attributed to the catalyst pore blocking by the PMHS-based resin, which is a typical by-product of reaction system using PMHS as H-donor [72]. To prove the reasonability of the inference, the characterizations of reused 5 wt.% KF/ZrO_2 by SEM, BET, XPS, and ICP-MS are conducted. Firstly, from the SEM image of the reused catalyst (Figure S1), it can be seen that the surface of the catalyst is covered by an unknown substrate. For the XPS spectra of reused 5 wt.% KF/ZrO_2 (Figure 5), the characteristic peak of silicon (102 eV) was detected, indicating that 5 wt.% KF/ZrO_2 is covered by PMHS-based resin. The BET isotherms and pore diameter analysis suggest that the pore diameter is reduced after use (Figures S2 and S3). Thus, the PMHS-based resin that is wrapping the 5 wt.% KF/ZrO_2 restricts the substrate to enter into the cavity of support, which decreases the contact of active compounds to substrate and weakens the catalytic activity of 5 wt.% KF/ZrO_2. Meanwhile, the sharp decrease of KF content is also attributed to the coverage of PMHS resin, which can be illustrated by the significant peak of silicon in the XPS spectrum (Figure 5). Except the effect of PMHS-

Table 3: Influence of hydrosilane type on the reduction of FUR to FFA.

Entry	Hydrosilane structure	Chemical name	Yield (%)	Conversion (%)	Selectivity (%)
1	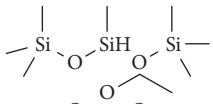	1,1,1,3,5,5,5-Heptamethyltrisiloxane	72	>99	72
2	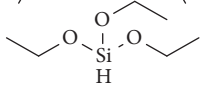	Triethoxysilane	75	>99	75
3	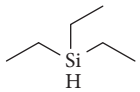	Triethylsilane	1	5	20
4	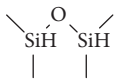	1,1,3,3-Tetramethyldisiloxane	>99	>99	100
5	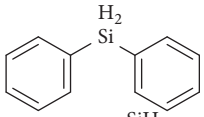	Diphenylsilane	99	>99	99
6	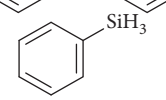	Phenylsilane	>99	>99	100
7	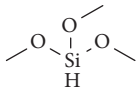	Trimethoxysilane	57	88	65
8	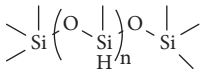	PMHS	97	99	98

Reaction conditions: 0.5 mmol FUR, 25 mg 5 wt.% KF/ZrO_2, 2 mL DMF, 2.5 equiv. H^- of hydrosilane, 25°C, and 30 min.

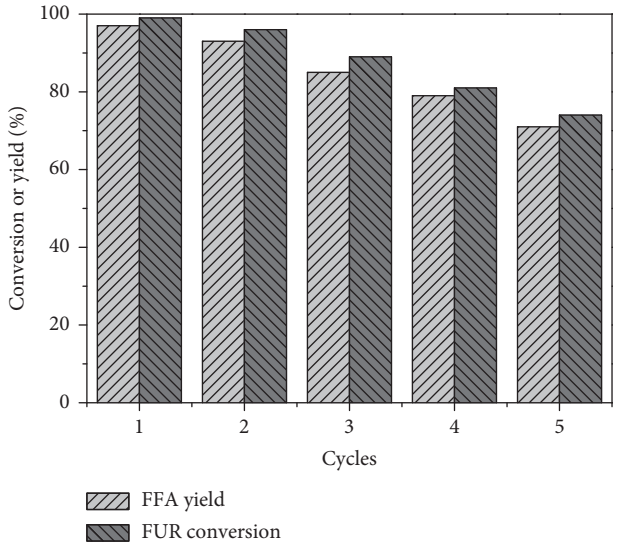

Figure 8: Catalyst recycling study of 5 wt.% KF/ZrO_2. Reaction conditions: 0.5 mmol FUR, 25 mg 5 wt.% KF/ZrO_2, 2 mL DMF, 2.5 equiv. H^- of PMHS, 25°C, and 30 min.

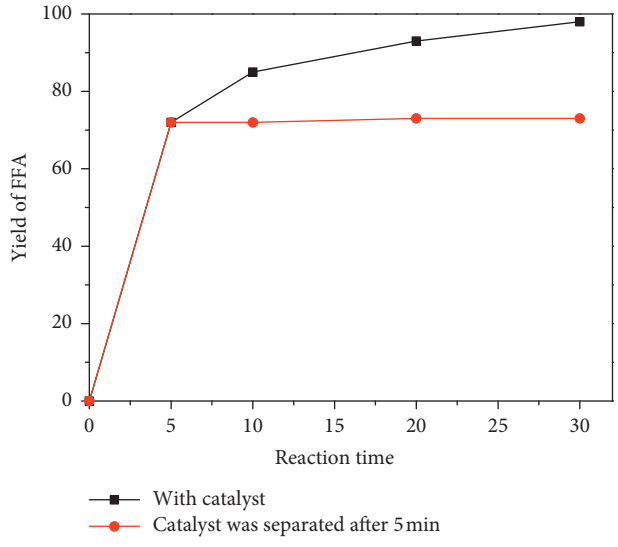

Figure 9: The FFA yield with or without the participation of 5 wt.% KF/ZrO_2. Reaction conditions: 0.5 mmol FUR, 25 mg 5 wt.% KF/ZrO_2, 2 mL DMF, 2.5 equiv. H^- of PMHS, 25°C, and 30 min.

based resin, the slight loss of KF is another factor for the decrease in the catalytic activity of 5 wt.% KF/ZrO_2 after use. The atomic analysis of fresh and reused 5 wt.% KF/ZrO_2 catalyst by ICP-MS (Table 2) indicates that KF was not significantly leached (by ca, 0.56%). Meanwhile, the hot filtration experiments (Figure 9) confirm the heterogeneous catalytic behavior of the solid catalyst. Therefore, the main factor that decreases the catalytic activity is the PMHS resin which covers the external surface of 5 wt.% KF/ZrO_2.

3. Conclusion

In summary, the KF/ZrO_2 catalyst was successfully prepared by the impregnation method and had good reactivity for the

reduction of FUR to FFA using PMHS as H-donor. For the support of the catalyst, ZrO_2 as a porosity material of chemical inertness maintains the original configuration after the process of impregnation. Meanwhile, 5 wt.% KF/ZrO_2 as an appropriate loading rate of KF keeps the porosity of support and high reactivity of KF. The benign reaction system was optimized, and thus, 97% FFA yield and 99% FUR conversion were achieved by this reaction system at 25°C after 0.5 h. Through the comparison of seven kinds of commercial hydrosilanes and PMHS, PMHS is considered as hydrosilane of the high price-performance ratio. The reusability of 5 wt.% KF/ZrO_2 is good, which further reduced the cost of the reaction system. After 5 times run, the FFA yield was slightly decreased from 97% to 71%, due to the pore of 5 wt.% KF/ZrO_2 covered by PMHS-based resin.

4. Materials and Experiments

4.1. Materials. Polymethylhydrosiloxane (>99.0%), potassium fluoride (>99.9%), 2-methylfuran (>99.9%), 1,1,3,3-tetramethyldisiloxane (>98.0%), nanotitanium dioxide (>99.8%), hydroxyapatite microspheres, and naphthalene (>99.0%) were purchased from Shanghai Aladdin Bio-Chem Technology Co., Ltd. Triethoxysilane (>97.0%), 1,1,1,3,5,5,5-heptamethyltrisiloxane (>98.0%), triethylsilane (>98.0%), trimethoxysilane (>95.0%), and phenylsilane (>97.0%) were bought from Tokyo Chemical Industry Co., Ltd. *N*,*N*-Dimethylformamide (>99.5%), methanol (>99.5%), and tetrahydrofuran (>99.5%) were purchased from Guangdong Guanghua Sci-Tech Co., Ltd. *n*-Butanol (>99.5%) and ethyl acetate (>99.5%) were obtained from Shanghai Shenbo Chemical Co., Ltd. Diphenylsilane (>97.0%) and zirconium dioxide nanopowder (>99.5%) were purchased from Alfa Aesar Chemicals Co., Ltd. Nanomagnesium oxide (>99.0%), montmorillonite K-10, and others were purchased from Beijing Innochem Technology Co., Ltd.

4.2. Preparation of Catalyst. A series of KF/support catalysts were prepared through an impregnation method. KF solution was prepared at first, where a desired amount of KF was dissolved into 2 mL pure water. Then, 1 g support was added into the solution. The mixture was heated at 60°C with stirring for 6 h. Finally, the mixture was dried at 80°C for 12 h, and the catalyst was ground for the test of catalytic activity. Through the impregnation method, active compound KF was distributed in the internal and external surface of the support by two steps. First, the support is completely immersed in the solution containing a moderate amount of KF until the cavity of support is full of KF solution by capillarity. Second, through a drying process, the solvent in the KF solution is completely volatilized, making the active compound KF be attached to the support surface.

4.3. Catalyst Characterization Techniques. BET (Brunauer–Emmett–Teller) surface areas of the porous materials were determined from nitrogen physisorption measurements at liquid nitrogen temperature on a Micromeritics ASAP 2460 instrument. Scanning electron microscopy (SEM) images were obtained by using field-emission scanning electron microscopy (FESEM; JEOL, EOL, JSM-6700F, 5 kV). Thermogravimetry (TG) analysis was determined by a NETZSCH STA 449 F3 Jupiter. XPS (X-ray photoelectron spectroscopy) measurements were recorded using a Physical Electronics Quantum 2000 Scanning ESCA Microprobe (Physical Electronics Inc., PHI, MN) equipped with a monochromatic Al Kα anode. The data of XRD (X-ray diffraction) of the powder samples were obtained by using a Rigaku International D/max-TTR III X-ray powder diffractometer with Cu Kα radiation and 2θ scanned from 5° to 80°. The quantitative elemental analysis of samples was completed by coupled plasma mass spectrometry (ICP-MS, Elan DRC II, PerkinElmer, Sciex).

4.4. Catalytic Transfer Hydrogenation. A plastic sealed tube is a vessel where the FFA hydrogenation reaction was carried out. In a general process, FUR (0.5 mmol, 0.048 g), KF/ZrO_2 (25 mg), DMF (2 mL), and PMHS were added successively into a 15 mL plastic tube and then the lid was covered. Afterward, the sealed tube filling with the reaction mixture was put into the oil bath that was kept at 25°C. Upon completion, methanol (2 mL) was added to quench the reaction, and the reaction mixture was filtered by a 0.2 μm filter membrane for GC analysis.

4.5. Product Analysis. The quantitative analysis of the reaction mixture was fulfilled by GC (Agilent 6890N) equipped with an HP-5 capillary column (30 m × 0.320 mm × 0.25 μm) and flame ionization detector (FID) detector. The programmed temperature for GC analysis is set as follows: maintaining at 60°C for 1 min, heating from 60 to 230°C in the rate of 10°C/min, and holding for 4 min. Naphthalene was employed as an internal standard for the quantitative analysis of the samples. The standard curves of FUR and FFA were recorded with GC by plotting different concentrations of FUR or FFA with specific concentrations of naphthalene, and the obtained curves are shown in Figures S5 and S6. The substrate conversion and product yield are calculated using the following equations, based on the standard curves made from commercial samples:

$$\text{conversion } (\%) = \left(1 - \frac{\text{mole of residual substrate}}{\text{mole of initial substrate}}\right) \times 100\%,$$

$$\text{yield } (\%) = \frac{\text{mole of product}}{\text{mole of initial substrate}} \times 100\%. \quad (1)$$

Data Availability

The data used to support the findings of this study are available from the corresponding author upon request.

Conflicts of Interest

The authors declare no conflicts of interest.

Authors' Contributions

Zhaozhuo Yu and Weibo Wu contributed equally to this work.

Acknowledgments

This study was financially supported by the National Natural Science Foundation of China (21576059, 21666008, and 21908033), Fok Ying-Tong Education Foundation (161030), Key Technologies R&D Program of China (2014BAD23B01), and Guizhou Science and Technology Foundation ([2018] 1037).

Supplementary Materials

SEM images (Figure S1), pore distribution (Figure S2), N2 adsorption-desorption isotherms (Figure S3), and TG curves (Figure S4) of solid catalysts, as well as standard curves of FUR (Figure S5) and FFA (Figure S6) are provided. (*Supplementary Materials*)

References

[1] H. Li, S. Yang, A. Riisager et al., "Zeolite and zeotype-catalysed transformations of biofuranic compounds," *Green Chemistry*, vol. 18, no. 21, pp. 5701–5735, 2016.

[2] K. Shikinaka, H. Sotome, Y. Kubota et al., "A small amount of nanoparticulated plant biomass, lignin, enhances the heat tolerance of poly(ethylene carbonate)," *Journal of Materials Chemistry A*, vol. 6, no. 3, pp. 837–839, 2018.

[3] S. Xu, M. E. Lamm, M. A. Rahman et al., "Renewable atom-efficient polyesters and thermosetting resins derived from high oleic soybean oil," *Green Chemistry*, vol. 20, no. 5, pp. 1106–1113, 2018.

[4] A. R. Alcantara and P. D. de Maria, "Recent advances on the use of 2-methyltetrahydrofuran (2-MeTHF) in biotransformations," *Current Green Chemistry*, vol. 5, no. 2, pp. 86–103, 2018.

[5] G. W. Huber, J. N. C. Huber, J. Christopher, and J. A. Barrett, "Production of liquid alkanes by aqueous-phase processing of biomass-derived carbohydrates," *Science*, vol. 308, no. 5727, pp. 1446–1450, 2005.

[6] D. Zhang, J. Wang, Y. Lin et al., "Present situation and future prospect of renewable energy in China," *Renewable and Sustainable Energy Reviews*, vol. 76, pp. 865–871, 2017.

[7] T. Wangchuk, C. He, L. D. Knibbs, M. Mazaheri, and L. Morawska, "A pilot study of traditional indoor biomass cooking and heating in rural Bhutan: gas and particle concentrations and emission rates," *Indoor Air*, vol. 27, no. 1, pp. 160–168, 2017.

[8] H. Li, W. Zhao, W. Dai et al., "Noble metal-free upgrading of multi-unsaturated biomass derivatives at room temperature: silyl species enable reactivity," *Green Chemistry*, vol. 20, no. 23, pp. 5327–5335, 2018.

[9] S. Saravanamurugan, A. Riisager, E. Taarning, and S. Meier, "Mechanism and stereoselectivity of zeolite-catalysed sugar isomerisation in alcohols," *Chemical Communications*, vol. 52, no. 86, pp. 12773–12776, 2016.

[10] F. H. Isikgor and C. R. Becer, "Lignocellulosic biomass: a sustainable platform for the production of bio-based chemicals and polymers," *Polymer Chemistry*, vol. 6, no. 25, pp. 4497–4559, 2015.

[11] C. Xu, R. A. D. Arancon, J. Labidi, and R. Luque, "Lignin depolymerisation strategies: towards valuable chemicals and fuels," *Chemical Society Reviews*, vol. 43, no. 22, pp. 7485–7500, 2014.

[12] M. J. Gilkey and B. Xu, "Heterogeneous catalytic transfer hydrogenation as an effective pathway in biomass upgrading," *ACS Catalysis*, vol. 6, no. 3, pp. 1420–1436, 2016.

[13] R. A. Sheldon, "Green and sustainable manufacture of chemicals from biomass: state of the art," *Green Chemistry*, vol. 16, no. 3, pp. 950–963, 2014.

[14] J.-P. Lange, E. van der Heide, J. van Buijtenen, and R. Price, "Furfural-A promising platform for lignocellulosic biofuels," *ChemSusChem*, vol. 5, no. 1, pp. 150–166, 2012.

[15] R. Mariscal, P. Maireles-Torres, M. Ojeda, I. Sádaba, and M. López Granados, "Furfural: a renewable and versatile platform molecule for the synthesis of chemicals and fuels," *Energy & Environmental Science*, vol. 9, no. 4, pp. 1144–1189, 2016.

[16] Z. Liu, D. Tian, J. Hu et al., "Functionalizing bottom ash from biomass power plant for removing methylene blue from aqueous solution," *Science of the Total Environment*, vol. 634, pp. 760–768, 2018.

[17] R. Jia, H. Lei, T. Hino, and A. Arulrajah, "Environmental changes in Ariake Sea of Japan and their relationships with Isahaya Bay reclamation," *Marine Pollution Bulletin*, vol. 135, pp. 832–844, 2018.

[18] G. D. Oreggioni, B. Singh, F. Cherubini et al., "Environmental assessment of biomass gasification combined heat and power plants with absorptive and adsorptive carbon capture units in Norway," *International Journal of Greenhouse Gas Control*, vol. 57, pp. 162–172, 2017.

[19] K. Yan and A. Chen, "Efficient hydrogenation of biomass-derived furfural and levulinic acid on the facilely synthesized noble-metal-free Cu–Cr catalyst," *Energy*, vol. 58, pp. 357–363, 2013.

[20] J. Wang, Z. Zhang, S. Jin, and X. Shen, "Efficient conversion of carbohydrates into 5-hydroxylmethylfurfan and 5-ethoxymethylfurfural over sufonic acid-functionalized mesoporous carbon catalyst," *Fuel*, vol. 192, pp. 102–107, 2017.

[21] C. Fang, Y. Li, Z. Yu, H. Li, and S. Yang, "Efficient catalytic upgrade of fructose to alkyl levulinates with phenylpyridine-phosphotungstate solid hybrids," *Current Green Chemistry*, vol. 6, no. 1, pp. 44–52, 2019.

[22] D. Darji, Y. Alias, and N. H. Abd Razak, "Effect of recycled imidazolium-based ionic liquids on biomass from rubber wood," *Current Green Chemistry*, vol. 4, pp. 74–81, 2017.

[23] H. Li, S. Saravanamurugan, S. Yang, and A. Riisager, "Direct transformation of carbohydrates to the biofuel 5-ethoxymethylfurfural by solid acid catalysts," *Green Chemistry*, vol. 18, no. 3, pp. 726–734, 2016.

[24] S. Zhang, M. Yang, J. Shao et al., "The conversion of biomass to light olefins on Fe-modified ZSM-5 catalyst: effect of pyrolysis parameters," *Science of The Total Environment*, vol. 628-629, pp. 350–357, 2018.

[25] R. Luque, "Catalytic biomass processing: prospects in future biorefineries," *Current Green Chemistry*, vol. 2, no. 1, pp. 90–95, 2015.

[26] H. Li, T. Yang, and Z. Fang, "Biomass-derived mesoporous Hf-containing hybrid for efficient Meerwein-Ponndorf-Verley reduction at low temperatures," *Applied Catalysis B: Environmental*, vol. 227, pp. 79–89, 2018.

[27] L. Filiciotto and R. Luque, "Biomass promises: a bumpy road to a renewable economy," *Current Green Chemistry*, vol. 5, no. 1, pp. 47–59, 2018.

[28] K. T. Malladi and T. Sowlati, "Biomass logistics: a review of important features, optimization modeling and the new trends," *Renewable and Sustainable Energy Reviews*, vol. 94, pp. 587–599, 2018.

[29] D. M. Alonso, S. G. Wettstein, and J. A. Dumesic, "Bimetallic catalysts for upgrading of biomass to fuels and chemicals," *Chemical Society Reviews*, vol. 41, no. 24, pp. 8075–8098, 2012.

[30] L. Zhang, G. Xi, K. Yu, H. Yu, and X. Wang, "Furfural production from biomass-derived carbohydrates and lignocellulosic residues via heterogeneous acid catalysts," *Industrial Crops and Products*, vol. 98, pp. 68–75, 2017.

[31] L. Zhang, G. Xi, Z. Chen, D. Jiang, H. Yu, and X. Wang, "Highly selective conversion of glucose into furfural over modified zeolites," *Chemical Engineering Journal*, vol. 307, pp. 868–876, 2017.

[32] W. Gong, C. Chen, Y. Zhang et al., "Efficient synthesis of furfuryl alcohol from H2-hydrogenation/transfer hydrogenation of furfural using sulfonate group modified Cu catalyst," *ACS Sustainable Chemistry & Engineering*, vol. 5, no. 3, pp. 2172–2180, 2017.

[33] Y. Nakagawa, K. Takada, M. Tamura, and K. Tomishige, "Total hydrogenation of furfural and 5-hydroxymethylfurfural over supported Pd-Ir alloy catalyst," *ACS Catalysis*, vol. 4, no. 8, pp. 2718–2726, 2014.

[34] Q. Yuan, D. Zhang, L. v. Haandel et al., "Selective liquid phase hydrogenation of furfural to furfuryl alcohol by Ru/Zr-MOFs," *Journal of Molecular Catalysis A: Chemical*, vol. 406, pp. 58–64, 2015.

[35] W. Huang, H. Li, B. Zhu, Y. Feng, S. Wang, and S. Zhang, "Selective hydrogenation of furfural to furfuryl alcohol over catalysts prepared via sonochemistry," *Ultrasonics Sonochemistry*, vol. 14, no. 1, pp. 67–74, 2007.

[36] S. Sitthisa and D. E. Resasco, "Hydrodeoxygenation of furfural over supported metal catalysts: a comparative study of Cu, Pd and Ni," *Catalysis Letters*, vol. 141, no. 6, pp. 784–791, 2011.

[37] V. Vetere, A. B. Merlo, J. F. Ruggera, and M. L. Casella, "Transition metal-based bimetallic catalysts for the chemoselective hydrogenation of furfuraldehyde," *Journal of the Brazilian Chemical Society*, vol. 21, no. 5, pp. 914–920, 2010.

[38] S. Sanjay, S. Naveen, M. Pravakar, K. A. Shah, J. K. Parikh, and D. Ajay K, "Optimization and kinetic studies on hydrogenation of furfural to furfuryl alcohol over SBA-15 supported bimetallic copper–cobalt catalyst," *Catalysis Letters*, vol. 145, no. 3, pp. 816–823, 2015.

[39] K. Yan, J. Liao, X. Wu, and X. Xie, "A noble-metal free Cu-catalyst derived from hydrotalcite for highly efficient hydrogenation of biomass-derived furfural and levulinic acid," *RSC Advances*, vol. 3, no. 12, pp. 3853–3856, 2013.

[40] R. V. Sharma, U. Das, R. Sammynaiken, and A. K. Dalai, "Liquid phase chemo-selective catalytic hydrogenation of furfural to furfuryl alcohol," *Applied Catalysis A: General*, vol. 454, pp. 127–136, 2013.

[41] R. Rao, A. Dandekar, R. T. K. Baker, and M. A. Vannice, "Properties of copper chromite catalysts in hydrogenation reactions," *Journal of Catalysis*, vol. 171, no. 2, pp. 406–419, 1997.

[42] H. Li, Y. Li, Z. Fang, and R. L. Smith, "Efficient catalytic transfer hydrogenation of biomass-based furfural to furfuryl alcohol with recycable Hf-phenylphosphonate nanohybrids," *Catalysis Today*, vol. 319, pp. 84–92, 2019.

[43] H. Li, W. Zhao, S. Saravanamurugan et al., "Control of selectivity in hydrosilane-promoted heterogeneous palladium-catalysed reduction of furfural and aromatic carboxides," *Communications Chemistry*, vol. 1, p. 32, 2018.

[44] J. Li, J.-l. Liu, H.-j. Zhou, and Y. Fu, "Catalytic transfer hydrogenation of furfural to furfuryl alcohol over nitrogen-doped carbon-supported iron catalysts," *ChemSusChem*, vol. 9, no. 11, pp. 1339–1347, 2016.

[45] H. Li, J. He, A. Riisager, S. Saravanamurugan, B. Song, and S. Yang, "Acid-base bifunctional zirconium *N*-alkyl-triphosphate nanohybrid for hydrogen transfer of biomass-derived carboxides," *ACS Catalysis*, vol. 6, no. 11, pp. 7722–7727, 2016.

[46] A. Martínez, M. A. Arribas, M. Derewinski, and A. Burkat-Dulak, "Enhanced sulfur resistance of bifunctional Pd/HZSM-5 catalyst comprising hierarchical carbon-templated zeolite," *Applied Catalysis A: General*, vol. 379, no. 1-2, pp. 188–197, 2010.

[47] Y. Zhu, G. Chuah, and S. Jaenicke, "Chemo- and regioselective Meerwein-Ponndorf-Verley and Oppenauer reactions catalyzed by Al-free Zr-zeolite beta," *Journal of Catalysis*, vol. 227, no. 1, pp. 1–10, 2004.

[48] M. De bruyn, M. Limbourg, J. Denayer et al., "Mesoporous Zr and Hf catalysts for chemoselective MPV reductions of unsaturated ketones," *Applied Catalysis A: General*, vol. 254, no. 2, pp. 189–201, 2003.

[49] Y. Zhu, G. Chuah, and S. Jaenicke, "Selective Meerwein–Ponndorf–Verley reduction of α, $\beta\alpha$, β-unsaturated aldehydes over Zr-zeolite beta," *Journal of Catalysis*, vol. 241, no. 1, pp. 25–33, 2006.

[50] D. Addis, S. Das, K. Junge, and M. Beller, "Selective reduction of carboxylic acid derivatives by catalytic hydrosilylation," *Angewandte Chemie International Edition*, vol. 50, no. 27, pp. 6004–6011, 2011.

[51] V. Bette, A. Mortreux, D. Savoia, and J.-F. Carpentier, "New developments in zinc-catalyzed asymmetric hydrosilylation of ketones with PMHS," *Tetrahedron*, vol. 60, no. 12, pp. 2837–2842, 2004.

[52] Z. Yu, F. Xu, Y. Li, H. Konno, H. Li, and S. Yang, "Tetraethylammonium fluoride-mediated a green hydrogen transfer process for selective reduction of biomass-derived aldehydes," *Current Green Chemistry*, vol. 6, no. 2, pp. 127–134, 2019.

[53] H. Li, W. Zhao, A. Riisager et al., "A Pd-Catalyzed in situ domino process for mild and quantitative production of 2,5-dimethylfuran directly from carbohydrates," *Green Chemistry*, vol. 19, no. 9, pp. 2101–2106, 2017.

[54] H. Li, W. Zhao, and Z. Fang, "Hydrophobic Pd nanocatalysts for one-pot and high-yield production of liquid furanic biofuels at low temperatures," *Applied Catalysis B: Environmental*, vol. 215, pp. 18–27, 2017.

[55] E. Vasilikogiannaki, I. Titilas, C. Gryparis, A. Louka, I. N. Lykakis, and M. Stratakis, "Efficient hydrosilylation of carbonyl compounds by 1,1,3,3-tetramethyldisiloxane catalyzed by Au/TiO_2," *Tetrahedron*, vol. 70, no. 36, pp. 6106–6113, 2014.

[56] E. Abele and E. Lukevics, "Recent advances in fluoride ion activation of silicon bonds in organic synthesis," *Main Group Metal Chemistry*, vol. 24, no. 6, p. 315, 2001.

[57] M. D. Drew, N. J. Lawrence, W. Watson, and S. A. Bowles, "The asymmetric reduction of ketones using chiral ammonium fluoride salts and silanes," *Tetrahedron Letters*, vol. 38, no. 33, pp. 5857–5860, 1997.

[58] S. R. Mirmasoomi, M. Mehdipour Ghazi, and M. Galedari, "Photocatalytic degradation of diazinon under visible light using TiO_2/Fe_2O_3 nanocomposite synthesized by ultrasonic-assisted impregnation method," *Separation and Purification Technology*, vol. 175, pp. 418–427, 2017.

[59] M. Shimokawabe, H. Asakawa, and N. Takezawa, "Characterization of copper/zirconia catalysts prepared by an impregnation method," *Applied Catalysis*, vol. 59, no. 1, pp. 45–58, 1990.

[60] J. H. Clark, "Fluoride ion as a base in organic synthesis," *Chemical Reviews*, vol. 80, no. 5, pp. 429–452, 1980.

[61] K. Revunova and G. I. Nikonov, "Base-catalyzed hydrosilylation of ketones and esters and insight into the mechanism," *Chemistry-A European Journal*, vol. 20, no. 3, pp. 839–845, 2014.

[62] J. A. Korpiel and R. D. Vidic, "Effect of sulfur impregnation method on activated carbon uptake of gas-phase mercury," *Environmental Science & Technology*, vol. 31, no. 8, pp. 2319–2325, 1997.

[63] F. Wang and Z. Zhang, "Catalytic transfer hydrogenation of furfural into furfuryl alcohol over magnetic γ-Fe_2O_3@HAP catalyst," *ACS Sustainable Chemistry & Engineering*, vol. 5, no. 1, pp. 942–947, 2017.

[64] M. Audemar, C. Ciotonea, K. De Oliveira Vigier et al., "Selective hydrogenation of furfural to furfuryl alcohol in the presence of a recyclable cobalt/SBA-15 catalyst," *ChemSusChem*, vol. 8, no. 11, pp. 1885–1891, 2015.

[65] T. V. Kotbagi, H. R. Gurav, A. S. Nagpure, S. V. Chilukuri, and M. G. Bakker, "Highly efficient nitrogen-doped hierarchically porous carbon supported Ni nanoparticles for the selective hydrogenation of furfural to furfuryl alcohol," *RSC Advances*, vol. 6, no. 72, pp. 67662–67668, 2016.

[66] Y. Wang, Y. Miao, S. Li, L. Gao, and G. Xiao, "Metal-organic frameworks derived bimetallic Cu-Co catalyst for efficient and selective hydrogenation of biomass-derived furfural to furfuryl alcohol," *Molecular Catalysis*, vol. 436, pp. 128–137, 2017.

[67] H. Tang, Y. Li, N. Liu, L. Fu, and Y. Liu, "A highly-efficient KF-modified nanorod support Zr–Ce oxide catalyst and its application," *ChemCatChem*, vol. 10, no. 20, pp. 4739–4746, 2018.

[68] X. Yan, Q. Zhang, M. Zhu, and Z. Wang, "Selective hydrogenation of benzene to cyclohexene over Ru-Zn/ZrO_2 catalysts prepared by a two-step impregnation method," *Journal of Molecular Catalysis A: Chemical*, vol. 413, pp. 85–93, 2016.

[69] B. Sathyaseelan, E. Manikandan, I. Baskaran et al., "Studies on structural and optical properties of ZrO_2 nanopowder for opto-electronic applications," *Journal of Alloys and Compounds*, vol. 694, pp. 556–559, 2017.

[70] E. Lukevics and M. Dzintara, "The alcoholysis of hydrosilanes," *Journal of Organometallic Chemistry*, vol. 295, no. 3, pp. 265–315, 1985.

[71] J. Lipowitz and S. A. Bowman, "Use of polymethylhydrosiloxane as a selective, neutral reducing agent for aldehydes, ketones, olefins, and aromatic nitro compounds," *The Journal of Organic Chemistry*, vol. 38, no. 1, pp. 162–165, 1973.

[72] S. Hanada, Y. Motoyama, and H. Nagashima, "Dual Si-H effects in platinum-catalyzed silane reduction of carboxamides leading to a practical synthetic process of tertiary-amines involving self-encapsulation of the catalyst species into the insoluble silicone resin formed," *Tetrahedron Letters*, vol. 47, no. 35, pp. 6173–6177, 2006.

Hindawi
Journal of Chemistry
Volume 2019, Article ID 4712807, 5 pages
https://doi.org/10.1155/2019/4712807

Research Article

High CO_2 Adsorption Enthalpy Enabled by Uncoordinated N-Heteroatom Sites of a 3D Metal-Organic Framework

Yongting Zhao[1] **and Yiming Xie**[2]

[1]*College of Chemistry and Chemical Engineering, Anshun University, Anshun 561000, China*
[2]*College of Materials Science and Engineering, Huaqiao University, Quanzhou 362021, China*

Correspondence should be addressed to Yongting Zhao; ydrmakeit2008@163.com

Received 11 October 2019; Accepted 28 November 2019; Published 21 December 2019

Guest Editor: Hu Li

A 3D metal-organic framework (MOF), $Mn_2L_2(H_2O)_2 \cdot (DMF)$ {H_2L = 5- (Pyridin-2-yl)-3, 3′-bi (1H-1,2,4-triazole)} (**1**) with uncoordinated N-heteroatom sites, has been obtained through hydrothermal method and structurally characterized by X-ray structural analysis, powder X-ray diffraction (PXRD), and thermal analysis (TGA). The framework of compound **1** exhibits fascinating adsorption properties and shows high adsorption enthalpy of CO_2. The experimental results prove which uncoordinated nitrogen heteroatom sites can markedly increase the reciprocity between host frame and CO_2 at room temperature.

1. Introduction

Biomass is a sustainable material, which has been developed as a promising feedstock for producing biofuels, and carbon dioxide (CO_2) from the burning of biofuels, as well as fossil oil, is considered as the main component of all the gases that cause the greenhouse effect resulting in various kinds of environmental unsteadiness [1–4]. Captured CO_2 has industrial, economical, and social importance in decreasing CO_2 emissions and in alleviating greenhouse effect. Due to its high specific surface area and adjustable structures, MOFs are certainly very promising as CO_2 adsorbents materials have been investigated over the last couple of decades. Numerous types of research on MOFs have illustrated the great potential for storage and separation [5–12]. A recent effort to improve the ability of MOFs to capture CO_2 is that increase the number of uncoordinated nitrogen atoms in the metal-organic frame [13–16], the enthalpy of CO_2 can be augmented due to the uncoordinated N-heteroatom sites of ligands [17, 18].

We noticed an interesting framework $Mn_2L_2(H_2O)_2 \cdot (DMF)$ reported by Dong et al. [19], which is constructed by Mn salt and H_2L ligand. As shown in Figure 1, the Mn center is octahedrally coordinated by one O atom from the terminal coordinated water and five N atoms from three different L ligands. Five of seven N atoms of the L ligand coordinate to three Mn centers, among which N1, N2, N4, and N6 atoms are in chelating mode, and N7 atom is in monodentate mode. Compound **1** has a 3D open framework including 1D channel and rich uncoordinated N-sites. Through the calculation of the PLATON program [20], the free solvent-accessible pore volume ratio in compound **1** is about 49.7% without taking into account the guest molecules. However, the microporosity of compound **1** has never been researched (the pore size distribution of the compound 1 is shown in Table 3S). Herein, we study the influence of uncoordinated N-heteroatom sites of compound **1** on the uptake and adsorption enthalpy of CO_2. As expected, it has high amusing adsorption properties and shows high adsorption enthalpy of CO_2 at ambient temperatures. In the conditions we adopted, the N-heteroatom which is uncoordinated can observably enhance the interaction between host framework and CO_2.

2. Experimental

2.1. Synthesis of $Mn_2L_2(H_2O)_2 \cdot (DMF)$. Compound **1** was synthesized according to the reported method [19]. The mixture of $MnSO_4 \cdot H_2O$ (0.0160 g, 0.1 mmol), H_2L (0.0213 g,

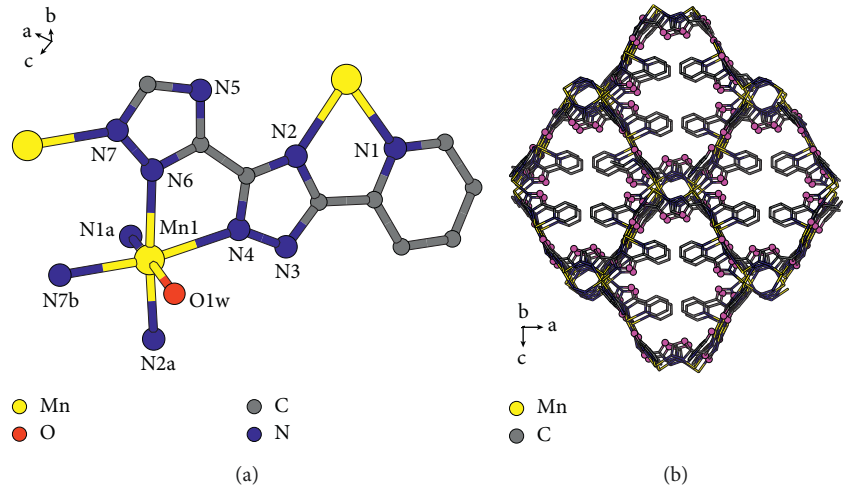

Figure 1: (a) Coordination environment of Mn (II) in compound 1; (b) the 1D channel of compound 1 (the pink atoms stand for uncoordinated N sites).

0.1 mmol), DMF (4.0 ml), and H_2O (4.0 ml) in a 25 ml Parr Teflon-lined stainless steel autoclave, heated at 160°C for 3 days, and then allowed to cool slowly to indoor temperature. Colorless octahedron crystals were acquired, rinsed with DMF, and dried at ambient temperatures. X-ray molecular structure analysis indicates that compound **1** in the orthorhombic I41, a space group, is identical to the reported one (crystal data of compound **1** are shown in Tables 1S and 2S). Elemental analysis (EA) for compound **1** $C_{21}H_{21}Mn_2N_{15}O_3$ (641.41) were given as follows: calculated: C 39.33, H 3.30, and N 32.76; found: C 39.14, H 3.43, and N 33.96; IR (KBr pellet, cm^{-1}) for compound **1** : 3370 (m), 1656 (w), 1610 (w), 1495 (w), 1419 (w), 1120 (s), 818 (m), 646 (m), and 507 (m).

2.2. Preparation of Activated Sample. Supercritical CO_2 activation experiments were accomplished on Tousimis™ Samdri® PVT-30. Ahead of activation, samples were thoroughly washed with DMF. Sample **1** was wrapped with a toilet paper and fixed by Flament, and then the sample was put in a tube and placed into the chamber of the supercritical drier. The chamber was charged by dry liquid CO_2 (99.8%), and the sample tube was permitted to purge for 5 min every 30 min. During the process, the chamber temperature was kept at ~0–10°C. Four hours later, the temperature of the chamber was raised to ~38°C, and the same chamber temperature was kept for one hour followed by slow venting one night. As-synthesized samples were soaked in liquid CO_2 at high pressure over the course of hours and then under dynamic vacuum conditions to form activated sample.

3. Results and Discussion

3.1. The Powdered X-Ray Diffraction and Thermogravimetric Analysis. It can be known that the compound **1** is the pure phase because the experimental PXRD patterns confirm well with the graph simulated from the research results (Figure 2(a)). Thermal analysis (TGA) in N_2 ambience with a heating rate of 10°C/min was done on a polycrystalline sample to study the thermostability of compound **1** from 25 to 800°C (Figure 3). The primary sample **1** indicated the first weight decrease in 6% takes place in the range of 30–100°C, corresponding to the release of surface solvent molecules and water molecules in the channel. The second weight decrease in 16% occurs at 100–200°C, which can owe to the loss of DMF molecules. The third weight decrease in 7% occurs at 200–450°C, which could be caused by the lost of coordinated water molecules. After this temperature, the framework starts to collapse.

3.2. The Study of Porosity. In order to evaluate the permanent porosity, N_2 adsorption and CO_2 adsorption experiments were carried out. Prior at gas adsorption, the sample was activated by supercritical CO_2 (SCD) methods. N_2 adsorption experiment at 77 K exhibits type I sorption isotherms, which is particular of porous materials. The maximum N_2 is 116.45 cm^3/g at 744.6 mmHg (Figure 4), corresponding to Langmuir and BET surface areas which were 326.25 and 232.48 m^2/g, severally. However, obvious hysteresis loop was observed. The possible reason is due to the flexibility of skeleton based on weak coordination bond because of Mn1 connection through monodentate coordination with N7, and the single bond between Mn1 with N7 can freely rotate. From the PXRD patterns between the as-synthesized and activated samples, we can see that the main peaks of compound **1** shift to high angles (Figure 2(b)), which reflected the flexibility of the framework.

The presence of the permanent porosity and oofy uncoordinated N-heteroatom sites indicates that compound **1** may have great potential for the CO_2 capture adhibition. Single-component CO_2 sorption isotherms were measured at 273 K and 298 K (Figure 5(a)). A hysteresis loop was also observed. The CO_2 uptake values were 32.4 cm^3/g at 273 K, and 20.85 cm^3/g at 298 K, respectively. The value of the uptake (32.4 cm^3/g) is higher compared with numerous

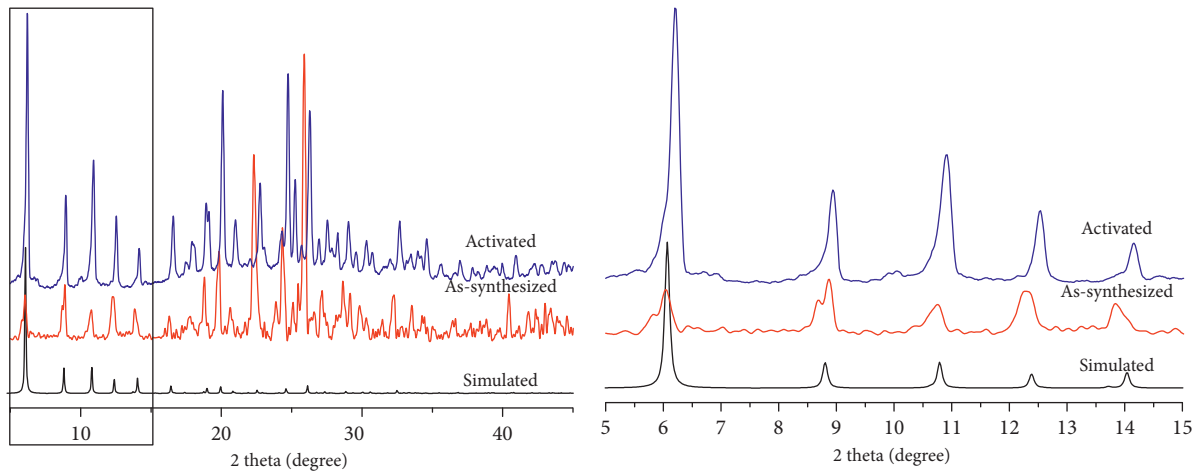

Figure 2: (a) The powder XRD patterns of compound **1** under different conditions. (b) The amplification of the 2theta in the range of 5–15 degrees.

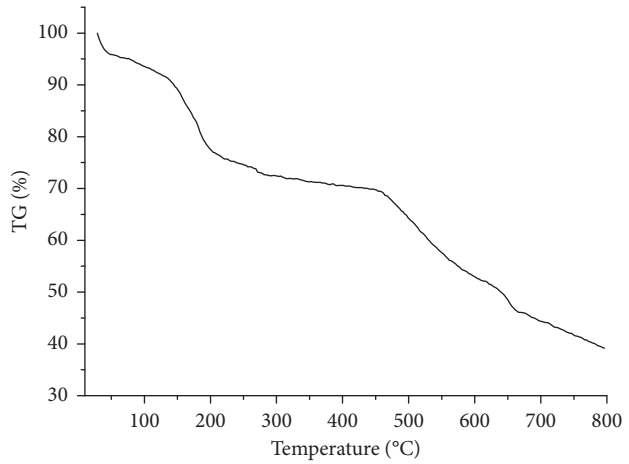

Figure 3: The TGA of compound **1**.

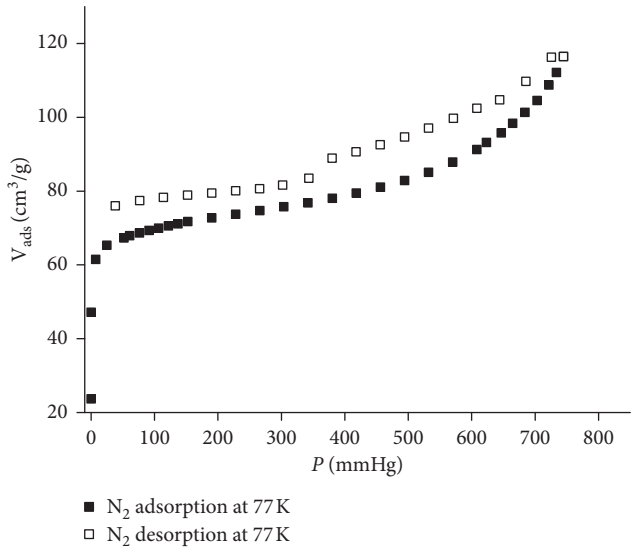

Figure 4: N_2 adsorption isotherms for compound 1 at 77 K.

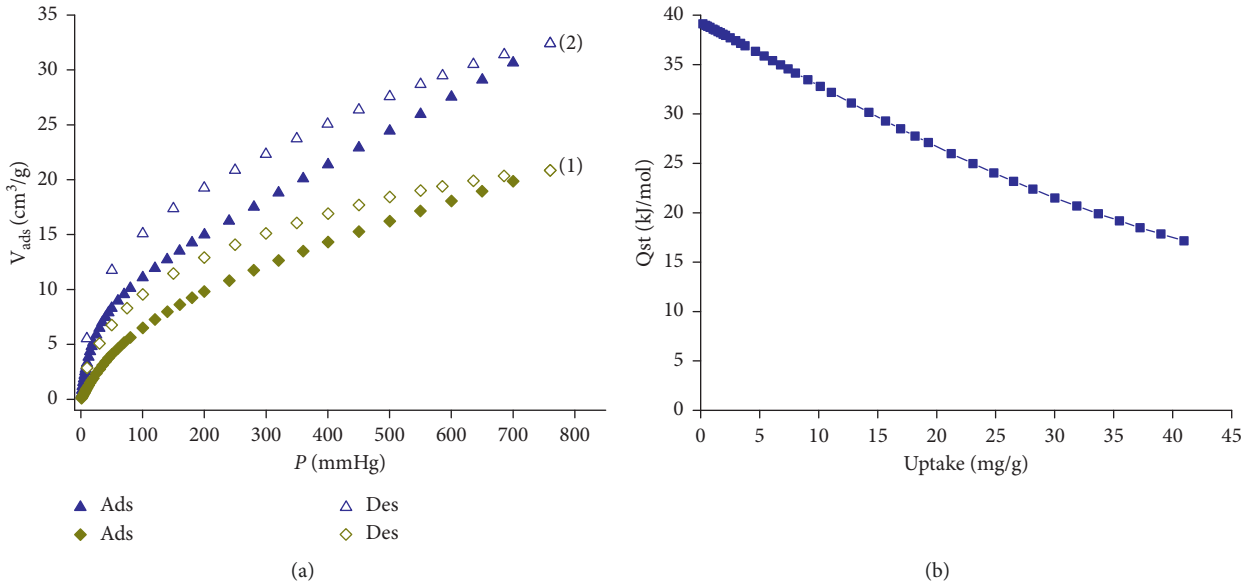

Figure 5: (a) CO_2 adsorption isotherms for compound 1 at 298 K (1) and 273 K (2) (b).

famous porous materials without uncoordinated N-sites, for instance ZIF-8, ZIF-68, ZIF-69, and ZIF-71 [21, 22].

In order to measure the powerful affinities to CO_2, the enthalpy of CO_2 adsorption for compound **1** was calculated by using the virial equation from the adsorption isotherms at two different temperatures (273 and 295 K). At zero loading, the enthalpy of CO_2 adsorption is 39.1 kJ/mol for compound **1** (Figure 5(b)), which is also higher than most of the famous MOFs, such as MOF-5, IR-MOF-3, MOF-253, and bio-MOF-1 [23–26]. These results suggest the N-heteroatom which uncoordinated can markedly enhance the binding strengths of CO_2 gas molecules with the framework.

4. Conclusion

In summary, here, we reported the gas adsorption of a microporous MOF containing N-heteroatom. In the conditions we adopted that the N-heteroatom which is uncoordinated can markedly enhance the interaction between the host framework and CO_2 under ambient conditions.

Data Availability

The data used to support the findings of this study are available from the corresponding author upon request.

Conflicts of Interest

The authors declare that they have no conflicts of interest.

Acknowledgments

This work was financially supported by the Youth Growth Science and Technology Personnel Foundation of Guizhou Education Department (no. KY[2018]331).

Supplementary Materials

Crystal data and structure refinement parameters for compound 1 is shown in Table 1S, and the selected bond lengths (Å) and angles (°) for compound 1 are shown in Table 2S. The X-ray molecular structure analysis indicates that compound 1 is in the orthorhombic I41, a space group. The pore size distribution of the compound 1 is shown in Table 3S. (*Supplementary Materials*)

References

[1] Z.-Z. Yang, Y.-N. Zhao, and L.-N. He, "CO_2 chemistry: task-specific ionic liquids for CO2 capture/activation and subsequent conversion," *RSC Advances*, vol. 1, no. 4, pp. 545–567, 2011.

[2] K. S. Lackner, S. Brennan, J. M. Matter, A. H. A. Park, A. Wright, and B. Van Der Zwaan, "The urgency of the development of CO_2 capture from ambient air," *Proceedings of the National Academy of Sciences*, vol. 109, no. 33, pp. 13156–13162, 2012.

[3] M. R. Allen, D. J. Frame, C. Huntingford et al., "Warming caused by cumulative carbon emissions towards the trillionth tonne," *Nature*, vol. 458, no. 7242, pp. 1163–1166, 2009.

[4] S. Solomon, G.-K. Plattner, R. Knutti, and P. Friedlingstein, "Irreversible climate change due to carbon dioxide emissions," *Proceedings of the National Academy of Sciences*, vol. 106, no. 6, pp. 1704–1709, 2009.

[5] K. Sumida, D. L. Rogow, J. A. Mason et al., "Carbon dioxide capture in metal-organic frameworks," *Chemical Reviews*, vol. 112, no. 2, pp. 724–781, 2012.

[6] J.-R. Li, R. J. Kuppler, and H.-C. Zhou, "Selective gas adsorption and separation in metal-organic frameworks," *Chemical Society Reviews*, vol. 38, no. 5, pp. 1477–1504, 2009.

[7] R. E. Morris and P. S. Wheatley, "Gas storage in nanoporous materials," *Angewandte Chemie International Edition*, vol. 47, no. 27, pp. 4966–4981, 2008.

[8] J. Zhang, H. Wu, T. J. Emge, and J. Li, "A flexible MMOF exhibiting high selectivity for CO2 over N_2, CH_4 and other

small gases," *Chemical Communications*, vol. 46, no. 48, pp. 9152–9154, 2010.

[9] W.-Q. Zhang, R.-D. Wang, Z.-B. Wu et al., "Comparative study on temperature-dependent CO_2 sorption behaviors of two isostructural N-Oxide-Functionalized 3D dynamic microporous MOFs," *Inorganic Chemistry*, vol. 57, no. 3, pp. 1455–1463, 2018.

[10] D. D. Borges, P. Normand, A. Permiakova et al., "Gas adsorption and separation by the Al-based metal-organic framework MIL-160," *The Journal of Physical Chemistry C*, vol. 121, no. 48, pp. 26822–26832, 2017.

[11] K.-J. Chen, D. G. Madden, T. Pham et al., "Tuning pore size in square-lattice coordination networks for size-selective sieving of CO_2," *Angewandte Chemie International Edition*, vol. 55, no. 35, pp. 10268–10272, 2016.

[12] B. Liu, H.-F. Zhou, L. Hou, and Y.-Y. Wang, "Functionalization of MOFs via a mixed-ligand strategy: enhanced CO_2 uptake by pore surface modification," *Dalton Transactions*, vol. 47, no. 15, pp. 5298–5303, 2018.

[13] Z. Zhang, Z.-Z. Yao, S. Xiang, and B. Chen, "Perspective of microporous metal-organic frameworks for CO_2 capture and separation," *Energy & Environmental Science*, vol. 7, no. 9, pp. 2868–2899, 2014.

[14] A. R. Millward and O. M. Yaghi, "Metal–Organic frameworks with exceptionally high capacity for storage of carbon dioxide at room temperature," *Journal of the American Chemical Society*, vol. 127, no. 51, pp. 17998-17999, 2005.

[15] Y. Zhao, H. Wu, T. J. Emge et al., "Enhancing gas adsorption and separation capacity through ligand functionalization of microporous metal-organic framework structures," *Chemistry—A European Journal*, vol. 17, no. 18, pp. 5101–5109, 2011.

[16] L. Wu, M. Xue, S.-L. Qiu, G. Chaplais, A. Simon-Masseron, and J. Patarin, "Amino-Modified MIL-68(In) with enhanced hydrogen and carbon dioxide sorption enthalpy," *Microporous and Mesoporous Materials*, vol. 157, pp. 75–81, 2012.

[17] F. Wang, H.-R. Fu, Y. Kang, and J. Zhang, "A new approach towards zeolitic tetrazolate-imidazolate frameworks (ZTIFs) with uncoordinated N-heteroatom sites for high CO_2 uptake," *Chemical Communications*, vol. 50, no. 81, pp. 12065–12068, 2014.

[18] A. Uzun and S. Keskin, "Site characteristics in metal organic frameworks for gas adsorption," *Progress in Surface Science*, vol. 89, no. 1, pp. 56–79, 2014.

[19] W.-W. Dong, D.-S. Li, J. Zhao, L.-F. Ma, Y.-P. Wu, and Y.-P. Duan, "Two solvent-dependent manganese (II) supramolecular isomers: solid-state transformation and magnetic properties," *CrystEngCOmm*, vol. 15, no. 27, pp. 5412–5416, 2013.

[20] A. L. Spek, *PLATON, A Multipurpose Crystallographic Tool*, Utrecht Universtiy, Utrecht, Netherlands, 2001.

[21] L. Ding and A. O. Yazaydin, "The effect of SO_2 on CO_2 capture in zeolitic imidazolate frameworks," *Physical Chemistry Chemical Physics*, vol. 15, no. 28, pp. 11856–11861, 2013.

[22] W. Morris, B. Leung, H. Furukawa et al., "A combined Experimental–Computational investigation of carbon dioxide capture in a series of isoreticular zeolitic imidazolate frameworks," *Journal of the American Chemical Society*, vol. 132, no. 32, pp. 11006–11008, 2010.

[23] Z. Zhao, Z. Li, and Y. S. Lin, "Adsorption and diffusion of carbon dioxide on Metal–Organic framework (MOF-5)," *Industrial & Engineering Chemistry Research*, vol. 48, no. 22, pp. 10015–10020, 2009.

[24] E. D. Bloch, D. Britt, C. Lee et al., "Metal insertion in a microporous Metal–Organic framework lined with 2, 2′-bipyridine," *Journal of the American Chemical Society*, vol. 132, no. 41, pp. 14382–14384, 2010.

[25] D. Farrusseng, C. Daniel, C. Gaudillère et al., "Heats of adsorption for seven gases in three Metal–Organic frameworks: systematic comparison of experiment and simulation," *Langmuir*, vol. 25, no. 13, pp. 7383–7388, 2009.

[26] J. An and N. L. Rosi, "Tuning MOF CO_2 adsorption properties via cation exchange," *Journal of the American Chemical Society*, vol. 132, no. 16, pp. 5578-5579, 2010.

Hindawi
Journal of Chemistry
Volume 2019, Article ID 8579528, 7 pages
https://doi.org/10.1155/2019/8579528

Research Article

Solid-Phase Preparation of Al-TiO_2 for Efficient Separation of Bioderived Product Danshensu

Fei Chang,[1] **Zhong Bing He**,[1] **and Quan Zhou**[2]

[1]*Institute of Comprehensive Utilization of Plant Resources, Kaili College, Kaili 556011, China*
[2]*Pharmaceutical and Bioengineering College, Hunan Chemical Vocational Technology College, Zhuzhou, Hunan 412000, China*

Correspondence should be addressed to Fei Chang; feichang1980@126.com

Received 2 June 2019; Revised 22 July 2019; Accepted 14 September 2019; Published 3 November 2019

Academic Editor: Dimosthenis L. Giokas

Four kinds of Al-TiO_2 solid samples with different Ti/Al ratios of 1 : 0.1, 1 : 0.09, 1 : 0.07, and 1 : 0.05 were synthesized via a solid-phase synthesis method and characterized by XRD, SEM, EDS, BET, and other techniques. The prepared solids were used for separation of the bioderived product danshensu, the content of which was determined by UV spectrophotometry. Moreover, the effects of extract concentration, PH value, adsorption time, and ethanol elution volume were investigated. The results showed that these Al-TiO_2 samples had good adsorption and desorption ability. Especially, the solid Al-TiO_2 with a Ti/Al ratio of 1 : 0.05 is more suitable for the separation of danshensu, exhibiting a higher adsorption (77.70%) under 2 h adsorption time and pH = 3; meanwhile, the high desorption rate (70.29%) was received under 80% ethanol and the sample concentration of 3.0 mg/mL.

1. Introduction

Danshensu significantly inhibits the growth of cancer cells and makes the tk/GCV (herpes simplex virus thymidine kinase/ganoside) system of cancer cells enhance the synergistic effect of killing and the effect of suicide gene bystanders (BE) [1]. The previous study also found that danshensu can significantly inhibit the rise of blood lipids in rabbits with a high-fat diet and can also inhibit the synthesis of endogenous cholesterol cells [2]. In the field of medicine, danshensu has a more broad application prospect. Therefore, the effective separation and purification of danshen sodium SSH (*Salvia scapiformis* Hance) on the full development and utilization of white tonic has great significance.

Salvia miltiorrhiza separation often uses the extraction or alcohol precipitation method [3–6], but there are bottlenecks such as separation difficulties and serious pollution problems of science and technology. In recent years, with the in-depth study of TiO_2 powder material, it was found that it not only has the basic characteristics of common materials but also has adjustable pore size, narrow pore size distribution, ordered structure, and larger specific surface area with a certain choice of adsorption properties and adsorption capacity [7] because of which it is widely used in the adsorption and separation of organic matter and metal ions [8]. Thus, the synthesis and properties of powder materials research and development have become the current focus of materials chemistry, physics, and traditional Chinese medicine and other disciplines [9–12], so as to achieve the powder material and drug substance molecules surface atoms or active sites selective adsorption [13].

In this study, the Al-TiO_2 samples were prepared by the solid-phase synthesis method for the first time. According to the different doping amounts, different adsorbent materials were obtained, and the influencing factors on the static adsorption of danshensu in SSH were studied by the concentration of extract, pH value, adsorption time, and elution volume fraction of ethanol. It provided a scientific theoretical basis for the effective development and utilization of this plant.

2. Experiments

2.1. Materials. Danshensu (HPLC ≥ 98%, Figure 1) standard was purchased from Beijing Solarbio Technology Co., Ltd.; tetrabutyl titanate (TBOT, 98%), hydrochloric acid (HCl),

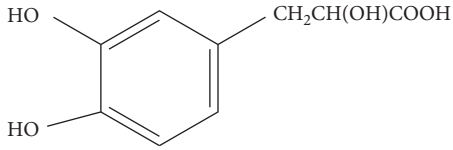

Figure 1: Chemical structure of danshensu.

sodium hydroxide barium chloride ($BaCl_2$), aluminum sulfate octadecanoate ($Al_2(SO_4)_3{\cdot}18H_2O$), cetyltrimethylammonium bromide (CTAB), anhydrous ethanol, and petroleum ether are analytical grade and purchased from Shanghai Aladdin Bio-Chem Technology Co., Ltd.

2.2. Preparation of Al-TiO_2. $Al_2(SO_4)_3{\cdot}18H_2O$ with a Ti/Al molar ratio of 1/0.1, 1/0.09, 1/0.07, and 1/0.05 was mixed with an appropriate amount of CTAB (20 wt.% of the total amount of $Al_2(SO_4)_3{\cdot}18H_2O$ and TBOT) and ground for 25 min in a mortar. Then, 3.403 g TBOT was added to the above mixture and was continuously ground for 20 min. After static standing for 6 h at room temperature, the reactor was transferred into 140°C muffle furnace for 2 h to obtain a white solid, followed by grinding with mortar and washing using a Brinell funnel with distilled water until no SO_4^{2-} (0.1 mol/L $BaCl_2$ solution test to determine). The resulting sample was dried at 110°C for 2 h and then placed into the muffle furnace at 1°C/min heating rate to 550°C for 6 h. The obtained product was cooled down to the room temperature to give Al-TiO_2.

2.3. Characterization of Al-TiO_2. XRD patterns were measured with the Bruker D8 advanced X-ray diffractometer (XRD) with Cu *Ka* radiation ($\lambda = 0.154$ nm) at 40 kV and 30 mA with a step size of 0.02. The SEM and EDS characterizations of the catalysts were studied using the S-3400H (Shimadzu) type scanning electron microscope (SEM). The Brunauer–Emmett–Teller (BET) surface areas were measured using the N_2 adsorption/desorption apparatus (Micromeritics ASAP 2460), and the pore size and pore volume distributions were calculated using the Barrett–Joyner–Halenda (BJH) model. FT-IR spectra were obtained using the S-65 spectrophotometer (Shimadzu). The UV-Vis spectra were recorded on the Shimadzu UV-2500 spectrophotometer.

2.4. Extraction of Danshensu. A certain amount of SSH powder was placed in a Soxhlet extractor and added petroleum ether reflow at 60°C for 12 h (defatted and bleached), petroleum ether removed by using a rotary evaporator, and dried at room temperature to obtain the solid powder. 15 g of the above powder was weighed, 50% ethanol was used as the extraction solvent (V/m = 40 : 1), and the solution was microwave extracted (power: 400 W, temperature: 40°C, and time: 5 min), filtered, and concentrated, and finally, danshensu was obtained.

2.5. Danshensu Detection. At 282 nm maximum absorption wavelength, with the concentration of danshensu as the abscissa and the absorbance as the ordinate, the linear equation was $Y = 0.01382X - 0.00443$ with the correlation coefficient $r = 0.99961$, and the concentration of danshensu in the range of 0.01–0.05 mg/mL has a good linearity by UV-Visible spectrophotometry [14].

2.6. Danshensu Static Adsorption and Desorption Experiments. A certain concentration of danshensu solution was removed accurately into a 250 mL triangle bottle with 1.0 g Al-TiO_2, and the appropriate time and the adsorption rate are calculated according to formula (1). Next, Al-TiO_2 was collected after adsorption, followed by putting into another triangle bottle by filtration. Ethanol was added, shaken at room temperature for 60 min, and left for 12 h. The supernatant was collected by centrifugation, the absorbance was measured by UV-Vis, and the desorption rate was calculated on the basis of formula (2).

The formula of adsorption rate calculation:

$$P_1 = \frac{(C_0V_0 - C_1V_1)}{C_0V_0} \times 100\%. \quad (1)$$

The formula of desorption rate calculation:

$$P_2 = \frac{C_2V_2}{(C_0V_0 - C_2V_2)} \times 100\%, \quad (2)$$

where P_1: adsorption rate, P_2: desorption rate, C_0: danshensu solution mass concentration (mg/mL) before adsorption, V_0: volume of danshensu solution before adsorption (mL), C1: danshensu mass concentration (mg/mL) after adsorption, V_1: volume of danshensu solution after adsorption (mL), C_2: danshensu concentration (mg/mL) after desorption, and V_2: volume of danshensu solution (mL) after desorption.

3. Results and Discussion

3.1. Characterization of Al-TiO_2

3.1.1. EDS Characterization. In order to confirm whether the Al^{3+} is doped into TiO_2, the four kinds of Al-TiO_2 were analyzed by EDS characterization, and the results are shown in Figure 1. As can be seen from Figure 2, all four samples are Al^{3+}-doped TiO_2. Among them, the contents of Al in samples A and B are higher than C and D, while B has the highest in the four samples, and C and D have the same basicity. This result preliminarily showed that the adsorption rates of danshensu by A and B are higher than those by C and D because Al^{3+} is a two-type metal, and danshensu is acidic, and amount of Al^{3+} directly affects the acidity and alkalinity of Al-TiO_2.

3.1.2. XRD. The Al-TiO_2 samples were characterized by XRD to understand the adsorption properties, and the results are shown in Figure 3. From the results, we can see that the Al-TiO_2 was prepared successfully, which is consistent with the EDS analysis. Also, with the increase of Al content, the XRD bands of Al-TiO_2 become sharper, indicating that the crystallinity of Al-TiO_2 is also increasing, leading to the permeability and compactness of Al-TiO_2 enhancement.

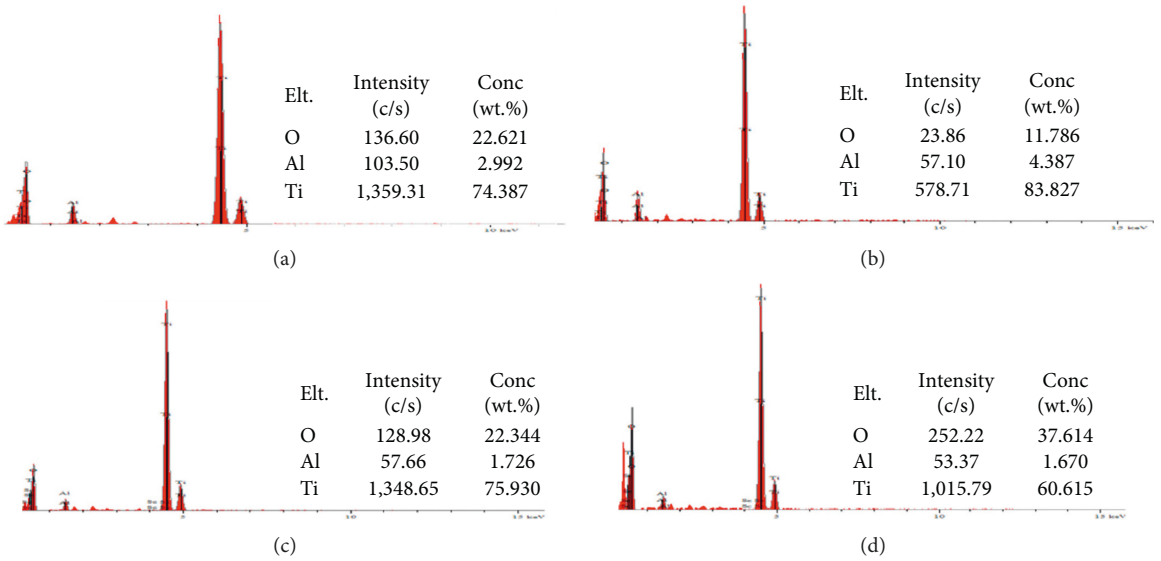

Figure 2: EDS analysis of Al-TiO_2 samples. (a) Ti/Al = 1 : 0.1; (b) Ti/Al = 1 : 0.09; (c) Ti/Al = 1 : 0.07; (d) Ti/Al = 1 : 0.05.

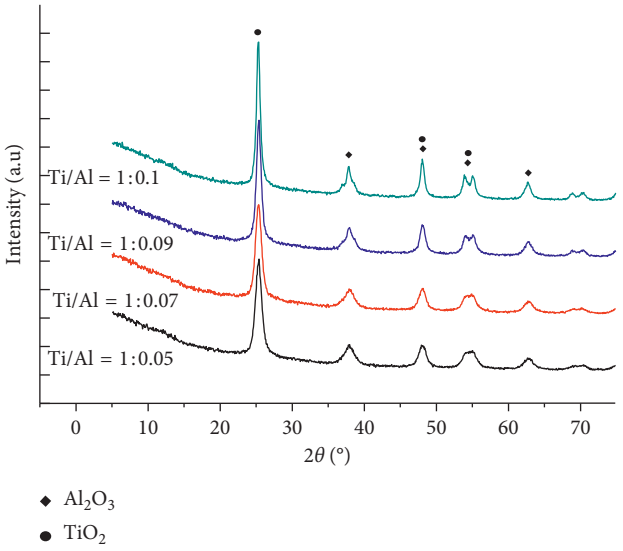

Figure 3: The XRD patterns of Al-TiO_2 samples.

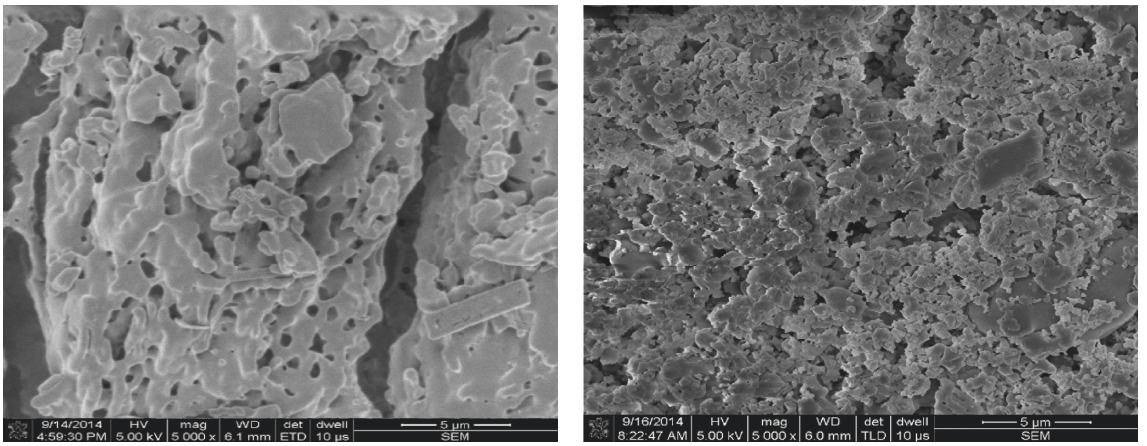

(a) (b)

Figure 4: Continued.

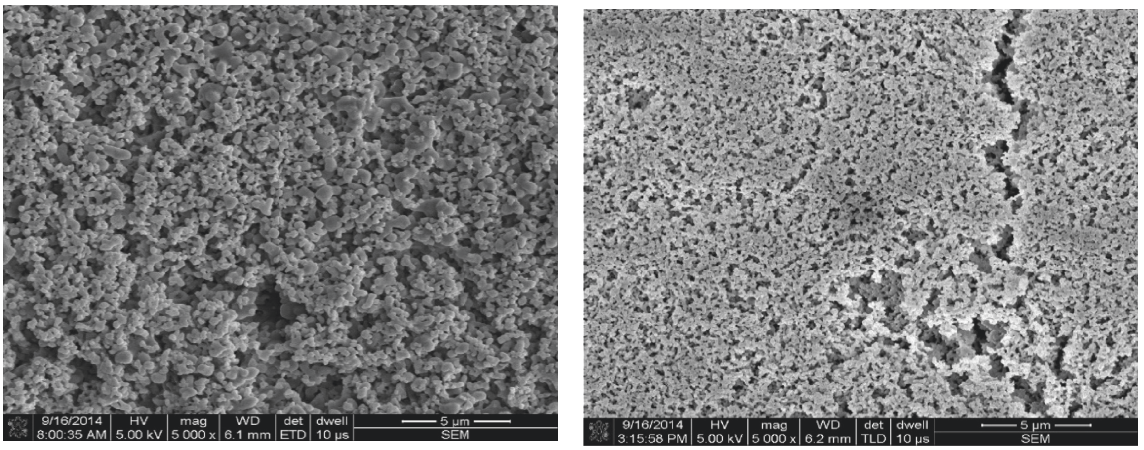

(c) (d)

Figure 4: SEM images of Al-TiO_2 powders with different Ti/Al ratios. (a) Ti/Al = 1/0.1; (b) Ti/Al = 1/0.09; (c) Ti/Al = 1/0.07; (d) Ti/Al = 1/0.05.

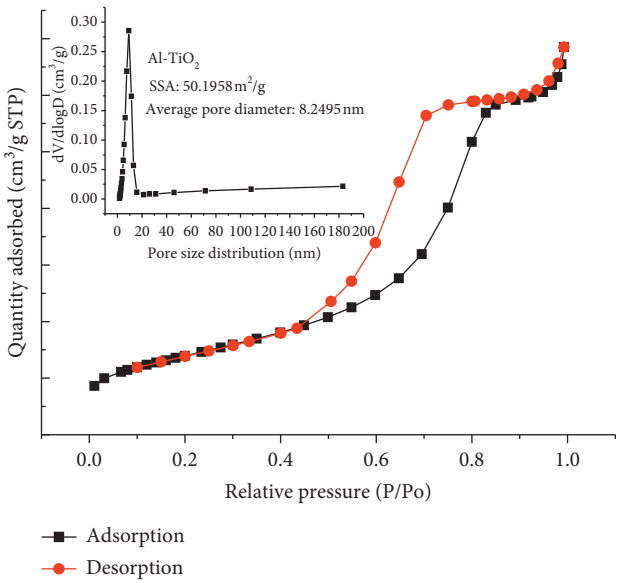

Figure 5: N_2 adsorption-desorption isotherms and pore size distribution of Al-TiO_2 (Ti/Al = 1/0.05).

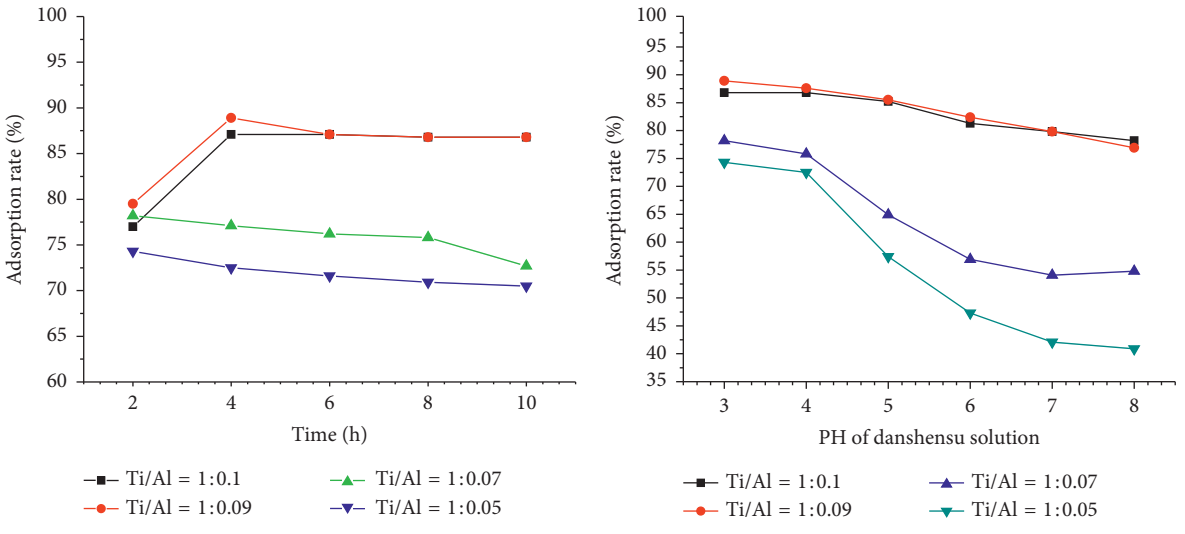

(a) (b)

Figure 6: Continued.

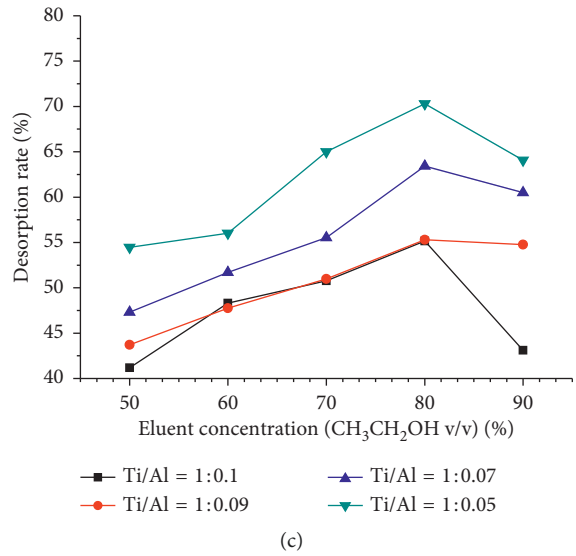

Figure 6: Results of adsorption and desorption condition optimization.

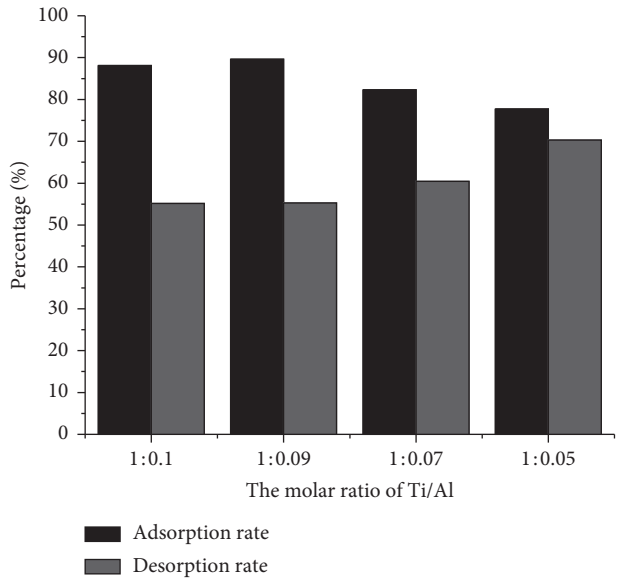

Figure 7: Results of adsorption and desorption of four Al-TiO_2 samples.

3.1.3. SEM. Material properties are closely related to their shape [15, 16], and the obtained SEM images of four different Al-TiO_2 samples are shown in Figure 4. As can be seen from Figure 4, the four Al-TiO_2 solids have a clear pore structure, but as the Al content decreases, the pore structure gradually becomes even, and the grain size of the Al-TiO_2 also decreases. In particular, Figure 4(d) is more obvious. It is preliminary judged that the four Al-TiO_2 samples have a good adsorption capacity.

3.1.4. BET. The N_2 adsorption-desorption isotherm of Al-TiO_2 (Ti/Al = 1/0.05) is shown in Figure 5. The Al-TiO_2 exhibited type IV isotherms with type H3 hysteresis loops. These observations indicated that the pores of Al-TiO_2 belong to the sheet-like stacked pores [17]. These observations were consistent with results from SEM studies. In addition, the specific surface area (SSA) of Al-TiO_2 is 50.1985 m^2/g, and the average pore size is 8.2495 nm.

3.2. Optimization of Static Adsorption and Desorption Conditions. In order to obtain the best adsorption and desorption conditions of the four Al-TiO_2 samples, the adsorption time, the pH value of the danshensu solution, and the eluent concentration were investigated, respectively, and the results are shown in Figure 6. It can be seen from the results of Figures 6(a) and 6(b) that all four Al-TiO_2 materials have good adsorption capacity. Among them, the adsorption capacity of Al-TiO_2 with Ti/Al = 1/0.1 and Ti/Al = 1/0.09 are stronger than that of Ti/Al = 1/0.07 and Ti/Al = 1/0.05, and the opposite results of the desorption capacity are shown with ethanol eluent in Figure 6(c). In addition, with the time extension, the adsorption capacity also increases, but the maximum adsorption rate was reached at 4 h (Figure 6(a)), and the pH value of the danshensu solution was inversely proportional to Al-TiO_2 adsorption capacity (Figure 6(b)). In which the adsorption rate is the highest when the the danshensu solution is pH = 3. At last, the result of the eluent concentration test showed that at 50–90% (v/v), the desorption rate increased with 50–80% ethanol concentration, the maximum desorption rate was received with 80% ethanol. Continuing to increase the ethanol concentration (90%), the desorption rate has a decreasing trend (Figure 6(c)), and the reason can be that danshensu was damaged by high concentrations of ethanol [18–20].

3.3. Test of Adsorption and Desorption. It can be seen from the results in Figure 7 that all four Al-TiO_2 samples have a good adsorption capacity. Among them, Al-TiO_2 with Ti/Al ratios 1/0.1 and 1/0.09 has the highest adsorption rate, but

the desorption capacity is poor. As the effective separation capability is used to measure the quality of material separation (desorption rate/adsorption rate), it can be calculated that the effective separation capability is 62.5%, 61.7%, 77.0%, and 90.3%, respectively. Thus, Al-TiO_2 with Ti/Al ratio 1/0.05 is most suitable for the separation of danshensu. The reason may be that it has a uniform pore structure [15, 21].

4. Conclusions

In conclusion, several Al-TiO_2 samples were prepared by solid-phase synthesis with TBOT and $Al_2(SO_4)_3{\cdot}18H_2O$. Then, the optimized Al-TiO_2 was used for separation of danshensu. The experimental results showed the following:

(1) Al-TiO_2 with Ti/Al ratios 1/0.1 and 1/0.09 has a higher adsorption rate, and the desorption rate is worse than that with Ti/Al ratios 1/0.07 and 1/0.05

(2) The optimal conditions for isolating danshensu solution are pH = 3, 4 h adsorption time, and 80% ethanol eluent

(3) The Al-TiO_2 sample with Ti/Al ratio 1/0.05 is the best material for separating danshensu under the best conditions

Data Availability

The data used to support the findings of this study are included within the article.

Conflicts of Interest

The authors declare that they have no conflicts of interest.

Acknowledgments

This work was financially supported by the Guizhou Provincial State University S&T Technology Joint Fund Program (Nos. LH [2015]7762, BS201503, and LH [2014]7222).

References

[1] H. Li, Y. H. Xie, Q. Yang et al., "Cardioprotective effect of paeonol and danshensu combination on isoproterenol-induced myocardial injury in rats," *PloS One*, vol. 7, no. 11, Article ID e48872, 2012.

[2] Y.-F. Ueng, Y.-H. Kuo, H.-C. Peng et al., "Diterpene quinone tanshinone IIA selectively inhibits mouse and human cytochrome p4501A2," *Xenobiotica*, vol. 33, no. 6, pp. 603–613, 2003.

[3] Y. Y. Wang, J. B. Zhu, L. Li, and Y. Jin, "Absorption and isolation of macroporous resin for five salvianolic acids from Salviae mitiorrhizae," *China Journal of Chinese Materia Medica*, vol. 33, no. 9, pp. 1004–1007, 2008.

[4] S. Kan, J. Li, W. Huang, L. Shao, and D. Chen, "Microsphere resin chromatography combined with microbial biotransformation for the separation and purification of salvianolic acid B in aqueous extract of roots of Salvia multiorrihza Bunge," *Journal of Chromatography A*, vol. 1216, no. 18, pp. 3881–3886, 2009.

[5] M. Zhang, H. Yang, X. Chen et al., "In-situ extraction and separation of salvianolic acid B from Salvia miltiorrhiza Bunge by integrated expanded bed adsorption," *Separation and Purification Technology*, vol. 80, no. 3, pp. 677–682, 2011.

[6] J.-C. Zhou, D.-W. Feng, and G.-S. Zheng, "Extraction of sesamin from sesame oil using macroporous resin," *Journal of Food Engineering*, vol. 100, no. 2, pp. 289–293, 2010.

[7] L. Kavan, J. Rathouský, M. Grätzel, V. Shklover, and A. Zukal, "Surfactant-templated TiO_2 (anatase): characteristic features of lithium insertion electrochemistry in organized nanostructures," *The Journal of Physical Chemistry B*, vol. 104, no. 50, pp. 12012–12020, 2000.

[8] J. Zhao, T. Wu, K. Wu, K. Oikawa, H. Hidaka, and N. Serpone, "Photoassisted degradation of dye pollutants. 3. Degradation of the cationic dye rhodamine B in aqueous anionic surfactant/TiO2Dispersions under visible light irradiation: evidence for the need of substrate adsorption on TiO2Particles," *Environmental Science & Technology*, vol. 32, no. 16, pp. 2394–2400, 1998.

[9] S. Paria and K. C. Khilar, "A review on experimental studies of surfactant adsorption at the hydrophilic solid-water interface," *Advances in Colloid and Interface Science*, vol. 110, no. 3, pp. 75–95, 2004.

[10] P. A. Kralchevsky, K. D. Danov, G. Broze, and A. Mehreteab, "Thermodynamics of ionic surfactant adsorption with account for the counterion binding: effect of salts of various valency," *Langmuir*, vol. 15, no. 7, pp. 2351–2365, 1999.

[11] R. Atkin, V. S. J. Craig, E. J. Wanless, and S. Biggs, "Mechanism of cationic surfactant adsorption at the solid-aqueous interface," *Advances in Colloid and Interface Science*, vol. 103, no. 3, pp. 219–304, 2003.

[12] Y. Li, N.-H. Lee, E. G. Lee, J. S. Song, and S.-J. Kim, "The characterization and photocatalytic properties of mesoporous rutile TiO_2 powder synthesized through self-assembly of nano crystals," *Chemical Physics Letters*, vol. 389, no. 1-3, pp. 124–128, 2004.

[13] J. Gao, F. Guan, Y. Zhao et al., "Preparation of ultrafine nickel powder and its catalytic dehydrogenation activity," *Materials Chemistry and Physics*, vol. 71, no. 2, pp. 215–219, 2001.

[14] F. A. M. Kang, F. Borges, C. Guimarães, J. L. F. C. Lima, C. Matos, and S. Reis, "Phenolic acids and derivatives: studies on the relationship among structure, radical scavenging activity, and physicochemical parameters," *Journal of Agricultural and Food Chemistry*, vol. 48, no. 6, pp. 2122–2126, 2000.

[15] M. Kang, "The superhydrophilicity of Al-TiO_2 nanometer sized material synthesized using a solvothermal method," *Materials Letters*, vol. 59, no. 24-25, pp. 3122–3127, 2005.

[16] Y. Yuan, J. Ding, J. Xu, J. Deng, and J. Guo, "TiO_2 nanoparticles co-doped with silver and nitrogen for antibacterial application," *Journal of Nanoscience and Nanotechnology*, vol. 10, no. 8, pp. 4868–4874, 2010.

[17] K. S. W. Sing, D. H. Everett, R. A. W. Haul et al., "Reporting physisorption data for gas/solid systems with special reference to the determination of surface area and porosity (Recommendations 1984)," *Pure and Applied Chemistry*, vol. 57, no. 4, pp. 603–619, 1985.

[18] Q. Yang, X. L. Zhang, X. Y. Li et al., "Coupling continuous ultrasound-assisted extraction with ultrasonic probe, solid-phase extraction and high-performance liquid chromatography for the determination of sodium Danshensu and four tanshinones in Salvia miltiorrhiza bunge," *Analytica Chimica Acta*, vol. 589, pp. 231–238, 2007.

[19] X. Gong, S. Wang, and H. Qu, "Comparison of two separation technologies applied in the manufacture of botanical

injections: second ethanol precipitation and solvent extraction," *Industrial & Engineering Chemistry Research*, vol. 50, no. 12, pp. 7542–7548, 2011.

[20] C. Ruizhan, Z. Shouqin, Z. Yonghong, B. Helong, and M. Fanlei, "Ultrahigh pressure extraction of Danshensu," *Transactions of the Chinese Society of Agricultural Engineering*, vol. 2008, no. 1, 2008.

[21] B. Y. Lee, S. H. Park, M. Kang, S. C. Lee, and S. J. Choung, "Preparation of Al/TiO2 nanometer photo-catalyst film and the effect of H2O addition on photo-catalytic performance for benzene removal," *Applied Catalysis A: General*, vol. 253, no. 2, pp. 371–380, 2003.

Hindawi
Journal of Chemistry
Volume 2019, Article ID 5256897, 12 pages
https://doi.org/10.1155/2019/5256897

Review Article

Formaldehyde Use and Alternative Biobased Binders for Particleboard Formulation: A Review

Stephen Warui Kariuki, Jackson Wachira, Millien Kawira, and Genson Murithi

Department of Physical Sciences, University of Embu, P.O. Box 6-60100, Embu, Kenya

Correspondence should be addressed to Stephen Warui Kariuki; stephowarui@yahoo.com

Received 30 June 2019; Revised 1 September 2019; Accepted 19 September 2019; Published 13 October 2019

Guest Editor: Zhichao Jin

Formaldehyde-based resins are conventionally used as a binder in formulation of particleboard. Epidemiologic studies have shown that formaldehyde is carcinogenic. Efforts to reduce the health hazard effects of the fomaldehyde-based resin in the particleboard formulation have included use of scavengers for formaldehydes and use of an alternative binder. Use of scavengers for the formaldehyde increases the cost and maintenance of particleboard formulation. There is no proof that scavengers eliminate the emission of formaldehyde from particleboard. Use of biobased binders in particleboard formulation provides an alternative for eliminating use of the formaldehyde-based resin. However, the alternative is hindered by challenges, which include limitations of physical and mechanical properties. The challenge has continuously been acted upon through research. The paper presents an overview of the use of starch as an alternative binder. Improvement over time of the starch and limitations thereof requires to be addressed. Use of the modified starch has shown increased particleboard performance. Mechanical strength, such as modulus of rupture, modulus of elasticity, and internal bonding in particleboards, however, remains to be a challenge.

1. Introduction

1.1. Formaldehyde-Based Resins and Particleboard Formulation. Formaldehyde is used in industries for the synthesis of resins and adhesives used during formulation of particleboard [1]. Phenol formaldehyde (PF) resins are used as adhesive for fixing together panels of exterior-grade plywood, the flakes of oriented strandboard panels, and particleboard [2]. Phenol formaldehyde resins provide high standards of physical and mechanical properties, which involve high strength and resistant to moisture. This prevents delamination and gives excellent temperature stability. This is due to the more flexible nature of phenolic resins [3]. However, high cost of PF is due to fluctuations in cost of phenols and undergoes hydrolysis to emit formaldehydes. Investigation aimed at use of cheaper and formaldehyde-free products as substitute of phenol-formaldehyde, based on not only environmental but also economic grounds. Lignin has comparatively low price and high phenolic moieties along with environmental considerations render it as a suitable substitute for phenols in the manufacture of PF [4, 5].

Urea formaldehyde (UF) resin is widely used as adhesives in the particleboard industry. UF is cheaper compared to PF. There are two major limitations of wood composite boards based on UF binders: first, high emission of formaldehyde during both production, and second, subsequent exploitaion of the boards [6]. Particleboard formulated with urea formaldehyde shown pronounced thickness swelling to water, and hence, they are unsuitable for outdoor use [7]. Measures used to reduce formaldehyde emissions involve decrease of the formaldehyde/urea molar ratio [8]. Unfortunately, the decrease in formaldehyde/urea ratio has resulted in deterioration of physical and mechanical properties of particleboard at the same time.

1.2. Formaldehyde Emission and Formaldehyde Scavangers. The other method used to reduce formaldehyde emission is by use of chemical additives called formaldehyde scavangers.

The most commonly used scavangers are compounds containing amine such as urea, ammonia, melamine, and dicyandiamide [9]. Melamine reacts with formaldehyde to form methylolamine as shown in equation (1) [10]:

$$C_3H_6N_6 + CH_2O \longrightarrow C_4H_8N_6O \quad (1)$$

Dicyandiamide reacts with two moles of formaldehyde as illustrated in equation (2) to form methyloldicyanamides [11]:

$$C_2H_4N_4 + 2CH_2O \longrightarrow C_4H_6N_4O \quad (2)$$

Urea reacts with formaldehyde to form monomethylolurea as shown in equation (3) [12, 13]. Urea formaldehyde resin is used in formulation of particleboard as a binder, other than a scavanger.

$$CO(NH_2)_2 + CH_2O \longrightarrow C_2H_6N_2O_2 \quad (3)$$

Sodium metabisulphite ($Na_2S_2O_5$) is a scavenger used in particleboards produced with urea formaldehyde and melamine formaldehyde resins. Sodium metabisulphite reacts with water to form sodium hydrogen sulfite, as shown in equation (4).

$$Na_2S_2O_5 + H_2O \longrightarrow 2NaHSO_3 \quad (4)$$

Sodium metabisulphite reacts with formaldehyde as a scavenger to form a bisulfite adduct [14] as shown in equation (5):

$$HCHO + NaHSO_3 \longrightarrow HOCH_2SO_3Na \quad (5)$$

Sodium hydrogen sulfite also reacts with sodium hydroxide to form sodium sulfite, as shown in equation (6):

$$NaHSO_3 + NaOH \longrightarrow H_2O + Na_2SO_3 \quad (6)$$

Sodium sulfite scavenger formaldehyde in the presence of water to form bisulfite adduct, as in equation (7) [14].

$$HCHO + Na_2SO_3 + H_2O \longrightarrow NaOH + NaSO_3CH_2OH \quad (7)$$

Ammonia is a good scavenger for the emitted formaldehyde [15]. Green tea catechin as a formaldehyde scavenger reduced formaldehyde from plywood manufactured with formaldehyde-based resin. Green tea extract reduced formaldehyde emissions from plywood [16]. Proanthocyanidic was found to protect kidney tissue against formaldehyde [17]. Tannin was mixed with low molecular phenol-formaldehyde resin in manufacture of plywood. It was used to scavenge against emitted formaldehyde [18].

Prolonged human exposure of formaldehyde lead to chronic toxicity and cancer [12, 19]. Formaldehyde can cause nasopharyngeal cancer [20]. Lu et al. [21] reported on genotoxic and cytotoxic modes of action for the carcinogenesis of inhaled formaldehyde in respiratory nasal epithelium [21]. An increased incidence of myeloid leukemia has been reported.

Increased exposure of formaldehyde to workers in a funeral homes resulted in mortality from myeloid leukemia [22] and lymphohematopoietic malignancies [23–25]. The most consistent pattern was death as a result of myeloid leukemis [26]. A study of 11,039 textile workers produced a certain relationship between the duration of formaldehyde exposure and leukemia-related deaths [27]. The exposure assessment based on 594 workers produced the mean exposure levels between 0.09 and 0.20 ppm, and the levels were relatively constant with no peaks or intermittent exposures. Leukemia had the highest standardized mortality ratio (SMR) with majority of occurrences from garment factory. The epidemiological literature on formaldehyde and leukemia is extensive. Many studies have shown a correlation between formaldehyde and cancer-related complications [26].

1.3. Use of Starch and Starch Derivatives as Substitutes for Particleboard Formulation. Adhesive technology is moving towards replacements of formaldehyde-based adhesives to use of biobased resources [28–30]. Various types of starch modification on its crystalline nature include chemical treatments such as oxidation using hypochlorite [31] and air [32], esterification [33], and cationization [34, 35]. Physical modification of starch includes mechanical activation [36], microwave [37, 38], ultrasonic degradation [39, 40], heat-moisture treatment [41], and enzymatic treatment [42–44]. The modified starch has been utilized in particleboard formulation [45–48].

Selamat et al. [46] compared physical and mechanical properties of particleboard formulated from rubberwood with urea formaldehydes and native starch, separately as binders. The native starch was extracted from oil palm trunk. Particleboard bonded with formaldehyde showed thickness swelling of 11.17% and water absorption of 82.08%, when compared to the native starch with thickness swelling of 82.08% and water absorption of 174.52% [46]. This shows that formaldehyde-based resin is more than twice better than the carboxymethyl starch, although the main drawback is emission of formaldehyde. Formaldehyde has been found to have carcinogenic properties [21, 49–51]. High water absorption of particleboard formulated with the carboxymethyl starch may be attributed to the presence of hydroxyl groups. Hydroxyl groups form hydrogen bonding with water. This increases water absorption and thickness swelling, thus affecting mechanical properties of the particleboards. Methylene diphenyl diisocyanate (MDI) were small and had better mechanical and chemical bonding ability [52]. Improvement in chemical bonding results in improvement in mechanical properties of the particleboard formulated.

Natural starch is in the disorganized metastable state and as such is easily dispersed in warm water [53]. Carboxymethylation therefore is a chemical modification method that is vital and versatile for transforming starch. Transformation of starch involves provision of water soluble polymers and intermediate of valuable functional attributes [54]. Carboxymethylation of starch (CMS) involves partial substitution of hydroxyl group (-OH) with ether group (-O-CH_2COOH). Starch reacts with monochloroacetic acid to produce carboxymethyl in the presence of sodium hydroxide in three different steps. Step one involves reaction of starch with starch, as shown in equation (8):

$$\mathrm{ROH} + \mathrm{NaOH} \longrightarrow \mathrm{RONa} + \mathrm{H_2O} \quad (8)$$

Step two involves the reaction between sodium salt formed with monochloroacetic acid to form sodium monochloroacetate (SMCA) as shown in equation (9):

$$\mathrm{RONa} + \mathrm{ClCH_2COONa} \longrightarrow \mathrm{ROCH_2COONa} + \mathrm{NaCl} \quad (9)$$

Alternatively, SMCA reacts with sodium hydroxide to form sodium glycolate:

$$\mathrm{NaOH} + \mathrm{ClCH_2COONa} \longrightarrow \mathrm{HOCH_2COONa} + \mathrm{NaCl} \quad (10)$$

Carboxylmethylation therefore improves the rheological property of the native starch that improves particleboard characteristics [54].

Starch in water undergoes limited reversible swelling, but the integrity of the crystal structure is such that it does not dissolve [55]. Starch gelatinization at low temperatures can be induced by addition of aqueous alkali [56]. Sodium hydroxide reacts with hydroxyl groups of starch thus improving the thickness swelling and water absorption of the native starch by 8% and 22%, respectively. This is attributed to reduction of hydroxyl groups that were reacted with sodium hydroxide. Another reason could be as a result of reaction between carboxylic group in monochloroacetic acid and hydroxyl groups in starch through esterification process. Particleboard bound with urea formaldehyde had the highest modulus of rupture (MOR) values for medium density of 9.63 N/mm^2, while those bound by the native starch gave the lowest of 3.38 N/mm^2. Same trend was found in modulus of elasticity and internal bonding with 3369.12 N/mm^2, 2068.95 N/mm^2 and 1.98 N/mm^2, 0.96 N/mm^2, respectively [46]. Improved mechanical strength from the native starch to carboxymethyl starch is attributed to the cross-linking of the composite material with highly branched carboxymethyl, leading to formation of stronger covalent bonds than hydrogen bonding found in the native starch. Carboxymethyl starch treatment improved the MOR, thus attaining the minimum Japanese Industrial Standard [46]. MOR is still very low compared to particleboard formulated from urea formaldehyde. There is no interaction between the functional groups of the lignocellulose material and the starch, which leaves a major deficit in reinforcement of the bond between the components of the particleboard. This presents a challenge that requires consideration. Treatment with sodium hydroxide and temperature reduces the sizes of starch making them disperse more within the lignocellulose matrix.

Despite the growing interest in bioplastics, the use of starch-based plastic is still limited due to its brittleness and moisture sensitivity. Addition of polyvinyl alcohol (PVA) reduces the brittleness of the bioplastic [57], and latex increases water resistance [58]. Shi and Tang [47] used polyvinyl alcohol solution with styrene-butadiene (SBR) latex and polymeric methyl diphenyl diioscyanate to modify corn starch. Particleboard formulated showed MOR range from 13.26 N/mm^2 to 16.54 N/mm^2, MOE range from 1508 N/mm^2 to 1768 N/mm^2, and IB range from 0.17 N/mm^2 to 0.32 N/mm^2 [47]. Starch-based adhesives gave the particleboard better prepressing property and sizing uniformity. Pan et al. [59] used polymeric methylene diphenyl diisocyanate to modify rice bran for making an adhesive for making particleboard. Average MOE for particleboard formulated was 2545 N/mm^2, MOR, 21 N/mm^2, and IB of 0.35 N/mm^2 [59]. The study showed that the rice bran adhesive produced can be used to replace a portion of the synthetic adhesive pMDI currently used for the fabrication of rice straw particleboard. Addition of PVA, latex, and SBR will improve moisture resistance, water absorption, and thickness swelling which in turn reduces mechanical properties.

Xu et al. [60] used butyl acrylate (BA) as a comonomer in synthesizing the corn starch-based wood adhesive. The bonding performance was close to that of commercial polivinyl alcohol solution. This cassava-based wood adhesive (SWA) improved in stability more than the corn starch-based wood adhesive. Improved stability was attributed by its low minimum film forming temperature (MFFT) and glass transition temperature (T_g) of the cassava starch [60]. Zhu and Zhuo [61] used butyl acryrate to modify the corn starch used for encapsulating carborxylic-containing compounds through graft copolymerization. The encapsulated organic materials showed low swellability, large encapsulating capacity, and low solubility in water [61]. Low swellability property is crucial in formulation of particleboards. Liu and Su [62] used butyl acrylate to modify potato starch through grafting via surface-initiated atom transfer radical polymerization [62]. Graft modification provides a significant route to alter physical and mechanical properties of biobased adhesives [63].

Starch contains many hydroxyl groups, which make it extremely polar leading to low interaction with nonpolar materials [64]. Starch-based adhesives wet the polar surfaces of cellulose, penetrate crevices and pores, and, thus, form strong bonds. Imam et al. [65] cross-linked corn starch with polyvinyl alcohol (PVOH) using hexamethoxy methylmelamine (HMMM) to bond lignocellulose materials together in an acidic medium. Under this condition, methoxy groups from HMMM reacted with the hydroxyl group from starch in the presence of PVOH to form ether bond [65], as in Scheme 1.

Ether bonds are covalent bonds which are stronger than hydrogen bonding in starch. The binder in formulated particleboard remained intact showing superior bond strength establishment. The boards fractured during mechanical testing. This is attributed to use of an acid media during particleboard formulation. The use of an acid media limits activation of functional groups in lignocellulose materials. Particleboard made from rice straw and the polyvinyl starch-based adhesive gave the following results: MOR, IB, and TS of up to 31 N/mm^2, 0.49 N/mm^2, and 20%, respectively [65]. Use of urea formaldehyde-based resin as a binder gave MOE, IB, and TS of up to 22.19 N/mm^2, 0.5 N/mm^2, and 75% [66]. Researchers worked with different particle sizes and found that the starch-based adhesive gave comparatively better physical and mechanical properties. Properties of polyvinyl alcohol-based resin were greatly influenced by the interaction between the adhesive and

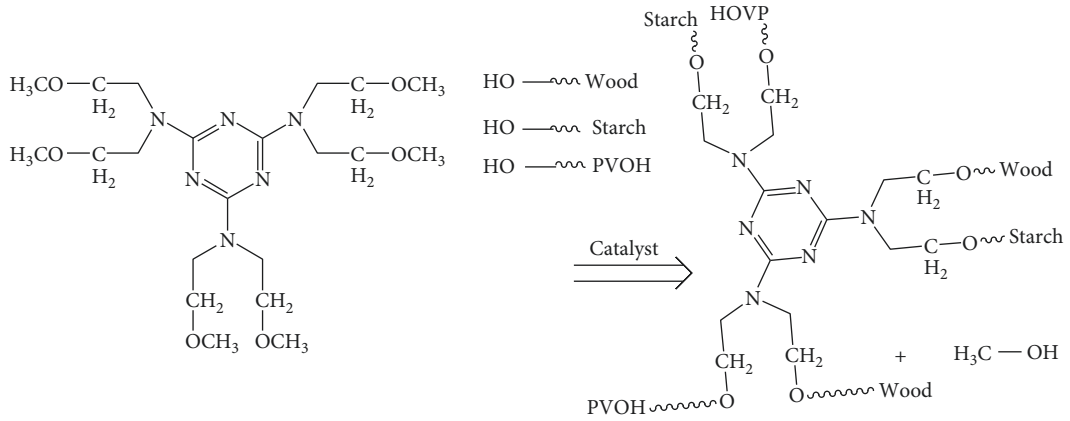

Scheme 1: Schematic chemical crosslinking reaction [65].

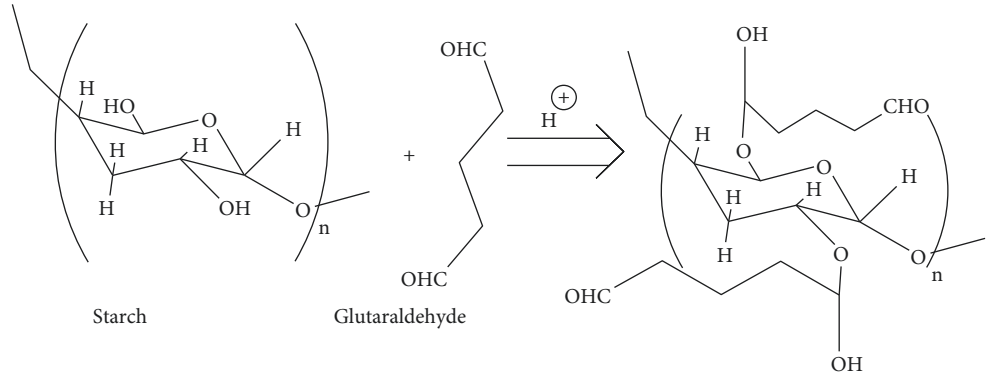

Scheme 2: Modified starch by glutaraldehyde.

lignocellulose material. These properties are still below expectations and can be boosted by use of an alkali, which activates functional groups in lignocellulose materials [67].

Akinyemi et al. [68] used glutaraldehyde to degrade the cassava starch in the presence of acidic medium. Hydroxyl groups in starch molecules were replaced by glutaraldehyde as indicated in Scheme 2.

The modified starch was used to bind wood chips in formulation of sawdust particleboard. Particleboard formulated using this modified starch gave the following results: MOE and MOR of 3232 N/mm^2, and 35.7 N/mm^2, respectively. Comparatively, melamine-formaldehyde (MF), was also used by Cui et al. [69] to obtain MOE and MOR of 2701 N/mm^2 and 14.21 N/mm^2, respectively [68]. MF undergoes hydrolysis leading to produce formaldehyde. Starch modified with glutaraldehyde gave better mechanical strength than their formaldehyde counterpart. Glutaraldehyde is harmful, and this has necessitated the use of sodium bisulfate as a scavenger to neutralize its effect [70]:

$$2Na^+HSO_3^- + OHC{-}(CH_2)_3{-}CHO \longrightarrow 2Na^+ \begin{matrix} OH \\ | \\ C \\ | \\ SO_3^- \end{matrix} {-}(CH_2)_3{-} \begin{matrix} OH \\ | \\ C \\ | \\ SO_3^- \end{matrix} \quad (11)$$

Starch reacts with polyurethane polymer via terminal hydroxyl group in starch through grafting [71], as shown in Scheme 3.

Polar hydroxyl groups are replaced with the hydrophobic aromatic urethane functional group [72]. Polyurethane has been used to modify castor oil starch used in formulation of particleboard made from sugarcane bagasse. The board had WA, TS, MOE, MOR, and IB of up to 20.1%, 20%, 22.6 N/mm^2, 2850 N/mm^2, and 1.18 N/mm^2, respectively [73]. Urea formaldehyde and melamine formaldehyde resin binders for sugarcane bagasse produced WA, TS, MOR, MOE, and IB of 64.87% and 32.52%, 24.71% and 12.66%, 757.8 N/mm^2 and 1053.28 N/mm^2, 3.66 N/mm^2 and 5.53 N/mm^2, and 0.2 N/mm^2 and 0.45 N/mm^2, respectively [74]. Formaldehyde-based resin produces formaldehyde which is a carcinogen. Although modified starch resin produced higher physical and mechanical properties compared to its formaldehyde-based resin, its properties are still very low. Mechanical properties of particleboard made using starch-based adhesive modified polyurethane improved by crosslinking with lignocellulose material.

Starches modified with octenyl succinic anhydride (OSA) have been used in a range of industrial applications, particularly as a food additive. OSA is hydrophobic and also has steric effects. Starch reacts with OSA to form starch octenyl succinate as shown in Scheme 4.

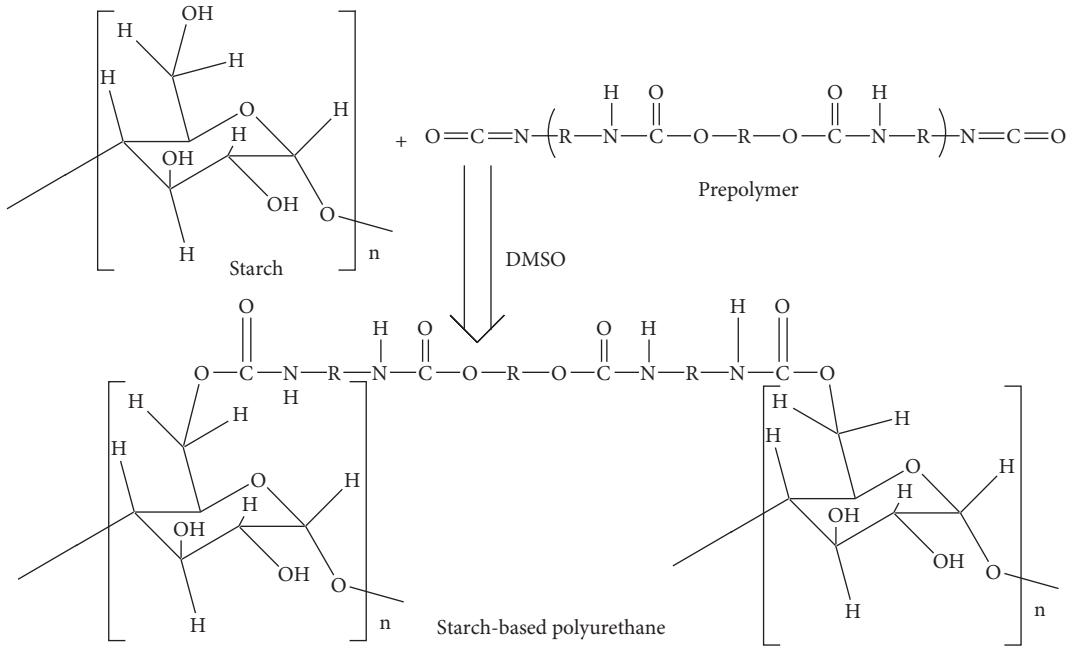

Scheme 3: Preparation of starch-based polyurethane [70].

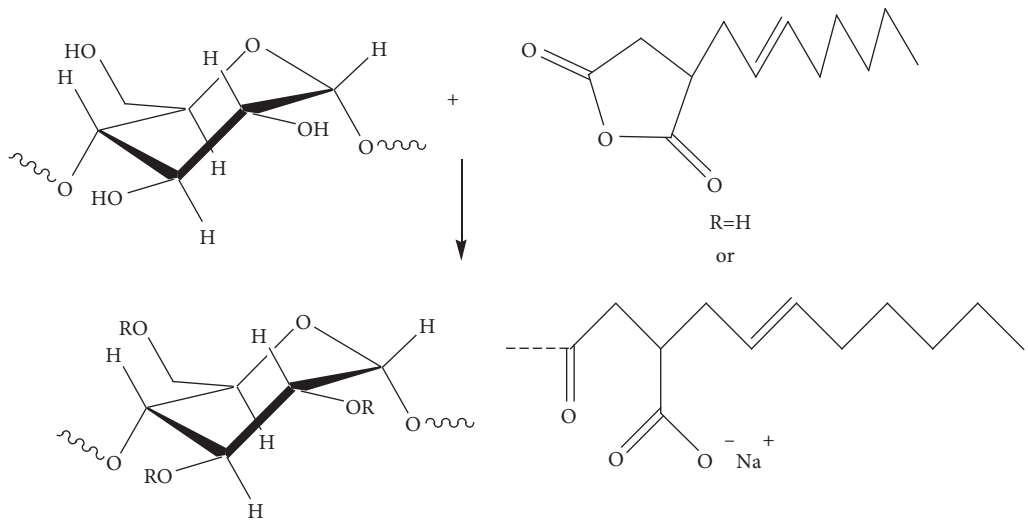

Scheme 4: Reaction showing starch modified with octenyl succinic anhydride (OSA).

Sweedman et al. [75] modified *indica* rice, maize, waxy maize, and potato with octenyl succinic anhydride (OSA) between the temperatures of 30 to 40°C. Due to hydrophobic and steric contributions of OSA and highly branched macromolecular starch structure, modified starch display useful stabilizing, encapsulating, interfacial, thermal, nutritional, and rheological properties [75]. Altuna et al. [76] modified starch with octenyl succinic anhydride to yield a hydrocolloid with amphiphilic properties, the octenyl succinylated starch. The octenyl succinylated starch finds wide application in the food industry mainly as emulsifier, encapsulating agent, and fat replacer [76]. Research investigating the reaction between OSA and modified waxy maize starch showed that OSA reacts with maltodextrine better than the native starch. This indicates incorporation of OSA into hydrated granules [77].

Succinic anhydride reacts with starch by refluxing with pyridin or by gelatinization of starch in aqueous pyridine. This is followed by a reaction with succinic anhydride in pyridine. Pyridine has a dual function in the reaction, activates starch, which makes it nucleophillic, and reacts with succinic anhydride to form succinyl pyridinium intermediate. The intermediate reacts with starch generating starch succinate and pyridine as shown in Scheme 5 [78].

Mehboob et al. [79] used succinic anhydride to modify the native sorghum starch and acid-thinned starch. Succinylation of starch introduces succinyl groups that have hydrophilic character to starch [79]. This group weakens

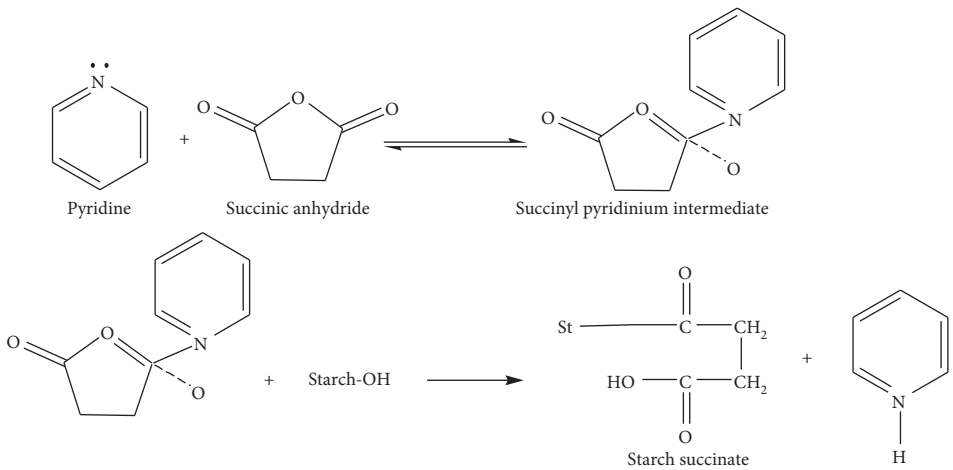

Scheme 5: Starch modification with succinate and pyridine.

internal bonding in starch granules and leads to solubilization of starch in cold water. Research has shown that succinylation reduced retrogradation in starches while the peak, cold paste and water-binding capacity, and set back viscosities improved [77]. Olayinka et al. [80] demonstarted that these parameters are increased by succinylation of red sorghum starch and decreased by modification of a white sorghum starch. The researcher stated that starch succinates have advantages such as high viscocity, greater thickening power and low gelatinization, and retrogradation [80]. Succinylated starches are used in preparation of nongelling creams due to the increase in viscosity of starch. Its improved hydrophilicity [79] makes them suitable for use as a binder in particleboards.

Hydroxypropylation is a common etherification method for starch through treatment with propylene oxide in an alkaline media [81]. Starch reacts with propylene oxide to form the hydroxylpropyl starch as shown in Scheme 6.

Hydroxypropylation decreases the ability of starch to recrystallize, which reduces the retrogradation property of starch, yielding a derivative that is stable at high temperatures [82]. Hydroxyl groups are substituted with hydroxylpropyl groups making its physicochemical properties similar to those of the carboxymethylation method. Hyroxypropyl groups disrupt inter- and intramolecular forces in starch, thus breaking hydrogen bond. This weakens the starch granules leading to its flexibility of amorphous region. Water uptake increases and thus an increase in the swellability [83]. Hydroxypropylation increases starch solubility in water and has stabilized solubility [84]. Hydroxypropylation reduces the number of hydroxyl groups in starch. This in turn reduces the hydrophilic properties of particleboards formulated with the hydropropylated starch. This will reduce water absorption and thickness selling of the particleboard.

Native starches are present in semicrystalline granular forms with certain thermal properties and functionality that have permitted its industrial use. Starch requires high heat to undergo a transition process, during which the granules break down into a mixture of polymers-in-solution, known as gelatinization. Sodium hydroxide solution reduces the temperature required by the starch to gelatinize [85].

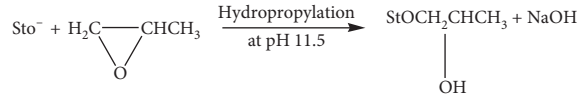

Scheme 6: Hydroxylpropylation of starch with propylene oxide.

Sodium hydroxide is meant to stabilize the viscosity of starch adhesives when they are subjected to high shearing action, heat for prolonged periods, or freeze-thaw cycles [86]. Starch reacts with sodium hydroxide to produce a cationated starch as shown in Scheme 7.

Other plasticizers apart from water and aqueous alkaline, include salt solution such as calcium chloride and potassium iodide [87]. Starch, a polyol, reacts with borax to form a borax-starch complex [88] as illustrated in Scheme 8.

Sodium hydroxide delignifies lignocellulose material by cleavage of the β-O-4 ether bond in which sodium cation and hydroxide ion participate [89], as illustrated in Scheme 9.

Activated starch reacts with lignin in lignocellulose material to form a plasticized starch blend [90] as shown in Figure 1.

Delignification takes place during cellulosic ethanol production to form free cellulose, hemicellulose, and lignin [91]. High concentration of sodium hydroxide converts cellulose and hemicellulose into organic acids, furfural, and hydroxymethyl furfural [92]. An organic acid such as lactic acid has been used in crosslinking of starch and furfural. Furfurals were used as a substitute of formaldehyde in particleboard formulation, respectively. Lignin hydroxyl groups are oxidized to carboxylic acid in the presence of sodium hydroxide as a catalyst [93]. Carboxylic acid reacts with starch hydroxyl groups to form an ester. Ester formation is the main linkage point between the lignocellulose materials and starch binders in the proposed composite formulation for particleboard.

Citric acid and sucrose are natural adhesives [45]. Citric acid is an organic polycarboxylic acid, which contains three carboxyl groups used as cross-linking agent for wood, through esterification [94], as shown in Figure 2.

Liao et al. [45] bonded sugarcane bagasse with commercial sucrose-based adhesive modified with citric acid in the production of particleboard. The board produced had a

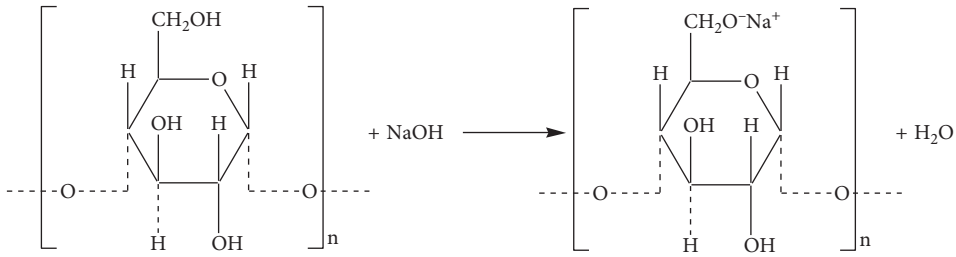

Scheme 7: Reaction between starch and sodium hydroxide.

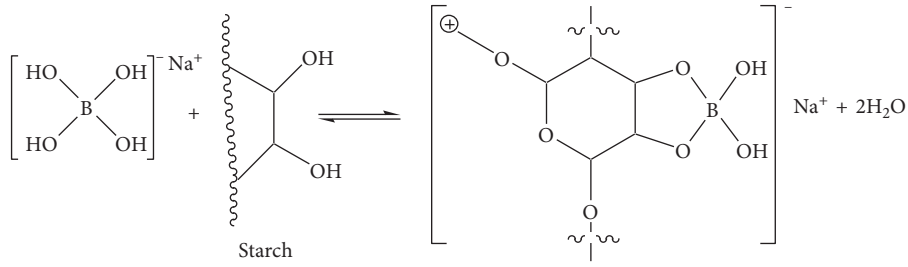

Scheme 8: Starch molecules crosslinked with borax.

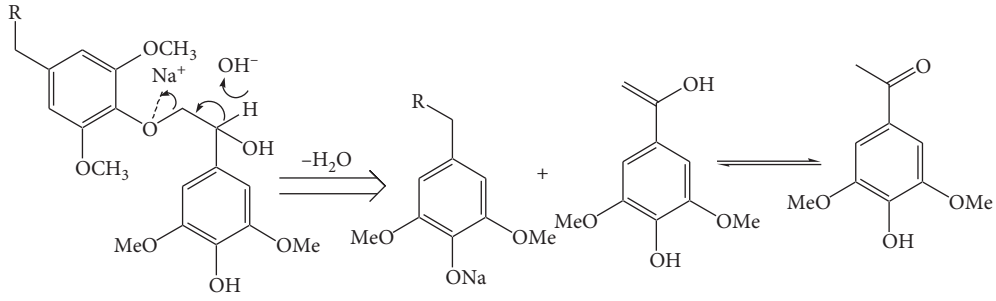

Scheme 9: Cleavage of the β-O-4 bond and formation of synringyl derivatives.

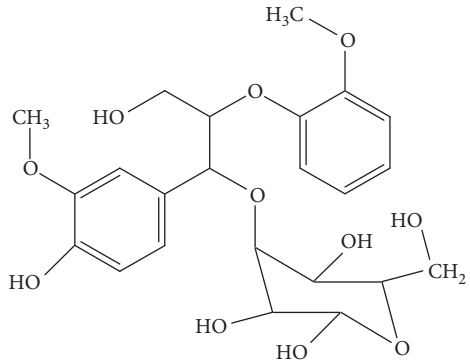

Figure 1: Ether bond formed between starch and lignocellulose material.

density of 0.45 g/cm^3, a low density particleboard [45]. Board density between 0.35 and 0.45 g/cm^3 produced modulus of rapture (MOR) of 6.2 N/mm^2 [45]. The particleboard showed good thermal insulation properties when used as building material for thermal insulation applications. Particleboards produced had a density of 0.40 g/cm^3 met the requirement of Chinese national forestry industry standard. Sugarcane bagasse is rich in sugar-containing compounds that make it suitable for particleboards manufacturing [45].

Starch hydrolyzed with and acid followed with oxidation lead to the formation of aldehyde starch [95] as shown in Scheme 10.

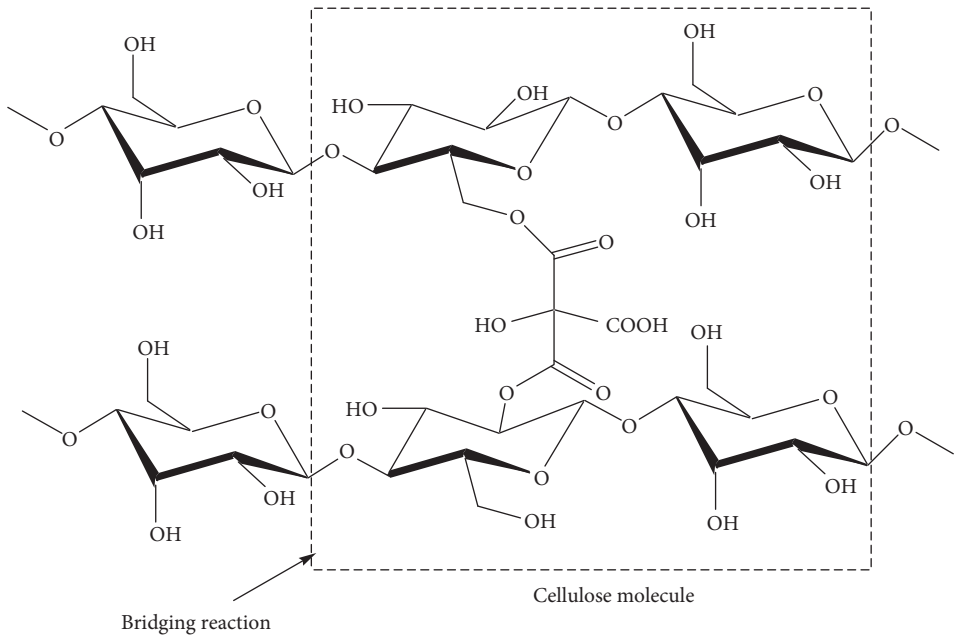

Figure 2: Reaction between citric acid and cellulose molecules [45].

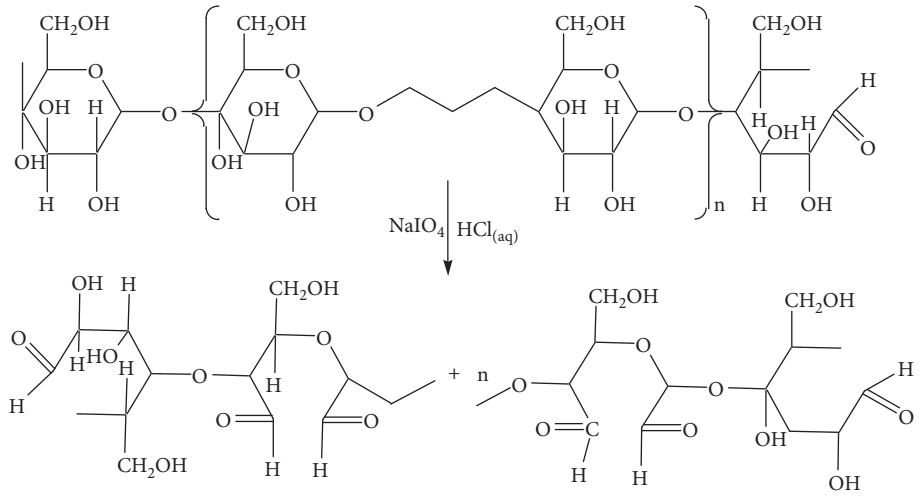

Scheme 10: Reaction of acid hydrolysis and oxidation of starch.

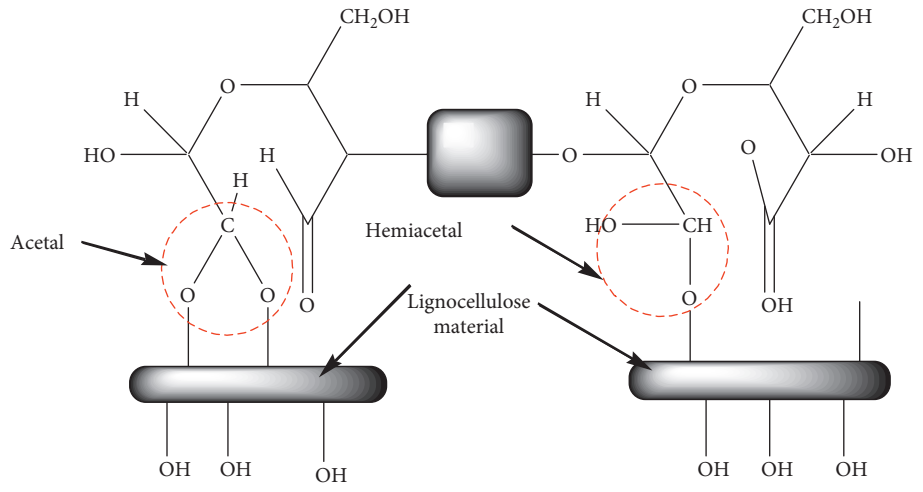

Figure 3: Acetal and hemiacetal bondage between lignocellulose material and modified starch.

Starch dialdehyde reacts with lignocellulose material to form acetal and hemiacetal bondage [96, 97] as proposed in Figure 3.

2. Conclusion

Starch structural and functional diversity make it suitable for different applications. Various modifications will change and improve functional properties of starch and facilitate its utilization for different purposes. Starch modified with other chemicals is used as a substitute for formaldehyde-based resin in particleboard formulations. Hydroxyl group modification in starch is achieved through the introduction of alkyl groups or oxidation to carboxylic acid. This reduces the hydroxyl functional groups that determine the water absorption and thickness swelling which in turn affect the mechanical properties of particleboard. Functional groups in lignocellulose materials determine the water and thickness swelling. Interaction between modified starch-based resin and lignocellulose materials improve properties of particleboard. Mechanical strength of particleboard made from starch-based resin is due to reaction between starch and lignocellulose materials. The hydroxyl group in starch and carboxylic group in lignocellulose materials react through condensation polymerization to form ester linkages. Esterification produces hydrophobic material that reduces water absorption. Esterification also results in formation of covalent bonding that increases the interaction between components of particleboards. This in turn increases the mechanical properties of the particleboard. Unmodified hydroxyl groups in both starch and lignocellulose materials undergo etherification forming a covalent bond through ether bond. Ether and ester linkages are covalent bonds, stronger than hydrogen bonding found between the untreated starch and lignocellulose materials. Physical and mechanical properties of particleboards produced from starch-based adhesives are improved by crosslinking of the starch and lignocellulose material using borax.

Disclosure

This review is part of Ph.D. research project without any research funds.

Conflicts of Interest

The authors declare no conflicts of interest.

References

[1] T. Salthammer, S. Mentese, and R. Marutzky, "Formaldehyde in the indoor environment," *Chemical Reviews*, vol. 110, no. 4, pp. 2536–2572, 2010.

[2] N. S. Çetin and N. Özmen, "Use of organosolv lignin in phenol-formaldehyde resins for particleboard production," *International Journal of Adhesion and Adhesives*, vol. 22, no. 6, pp. 477–480, 2002.

[3] C. A. Finch and A. Pizzi, *Wood Adhesives: Chemistry and Technology*, Marcel Dekkar, New York, NY, USA, 1984.

[4] M. Ghorbani, F. Liebner, H. W. G. Herwijnen et al., "Lignin phenol formaldehyde resoles: the impact of lignin type on adhesive properties," *Journal for BioResource*, vol. 11, pp. 6727–6741, 2016.

[5] A. Pizzi, "Recent developments in eco-efficient bio-based adhesives for wood bonding: opportunities and issues," *Journal of Adhesion Science and Technology*, vol. 20, no. 8, pp. 829–846, 2006.

[6] A. Pizzi and K. L. Mittal, *Handbook of Adhesive Technology; Chapter 31*, Marcel Dekker, New York, NY, USA, 2003.

[7] R. M. Rowell, *Handbook of Wood Chemistry and Wood Composites*, CRC Press, Boca Raton, FL, USA, 2013.

[8] Z. Que, T. Furuno, S. Katoh, and Y. Nishino, "Effects of urea-formaldehyde resin mole ratio on the properties of particleboard," *Building and Environment*, vol. 42, no. 3, pp. 1257–1263, 2007.

[9] F. C. Dupre, M. E. Foucht, W. P. Freese, K. D. Gabrielson, B. D. Gapud, and H. W. Ingram, "Cyclic urea formaldehyde prepolymer for use in phenol formaldehyde and melamine formaldehyde resin based binders," US Patent US 0,054,994, 2002.

[10] D. J. Merline, S. Vukusic, and A. A. Abdala, "Melamine formaldehyde: curing studies and reaction mechanism," *Polymer Journal*, vol. 45, no. 4, pp. 413–419, 2012.

[11] Y. Li, C. Ji, Y. Lu et al., "In situ synthesis of carbon/g-C_3N_4 composites for visible light catalysis by facile one-step pyrolysis of partially formaldehyde-modified dicyandiamide," *Materials Chemistry and Physics*, vol. 214, pp. 28–33, 2018.

[12] S. Boran, M. Usta, and E. Gümüşkaya, "Decreasing formaldehyde emission from medium density fiberboard panels produced by adding different amine compounds to urea formaldehyde resin," *International Journal of Adhesion and Adhesives*, vol. 31, no. 7, pp. 674–678, 2011.

[13] J. I. De Jong and J. de Jonge, "The reaction of urea with formaldehyde," *Recueil Des Travaux Chimiques Des Pays-Bas*, vol. 71, no. 7, pp. 643–660, 2010.

[14] N. A. Costa, J. Pereira, J. Ferra et al., "Scavengers for achieving zero formaldehyde emission of wood-based panels," *Wood Science and Technology*, vol. 47, no. 6, pp. 1261–1272, 2013.

[15] A. Marsal, S. Cuadros, A. M. Manich, F. Izquierdo, and J. Font, "Reduction of the formaldehyde content in leathers treated with formaldehyde resins by means of plant polyphenols," *Journal of Cleaner Production*, vol. 148, pp. 518–526, 2017.

[16] A. Takagaki, K. Fukai, F. Nanjo, Y. Hara, M. Watanabe, and S. Sakuragawa, "Application of green tea catechins as formaldehyde scavengers," *Journal for the Japan Wood Research*, vol. 46, p. 237, 2000.

[17] E. Bakar, E. Ulucam, and A. Cerkezkayabekir, "Protective effects of proanthocyanidin and vitamin E against toxic effects of formaldehyde in kidney tissue," *Biotechnic & Histochemistry*, vol. 90, no. 1, pp. 69–78, 2014.

[18] Y. B. Hoong, M. T. Paridah, Y. F. Loh, M. P. Koh, C. A. Luqman, and A. Zaidon, "Acacia mangium tannin as formaldehyde scavenger for low molecular weight phenol-formaldehyde resin in bonding tropical plywood," *Journal of Adhesion Science and Technology*, vol. 24, no. 8–10, pp. 1653–1664, 2010.

[19] B. Meyer, W. E. Johns, and J. K. Woo, "Formaldehyde release from sulfur-modified urea-formaldehyde resin systems," *Journal for Forest Products*, vol. 30, pp. 24–31, 1980.

[20] K.-H. Kim, S. A. Jahan, and J.-T. Lee, "Exposure to formaldehyde and its potential human health hazards," *Journal of Environmental Science and Health, Part C*, vol. 29, no. 4, pp. 277–299, 2011.

[21] K. Lu, L. B. Collins, H. Ru, E. Bermudez, and J. A. Swenberg, "Distribution of DNA adducts caused by inhaled formaldehyde is consistent with induction of nasal carcinoma but not leukemia," *Toxicological Sciences*, vol. 116, no. 2, pp. 441–451, 2010.

[22] M. Hauptmann, P. A. Stewart, J. H. Lubin et al., "Mortality from lymphohematopoietic malignancies and brain cancer among embalmers exposed to formaldehyde," *JNCI Journal of the National Cancer Institute*, vol. 101, no. 24, pp. 1696–1708, 2009.

[23] R. B. Hayes, A. Blair, P. A. Stewart, R. F. Herrick, and H. Mahar, "Mortality of U.S. embalmers and funeral directors," *American Journal of Industrial Medicine*, vol. 18, no. 6, pp. 641–652, 1990.

[24] J. Walrath and J. F. Fraumeni, "Mortality patterns among embalmers," *International Journal of Cancer*, vol. 31, no. 4, pp. 407–411, 1983.

[25] J. Walrath and J. F. Fraumeni, "Cancer and other causes of death among embalmers," *Journal for Cancer Research*, vol. 44, no. 10, pp. 4638–4641, 1984.

[26] L. Zhang, L. E. B. Freeman, J. Nakamura et al., "Formaldehyde and leukemia: epidemiology, potential mechanisms, and implications for risk assessment," *Journal for Environmental and Molecular Mutagenesis*, vol. 51, pp. 181–191, 2010.

[27] L. E. Pinkerton, M. Hein, and L. Stayner, "Mortality among a cohort of garment workers exposed to formaldehyde: an update," *Occupational and Environmental Medicine*, vol. 61, no. 3, pp. 193–200, 2004.

[28] M. Irle, C. Belloncle, B. Guezguez, L. . , R., and R. Chauvin, "An investigation of a "green" extender for synthetic adhesives," in *Proceedings of the ARBORA Conference*, pp. 20-21, Bordeaux, France, November 2008.

[29] S. Kim, "The reduction of formaldehyde and VOCs emission from wood-based flooring by green adhesive using cashew nut shell liquid (CNSL)," *Journal of Hazardous Materials*, vol. 182, no. 1–3, pp. 919–922, 2010.

[30] Y. Liu and K. Li, "Chemical modification of soy protein for wood adhesives," *Macromolecular Rapid Communications*, vol. 23, no. 13, pp. 739–742, 2002.

[31] K. F. Patel, H. U. Mehta, and H. C. Srivastava, "Kinetics and mechanism of oxidation of starch with sodium hypochlorite," *Journal of Applied Polymer Science*, vol. 18, no. 2, pp. 389–399, 1974.

[32] D. Gumul, H. Gambuś, and M. Gibiński, "Air oxidation of potato starch over zinc (II) catalyst," *Journal on Carbohydrate Polymers*, vol. 8, pp. 45–50, 2014.

[33] Z. Qiao, J. Gu, S. Lv, J. Cao, H. Tan, and Y. Zhang, "Preparation and properties of normal temperature cured starch-based wood adhesive," *Journal on BioResources*, vol. 11, pp. 4839–4849, 2016.

[34] C. Siau, A. Karim, M. Norziah, and W. Wan Rosli, "Effects of cationization on DSC thermal profiles, pasting and emulsifying properties of sago starch," *Journal of the Science of Food and Agriculture*, vol. 84, no. 13, pp. 1722–1730, 2004.

[35] F. Xie, L. Yu, H. Liu, and L. Chen, "Starch modification using reactive extrusion," *Journal on Starch*, vol. 58, pp. 131–139, 2016.

[36] Z. Huang, J. Lu, X. Li, and Z. Tong, "Effect of mechanical activation on physico-chemical properties and structure of cassava starch," *Carbohydrate Polymers*, vol. 68, no. 1, pp. 128–135, 2007.

[37] S. Emami, A. Perera, V. Meda, and R. T. Tyler, "Effect of microwave treatment on starch digestibility and physico-chemical properties of three barley types," *Food and Bioprocess Technology*, vol. 5, no. 6, pp. 2266–2274, 2012.

[38] G. Lewandowicz, T. Jankowski, and J. Fornal, "Effect of microwave radiation on physico-chemical properties and structure of cereal starches," *Carbohydrate Polymers*, vol. 42, no. 2, pp. 193–199, 2000.

[39] R. Czechowska-Biskup, B. Rokita, S. Lotfy, P. Ulanski, and J. M. Rosiak, "Degradation of chitosan and starch by 360-kHz ultrasound," *Journal on Carbohydrate Polymers*, vol. 60, no. 2, pp. 175–184, 2013.

[40] Z. Luo, X. Fu, X. He, F. Luo, Q. Gao, and S. Yu, "Effect of ultrasonic treatment on the physicochemical properties of maize starches differing in amylose content," *Journal on Starch—Stärke*, vol. 60, no. 11, pp. 646–653, 2013.

[41] A. Gunaratne and R. Hoover, "Effect of heat-moisture treatment on the structure and physicochemical properties of tuber and root starches," *Carbohydrate Polymers*, vol. 49, no. 4, pp. 425–437, 2002.

[42] H.-J. Chung, H. S. Lim, and S.-T. Lim, "Effect of partial gelatinization and retrogradation on the enzymatic digestion of waxy rice starch," *Journal of Cereal Science*, vol. 43, no. 3, pp. 353–359, 2006.

[43] B. Kaur, F. Ariffin, R. Bhat, and A. A. Karim, "Progress in starch modification in the last decade," *Food Hydrocolloids*, vol. 26, no. 2, pp. 398–404, 2012.

[44] Y. N. Shariffa, A. A. Karim, A. Fazilah, and I. S. M. Zaidul, "Enzymatic hydrolysis of granular native and mildly heat-treated tapioca and sweet potato starches at sub-gelatinization temperature," *Food Hydrocolloids*, vol. 23, no. 2, pp. 434–440, 2009.

[45] R. Liao, J. Xu, and K. Umemura, "Low density sugarcane bagasse particleboard bonded with citric acid and sucrose: effect of board density and additive," *Journal for Bioresources*, vol. 11, pp. 2174–2185, 2016.

[46] M. E. Selamat, O. Sulaiman, R. Hashim et al., "Measurement of some particleboard properties bonded with modified carboxymethyl starch of oil palm trunk," *Measurement*, vol. 53, pp. 251–259, 2014.

[47] J. Y. Shi and Y. Y. Tang, "Study on the rice straw-particleboard by starch-based API adhesive," *Advanced Materials Research*, vol. 113-116, pp. 1017–1020, 2010.

[48] I. Spiridon, C.-A. Teaca, and R. Bodirlau, "Preparation and characterization of adipic acid-modified starch microparticles/plasticized starch composite films reinforced by lignin," *Journal of Materials Science*, vol. 46, no. 10, pp. 3241–3251, 2010.

[49] M. Blackwell, H. Kang, A. Thomas, and P. Infante, "Formaldehyde: evidence of carcinogenicity," *American Industrial Hygiene Association Journal*, vol. 42, pp. 34–46, 1981.

[50] J. A. Swenberg, B. C. Moeller, and K. Lu, "Formaldehyde carcinogenicity research. 30 years and counting for mode of action, epidemiology, and cancer risk assessment," *Journal on Toxicologic Pathology*, vol. 41, pp. 143–148, 2013.

[51] USNTP, "National toxicology program (NTP)," Report on Carcinogens, Depart-ment of Health and Human Services, Public Health Service, National Toxicology Pro-Gram, USNTP, Patuxent River, MD, USA, 12th edition, 2011.

[52] X. Mo, E. Cheng, D. Wang, and X. S. Sun, "Physical properties of medium-density wheat straw particleboard using different adhesives," *Industrial Crops and Products*, vol. 18, no. 1, pp. 47–53, 2003.

[53] W. A. Mitchell, "Starch solubility," *Journal of Chemical Education*, vol. 54, no. 2, p. 132, 1977.

[54] P. M. Ganorkar and A. S. Kulkarni, "Studies on preparation and functional properties of carboxymethyl starch from sorghum," *Journal for Food Research*, vol. 20, pp. 2205–2210, 2013.

[55] S. A. Roberts and R. E. Cameron, "The effects of concentration and sodium hydroxide on the rheological properties of potato starch gelatinisation," *Carbohydrate Polymers*, vol. 50, no. 2, pp. 133–143, 2002.

[56] M. Wooton and P. Ho, "Alkali gelatinisation of wheat starch," *Journal for Starch—StaËrke*, vol. 41, pp. 261–265, 1989.

[57] H. Judawisastra, R. D. R. Sitohang, L. Marta, and Mardiyati, "Water absorption and its effect on the tensile properties of tapioca starch/polyvinyl alcohol bioplastics," *IOP Conference Series: Materials Science and Engineering*, vol. 223, Article ID 012066, 2017.

[58] S. H. Imam, L. Mao, L. Chen, and R. V. Greene, "Wood adhesive from crosslinked poly(vinyl alcohol) and partially gelatinized starch: preparation and properties," *Starch—Stärke*, vol. 51, no. 6, pp. 225–229, 1999.

[59] Z. Pan, A. Cathcart, and D. Wang, "Properties of particleboard bond with rice bran and polymeric methylene diphenyl diisocyanate adhesives," *Industrial Crops and Products*, vol. 23, no. 1, pp. 40–45, 2006.

[60] Q. Xu, J. Wen, and Z. Wang, "Preparation and properties of cassava starch-based wood adhesives," *Journal on BioResources*, vol. 11, pp. 6756–6767, 2016.

[61] Z. Zhu and R. Zhuo, "Controlled release of carboxylic-containing herbicides by starch-g-poly(butyl acrylate)," *Journal of Applied Polymer Science*, vol. 81, no. 6, pp. 1535–1543, 2001.

[62] P. Liu and Z. Su, "Surface-initiated atom transfer radical polymerization (SI-ATRP) of *n*-butyl acrylate from starch granules," *Carbohydrate Polymers*, vol. 62, no. 2, pp. 159–163, 2005.

[63] K. C. Gupta and S. Sahoo, "Graft copolymerization of acrylonitrile and ethyl methacrylate comonomers on cellulose using ceric ions," *Biomacromolecules*, vol. 2, no. 1, pp. 239–247, 2001.

[64] Y.-P. Wu, Q. Qi, G.-H. Liang, and L.-Q. Zhang, "A strategy to prepare high performance starch/rubber composites: in situ modification during latex compounding process," *Carbohydrate Polymers*, vol. 65, no. 1, pp. 109–113, 2006.

[65] S. H. Imam, S. H. Gordon, L. Mao, and L. Chen, "Environmentally friendly wood adhesive from a renewable plant polymer: characteristics and optimization," *Polymer Degradation and Stability*, vol. 73, no. 3, pp. 529–533, 2001.

[66] X. Li, Z. Cai, J. E. Winandy, and A. H. Basta, "Selected properties of particleboard panels manufactured from rice straws of different geometries," *Bioresource Technology*, vol. 101, no. 12, pp. 4662–4666, 2010.

[67] X. Erdocia, R. Prado, M. Á. Corcuera, and J. Labidi, "Base catalyzed depolymerization of lignin: influence of organosolv lignin nature," *Biomass and Bioenergy*, vol. 66, pp. 379–386, 2014.

[68] A. B. Akinyemi, J. O. Afolayan, and E. O. Oluwatobi, "Some properties of composite corn cob and sawdust particle boards," *Construction and Building Materials*, vol. 127, pp. 436–441, 2016.

[69] J. Cui et al., "Enhancement of mechanical strength of particleboard using environmentally friendly pine (Pinus pinaster L.) tannin adhesives with cellulose nanofibers," *Journal for Annals of Forest Science*, vol. 72, no. 1, pp. 27–32, 2015.

[70] S. L. P. Jordan, "Inactivation of glutaraldehyde by reaction with sodium bisulfite," *Journal of Toxicology And Environmental Health*, vol. 47, no. 3, pp. 299–309, 1996.

[71] M. Barikani and M. Mohammadi, "Synthesis and characterization of starch-modified polyurethane," *Carbohydrate Polymers*, vol. 68, no. 4, pp. 773–780, 2007.

[72] F. Zia, K. M. Zia, M. Zuber, S. Kamal, and N. Aslam, "Starch based polyurethanes: a critical review updating recent literature," *Carbohydrate Polymers*, vol. 134, pp. 784–798, 2015.

[73] J. Fiorelli, D. D. L. Sartori, J. C. M. Cravo et al., "Sugarcane bagasse and castor oil polyurethane adhesive-based particulate composite," *Materials Research*, vol. 16, no. 2, pp. 439–446, 2013.

[74] R. M. De Barros Filho, L. M. Mendes, K. M. Novack, L. O. Aprelini, and V. R. Botaro, "Hybrid chipboard panels based on sugarcane bagasse, urea formaldehyde and melamine formaldehyde resin," *Industrial Crops and Products*, vol. 33, no. 2, pp. 369–373, 2011.

[75] M. C. Sweedman, M. J. Tizzotti, C. Schäfer, and R. G. Gilbert, "Structure and physicochemical properties of octenyl succinic anhydride modified starches: a review," *Carbohydrate Polymers*, vol. 92, no. 1, pp. 905–920, 2013.

[76] L. Altuna, M. L. Herrera, and M. L. Foresti, "Synthesis and characterization of octenyl succinic anhydride modified starches for food applications. A review of recent literature," *Food Hydrocolloids*, vol. 80, pp. 97–110, 2018.

[77] Z. Sui, K. C. Huber, and J. N. BeMiller, "Effects of the order of addition of reagents and catalyst on modification of maize starches," *Carbohydrate Polymers*, vol. 96, no. 1, pp. 118–130, 2013.

[78] P. Bhandari and R. S. Singhal, "Studies on the optimisation of preparation of succinate derivatives from corn and amaranth starches," *Carbohydrate Polymers*, vol. 47, no. 3, pp. 277–283, 2002.

[79] S. Mehboob, T. M. Ali, F. Alam, and A. Hasnain, "Dual modification of native white sorghum (sorghum bicolor) starch via acid hydrolysis and succinylation," *LWT—Food Science and Technology*, vol. 64, no. 1, pp. 459–467, 2015.

[80] O. O. Olayinka, B. I. Olu-Owolabi, and K. O. Adebowale, "Effect of succinylation on the physicochemical, rheological, thermal and retrogradation properties of red and white sorghum starches," *Food Hydrocolloids*, vol. 25, no. 3, pp. 515–520, 2011.

[81] J. Singh, L. Kaur, and O. J. McCarthy, "Factors influencing the physico-chemical, morphological, thermal and rheological properties of some chemically modified starches for food applications—a review," *Food Hydrocolloids*, vol. 21, no. 1, pp. 1–22, 2007.

[82] J. Pal, R. S. Singhal, and P. R. Kulkarni, "Physicochemical properties of hydroxypropyl derivative from corn and amaranth starch," *Carbohydrate Polymers*, vol. 48, no. 1, pp. 49–53, 2002.

[83] N. Masina, Y. E. Choonara, P. Kumar et al., "A review of the chemical modification techniques of starch," *Carbohydrate Polymers*, vol. 157, pp. 1226–1236, 2017.

[84] A. Besheer, G. Hause, J. Kressler, and K. Mäder, "Hydrophobically modified hydroxyethyl starch: synthesis, characterization, and aqueous self-assembly into nano-sized polymeric micelles and vesicles," *Biomacromolecules*, vol. 8, no. 2, pp. 359–367, 2007.

[85] I. D. Evans and D. R. Haisman, "The effect of solutes on the gelatinization temperature range of potato starch," *Starch—Stärke*, vol. 34, no. 7, pp. 224–231, 1982.

[86] A. A. Ragheb, I. Abdel-Thalouth, and S. Tawfik, "Gelatinization of starch in aqueous alkaline solutions," *Starch—Stärke*, vol. 47, no. 9, pp. 338–345, 1995.

[87] J. Jane, "Starch properties, modifications, and applications," *Journal of Macromolecular Science, Part A*, vol. 32, no. 4, pp. 751–757, 1995.

[88] P. Erdem, E. A. Bursali, and M. Yurdakoc, "Preparation and characterization of tannic acid resin: study of boron adsorption," *Environmental Progress & Sustainable Energy*, vol. 32, no. 4, pp. 1036–1044, 2012.

[89] V. M. Roberts, V. Stein, T. Reiner, A. Lemonidou, X. Li, and J. A. Lercher, "Towards quantitative catalytic lignin depolymerization," *Chemistry—A European Journal*, vol. 17, no. 21, pp. 5939–5948, 2011.

[90] R.-L. Wu, X.-L. Wang, F. Li, H.-Z. Li, and Y.-Z. Wang, "Green composite films prepared from cellulose, starch and lignin in room-temperature ionic liquid," *Bioresource Technology*, vol. 100, no. 9, pp. 2569–2574, 2009.

[91] Z. Wang, D. R. Keshwani, A. P. Redding, and J. J. Cheng, "Sodium hydroxide pretreatment and enzymatic hydrolysis of coastal Bermuda grass," *Bioresource Technology*, vol. 101, no. 10, pp. 3583–3585, 2010.

[92] D. B. Hodge, M. N. Karim, D. J. Schell, and J. D. McMillan, "Soluble and insoluble solids contributions to high-solids enzymatic hydrolysis of lignocellulose," *Bioresource Technology*, vol. 99, no. 18, pp. 8940–8948, 2008.

[93] X. Gu, C. Kanghua, H. Ming, Y. Shi, and Z. Li, "La-modified SBA-15/H_2O_2 systems for the microwave assisted oxidation of organosolv beech wood lignin," *Maderas. Ciencia Y Tecnología*, vol. 14, no. 1, pp. 31–41, 2012.

[94] S. B. Vukusic, D. Katovic, C. Schramm, J. Trajkovic, and B. Sefc, "Polycarboxylic acids as non-formaldehyde anti-swelling agents for wood," *Holzforschung*, vol. 60, no. 4, pp. 439–444, 2006.

[95] Y. Zuo, W. Liu, J. Xiao, X. Zhao, Y. Zhu, and Y. Wu, "Preparation and characterization of dialdehyde starch by one-step acid hydrolysis and oxidation," *International Journal of Biological Macromolecules*, vol. 103, pp. 1257–1264, 2017.

[96] T. Saito and A. Isogai, "Introduction of aldehyde groups on surfaces of native cellulose fibers by TEMPO-mediated oxidation," *Colloids and Surfaces A: Physicochemical and Engineering Aspects*, vol. 289, no. 1–3, pp. 219–225, 2006.

[97] B. Sun, Q. Hou, Z. Liu, and Y. Ni, "Sodium periodate oxidation of cellulose nanocrystal and its application as a paper wet strength additive," *Cellulose*, vol. 22, no. 2, pp. 1135–1146, 2015.

Hindawi
Journal of Chemistry
Volume 2019, Article ID 9585140, 5 pages
https://doi.org/10.1155/2019/9585140

Research Article

Kinetic Study of Biodangerous Methylmercury Degradation under Various Light Conditions

Yutao Zhang,[1,2] **Xia Chen**,[3] **Qixia Jiang**,[4] **Xiaojuan Zhang**,[1] **and Qiuyun Zhang**[1]

[1]*Engineering Technology Center of Control and Remediation of Soil Contamination of Provincial Science & Technology Bureau, Anshun University, Anshun, Guizhou 561000, China*
[2]*College of Resource and Environmental Engineering, Anshun University, Anshun, Guizhou 561000, China*
[3]*College of Elemental Education, Jining University, Jining, Shandong 273100, China*
[4]*Zoucheng Senior School of Vocational Technology, Jining, Shandong 273500, China*

Correspondence should be addressed to Yutao Zhang; zyt0516@126.com and Qiuyun Zhang; sci_qyzhang@126.com

Received 5 June 2019; Accepted 15 July 2019; Published 25 July 2019

Guest Editor: Hu Li

Methylmercury (MeHg) has remarkable toxicological effects on humans, plants, and other lives in the environment, which may restrict the comprehensive utilization of biomass source in view of possibly forming biohazardous waste. In this study, a kinetic study of MeHg degradation under UVB, UVA, natural light, and dark was carried out. The result showed that light radiation enhanced MeHg degradation but had no significant influence on the final balance between MeHg and inorganic mercury (Hg^{2+}) in pure water. The balance is of great importance and can be used as a key fundamental to estimate MeHg cycling in other complicated aquatic environments. MeHg degradation was identified to be second-order reaction using the fitting optimization level of the regression equation, and the second-order rate constants were 1.61, 0.82, and 0.91 $L{\cdot}ng^{-1}{\cdot}d^{-1}$, half-lives were calculated to be 0.62, 1.3, and 1.08 d for UVB, UVA, and natural light, respectively. A possible MeHg degradation mechanism was proposed, and it could perfectly explain the results obtained in this paper and some previous studies.

1. Introduction

In the past decades, the extensive industrial and agricultural use of mercury and its compounds had resulted in serious contamination to fresh water and sea water [1–3]. Mercury-contaminated water may pose a risk to aquatic life [4] and subsequently to mankind through the food chains [5]. In addition, the possible formation of biohazardous waste from the toxin-rich biomass may restrict the comprehensive utilization of those renewable resources.

The ecological and toxicological effects of mercury are positively dependent on chemical species [6, 7]. As a potent neurotoxin to human and other lives in the environment, MeHg is many times more toxic than the corresponding inorganic metal ion [8], owing to its lipophilic and protein binding properties [9, 10]. Fortunately, aquatic MeHg content is kept at a low level because both of mercury methylation and demethylation processes are going on in the environment. Research showed that photoinduced degradation of MeHg was thought to be an important process in the biogeochemical cycling of mercury [11, 12]. Both radiation intensity and light wavelength hold the capacity to influencing MeHg degradation [13]. Some kinetic studies were carried out to calculate the reaction rate of photoinduced MeHg degradation, but significant differences were observed in the obtained results, varying over orders of magnitude [11, 14–16]. These inconsistent results indicate that the mechanism of MeHg degradation may be different under various environmental conditions. Additionally, dissolved organic matter [17, 18], some ions (e.g., Cl^- and NO_3^-) [13, 19], and radicals (e.g., $^{\cdot}OH$ and $^1O_2$) [20] in water also influence reaction rate significantly. However, no matter how many influencing factors act on and which mechanism undergoes in the process of MeHg degradation, the pure chemical balance between MeHg and inorganic mercury ion

(Hg^{2+}) is always the key fundamental to estimate the MeHg cycling in each aquatic ecosystem.

MeHg pool in an aquatic system was determined by the net result of processes, e.g., input, export, internal formation, and degradation of MeHg. Hence, experiments under simple conditions which start with only MeHg degradation and end with the chemical balance in an isolated system (without MeHg input or export) under constant temperature are most suitable to study the kinetic information of MeHg degradation. The kinetic data of these experiments can be used as a fundamental to establish the MeHg cycling model in a complicated aquatic system when other environmental factors were taken into account additionally. Therefore, this study was carried out in pure water and the objectives were to (1) establish chemical balances between MeHg and inorganic mercury under various light conditions and (2) estimate the kinetic data of MeHg degradation under UV irradiation, natural light, and darkness.

2. Materials and Methods

2.1. Preparation of Stock Solution. Clean techniques were used, and disposable gloves were worn throughout the experiments to minimize any exotic contamination. All the glassware was soaked in nitric acid for approximately 24 h and sterilized subsequently, and reaction solutions were prepared with ultrapure water (18.2 MΩ·cm^{-1}). Stock solution of 1 ng·Hg·L^{-1} CH_3HgCl (GR, Seattle, WA, USA) solutions was prepared, and its pH was adjusted to be 5.5 with nitric acid or sodium hydroxide. The stock solution was stored in brown quartz bottles, which were wrapped in an aluminum foil and kept in a refrigerator at 4°C.

2.2. Experimental Design. 100 mL of 1 ng·Hg·L^{-1} CH_3HgCl solution was poured into bottles (borosilicate glass, 100 mL) and a very small space was left over the solution to minimize mercury lost from the reaction system. Then, the bottles were sealed with parafilm and incubated in a dark box whose inside wall was covered with aluminum foil to get ambient light. 8 UV bulbs (8 watt) were equipped in the box. The experiment lasted for 3 weeks, and 3 bottles were taken out each time at 1 d, 2 d, 4 d, 6 d, 9 d, 12 d, and 17 d for determination of MeHg concentration. Being the dominant component of UV in sunlight, UVA (365 nm) and UVB (310 nm) were employed to study the photoinduced decomposition of methylmercury in this study. The experiment was conducted under UVA, UVB, natural light, and dark, respectively, at 25°C in an air-conditioned room. Under natural light treatment, the dark box was open and the reaction solution was determined for MeHg concentration at midday to get similar light intensity (about 80–90 klx). Under dark treatment, the box was closed and all the bottles were wrapped with an aluminum foil. Under UV irradiation, 365 and 310 nm bulbs were employed to represent UVA and UVB radiations. A mini fan was equipped in a hole on the side wall of the box to keep air circulating and get constant temperature when the UV bulbs were turned on. We verified the accuracy and the precision of the data in various aspects such as blank value assay, recovery rate experiment, and parallel determination experiment.

2.3. Data Analysis. MeHg concentration was determined using the method of 1630 [21], and all data were analyzed by SPSS 10.0 and Origin 8.0 software for Windows. The reaction kinetic order was determined using the fitting optimization level of the regression equation.

3. Results and Discussion

3.1. MeHg Demethylation Trend under Various Light Treatments. Many researchers have identified that solar UV could decrease MeHg content in surface water using field experiments [11, 16]. The photoinduced demethylation process was influenced by environmental factors (e.g., DOM, salinity, nitrate, photoreactive trace metals, and chloride) [13, 16, 20, 22]. The experiment in this study was conducted in lab, and all of the influencing factors were well controlled with light radiation as the only variable factor; data obtained in this study were much more purposeful and meaningful for further understanding of the photoinduced MeHg degradation process. MeHg concentration decreased at a faster rate in the first 6 days after the experiment started and at a lower rate in the following 15 days in all the treatments of dark, natural light, UVA, and UVB (Figure 1).

Although MeHg concentration decreased in all of the treatments with different radiations, a significant difference was observed in reaction rate between different light treatments, in an order of UVB > natural light > UVA > dark. As Figure 1 shows, 90% of MeHg degraded in the prior 6 days under UVB radiation; UVA which was similar to natural light resulted in about 80% of MeHg degradation. However, in the same 6 days, only 65% of MeHg degraded in the samples treated with dark. The result suggested that light wavelength has a great influence on MeHg demethylation. According to the previous reports, $^{\cdot}OH$, produced in the Fenton reaction, should account for the fastest MeHg degradation induced by UVB treatment [20, 22]. Although UVB gave the fastest degradation rate in this study, it is noted that UVA dominates MeHg cycling in the aquatic environment [15], as it accounts for 98% UV light. Although samples treated under dark gave the slowest degradation rate, 90% MeHg degraded after 17 d as well, suggesting that photoinduced demethylation was not the only pathway accounting for the loss of MeHg which also occurred without light radiation.

In conclusion, light radiation indeed enhanced MeHg degradation rate, but it was not essential for MeHg demethylation in the aquatic system. Most probably, MeHg demethylation undergoes different mechanisms under corresponding light treatments.

3.2. Chemical Balance of MeHg Demethylation Reaction. It was unexpected to find such a similar final reaction state treated with UVB, UVA, natural light, and dark after

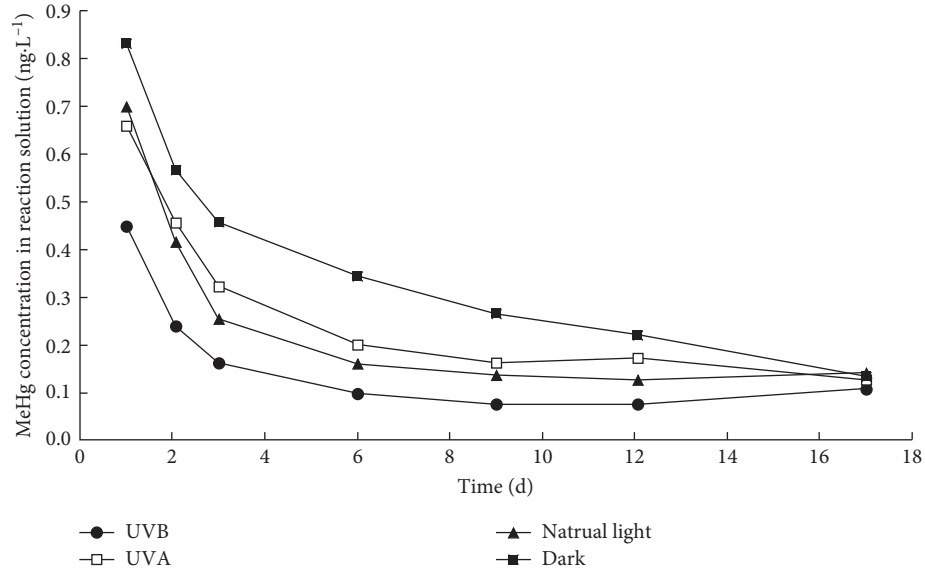

Figure 1: MeHg concentration variation with time. Initial MeHg concentration was 1 ng·Hg·L^{-1}.

incubation of 17 days, as Figure 2 shows. The ratios of MeHg to total mercury in the reaction solution were 10.51%, 11.45%, 11.60%, and 12.60% for UVB, UVA, natural light, and dark, respectively, and the differences between these ratios were rather less significant than imagined. This unexpected result verified that light radiation has a great influence on the MeHg degradation rate and most probably also to the reaction mechanism indeed, but it cannot significantly affect the final reaction balance of MeHg degradation in an isolated reaction system. However, in an open aquatic system, environmental factors such as dissolved organic matter, pH, sulfur, trace elements content, and so on will shift the balance to MeHg or Hg^{2+} side.

In this study, the experiments were conducted in a lab with constant pH and temperature, and the result was influenced entirely by light radiation. Hence, the similar balance between MeHg and inorganic mercury under various light irradiations is of great implication for the researchers to understand MeHg cycling (input, output, in situ formation, and decomposition) further in an aquatic system. For example, if the ratio of MeHg and total mercury was over than 12% in lake water, most probably, some environmental factors of this aquatic system were more suitable for MeHg formation or more external MeHg was inputted to this lake. These potential factors (in situ formation and external source) should be the focus when MeHg cycling in this lake was estimated.

3.3. Kinetic Study of MeHg Degradation under Various Light Radiations. Plots of $\ln[\mathrm{MeHg}]_i/[\mathrm{MeHg}]_t$ versus t and $1/[\mathrm{MeHg}]_t$ versus t were used to validate whether MeHg degradation follows first-order or second-order reactions, respectively, where $[\mathrm{MeHg}]_t$ means MeHg content (ng·Hg·L^{-1}) at time t and $[\mathrm{MeHg}]_i$ means initial MeHg concentration, always 1 ng·Hg·L^{-1} in this study. The fitting coefficients, reaction rate constants, and half-lives, which were calculated following both first- and second-order kinetic equations, are presented in Table 1.

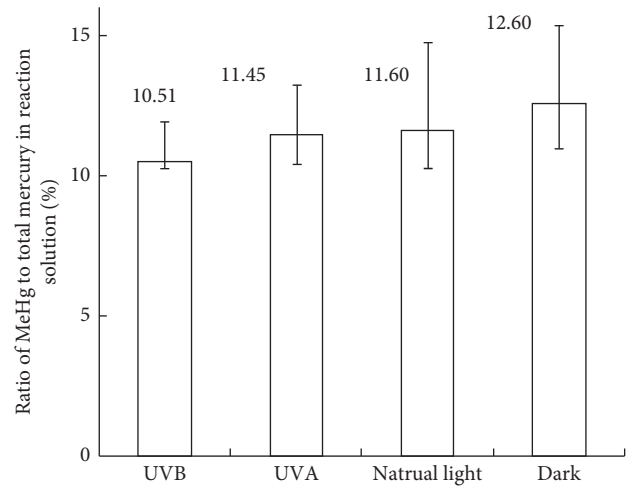

Figure 2: Ratio of MeHg to total mercury in reaction solution at the end of the experiment.

It is noted that the data obtained after equilibrium conversion were not meaningful to calculate the rate constant. Hence, data obtained in the prior 9 days were used to study kinetic information for UVB, UVA, and natural light treatments and 17 days for dark treatment, respectively.

The results show that, under UVB, UVA, and natural light, the second-order equation is much better than the first-order equation to fit MeHg degradation. The fitting coefficients of the second-order equation were 0.94, 0.85, and 0.86, compared with that of first-order one 0.18, 0.38, and 0.48 for UVB, UVA, and natural light, respectively (Table 1). These data suggest that, under light radiation, MeHg degradation is a second-order reaction rather than

Table 1: Kinetic information of MeHg degradation under different light conditions.

Treatments	Rate constants				Fitting coefficients			
	UVB	UVA	Natural light	Dark	UVB	UVA	Natural light	Dark
First-order reaction ($1\,d^{-1}$)	0.35	0.19	0.21	0.13	0.18	0.38	0.45	0.83
Second-order reaction ($L{\cdot}ng^{-1}{\cdot}d^{-1}$)	1.61	0.82	0.91	0.43	0.94	0.85	0.86	0.90
Half-life (d)	0.62	1.30	1.08	—	—	—	—	—
△pH	0.2	0.1	0.1	−1.6	—	—	—	—

*△pH means the pH changes of the solution before and after the incubation period.

the first-order reaction. Under dark treatment, fitting coefficients of the first-order and second-order equations were very close, 0.83 and 0.89, and it is not enough to validate the reaction order. A hypothesis was proposed that MeHg degradation under light radiation follows an entirely different chemical mechanism from that under dark. Additionally, pH decreased by 1.6 (from 5.5 to 3.9) for solution treated under dark, while no significant pH change was observed in the solution treated under light radiation (Table 1). The difference in pH change under light and dark supports the hypothesis we proposed.

Under reaction conditions in this study, the second-order rate constants of MeHg degradation were 1.61, 0.82, and 0.91 $L{\cdot}ng^{-1}{\cdot}d^{-1}$, and the half-lives were calculated to be 0.62, 1.3, and 1.08 d for UVB, UVA, and natural light, respectively. Kinetic data under dark treatment could not be calculated, because the reaction order under dark could not be decided based on the data obtained in this study (Table 1).

3.4. Proposed Mechanisms of Photoinduced Methylmercury Degradation. As shown in Figure 1 and kinetic data in Table 1, light irradiation can accelerate methylmercury degradation, as many previous studies have reported. Since methylmercury can be degraded directly by UV irradiation with wavelengths lower than 254 nm [23], direct degradation of methylmercury cannot occur with the light source of 310 and 365 nm in this study. Hence, we can conclude that indirect photolysis may be the dominant pathway for methylmercury degradation in this study. Previous studies have validated that hydroxyl radicals ($^{\cdot}OH$) play an important role in the indirect photolysis process of methylmercury due to its powerful and nonselective reactivity. For example, Zepp et al. [24] and Chen et al. [20] determined the reaction kinetics of methylmercury and $^{\cdot}OH$ using the steady-state kinetic technique. In this study, $^{\cdot}OH$ can be produced through photolysis of nitrate ions which was introduced into the reaction system with nitric acid when adjusting pH of the solution.

This hypothesis could be demonstrated with the following equations:

$$NO_3^- \xrightarrow{hv} NO_2 + {}^{\cdot}O^- \quad (1)$$

$${}^{\cdot}O^- + H_2O \longrightarrow {}^{\cdot}OH + OH^- \quad (2)$$

According to kinetic information obtained in this study, a possible mechanism was proposed as follows:

$$\begin{aligned} CH_3HgCl + {}^{\cdot}OH &\longrightarrow CH_3 + HgOHCl \\ CH_3HgCl + {}^{\cdot}OH &\longrightarrow CH_3OH + {}^{\cdot}HgCl \\ {}^{\cdot}HgCl &\longrightarrow Hg^0 + {}^{\cdot}Cl \\ {}^{\cdot}HgCl + {}^{\cdot}HgCl &\longrightarrow Hg^0 + HgCl_2 \end{aligned} \quad (3)$$

The possible side reactions are listed as follows:

$$\begin{aligned} {}^{\cdot}CH_3 + {}^{\cdot}CH_3 &\longrightarrow CH_3 - CH_3 \\ {}^{\cdot}CH_3 + {}^{\cdot}OH &\longrightarrow CH_3OH \\ {}^{\cdot}CH_3 + {}^{\cdot}Cl &\longrightarrow CH_3Cl \\ CH_3OH &\xrightarrow{{}^{\cdot}OH} CH_2O \end{aligned}$$

The proposed mechanism gives perfect explanation to some previous studies. For example, Inoko and coworkers studied the photochemical decomposition of MeHg using mercury lamps and identified CH_3Cl and CH_3CH_3 as products in solution [23]. In addition, Chen et al. found CH_2O in MeHg decomposition products [20].

4. Conclusions

The MeHg degradation rate increases with decreasing radiation wavelength. Light radiation enhances the MeHg degradation but does not influence the final chemical balance between MeHg and inorganic mercury in an isolated aquatic reaction system. This ratio obtained in this study can be used as an important fundamental to estimate MeHg cycling in some complicated aquatic systems, where many environmental influencing factors are involved. Kinetic study shows that MeHg degradation is a second-order reaction and the half-life is 1.08 d under natural light in pure water.

Data Availability

The data used to support the findings of this study are available from the corresponding author upon request.

Conflicts of Interest

The authors declare that they have no conflicts of interest.

Acknowledgments

This study was supported by the joint science and technology funds of the Guizhou S&T Department, Anshun City People's Government and Anshun University (no. LH [2016]7278), Creative Research Groups support program of

Guizhou Education Department (no. KY [2017]049), and Construction Projects of Innovation Platform from Science and Technology Bureau in Anshun (no. [2016]-4).

References

[1] S. Heaven, M. A. Ilyushchenko, W. Tanton, S. M. Ullric, and E. P. Yanin, "Mercury in the River Nura and its floodplain, Central Kazakhstan: river sediments and water," *Science of the Total Environment*, vol. 260, no. 1–3, pp. 35–44, 2000.

[2] W. Zhu, Y. Song, G. A. Adediran et al., "Mercury transformations in resuspended contaminated sediment controlled by redox conditions, chemical speciation and sources of organic matter," *Geochimica et Cosmochimica Acta*, vol. 220, pp. 158–179, 2017.

[3] R. Cesário, L. Poissant, M. Pilote, N. J. O'Driscoll, A. M. Mota, and J. Canário, "Dissolved gaseous mercury formation and mercury volatilization in intertidal sediments," *Science of the Total Environment*, vol. 603-604, pp. 279–289, 2017.

[4] Z. Y. Gao, M. M. Li, J. Wang, J. Yan, C. C. Zhou, and C. H. Yan, "Blood mercury concentration, fish consumption and anthropometry in Chinese children: a national study," *Environment International*, vol. 110, pp. 14–21, 2017.

[5] G. J. Myers, P. W. Davidson, C. Cox, C. Shamlaye, E. Cernichiari, and T. W. Clarkson, "Twenty-seven years studying the human neurotoxicity of methylmercury exposure," *Environmental Research*, vol. 83, no. 3, pp. 275–285, 2000.

[6] T. W. Clarkson, "Human toxicology of mercury," *Journal of Trace Elements in Experimental Medicine*, vol. 11, no. 23, pp. 303–317, 1972.

[7] L. Mínguez-Alarcón, M. C. Afeiche, P. L. Williams et al., "Hair mercury (Hg) levels, fish consumption and semen parameters among men attending a fertility center," *International Journal of Hygiene & Environmental Health*, vol. 221, no. 2, pp. 174–182, 2018.

[8] D. W. Boening, "Ecological effects, transport, and fate of mercury: a general review," *Chemosphere*, vol. 40, no. 12, pp. 1335–1351, 2000.

[9] F. Zahir, S. J. Rizwi, S. K. Haq, and R. H Khan, "Low dose mercury toxicity and human health," *Environmental Toxicology and Pharmacology*, vol. 20, no. 2, pp. 351–360, 2005.

[10] D. Zhang, Y. Yin, Y. Li, Y. Cai, and J. Liu, "Critical role of natural organic matter in photodegradation of methylmercury in water: molecular weight and interactive effects with other environmental factors," *Science of the Total Environment*, vol. 578, pp. 535–541, 2016.

[11] C. R. Hammerschmidt and W. F. Fitzgerald, "Photodecomposition of methylmercury in an Arctic Alaskan lake," *Environmental Science & Technology*, vol. 40, no. 4, pp. 1212–1216, 2006.

[12] J. A. Fleck, M. Marvin-DiPasquale, C. A. Eagles-Smith et al., "Mercury and methylmercury in aquatic sediment across western North America," *Science of the Total Environment*, vol. 568, pp. 727–738, 2016.

[13] R. Sun, D. Wang, Y. Zhang et al., "Photo-degradation of monomethylmercury in the presence of chloride ion," *Chemosphere*, vol. 91, no. 11, pp. 1471–1476, 2013.

[14] P. Seller, C. A. Kelly, J. W. M. Rudd, and A. R. Machutchon, "Photodegradation of methylmercury in lakes," *Nature*, vol. 380, no. 6576, pp. 694–697, 1996.

[15] I. Lehnherr and V. L. Louis, "Importance of ultraviolet radiation in the photodemethylation of methylmercury in freshwater ecosystems," *Environmental Science & Technology*, vol. 43, no. 15, pp. 5692–5698, 2009.

[16] F. J. Black, B. A. Poulin, and A. R. Flegal, "Factors controlling the abiotic photo-degradation of monomethylmercury in surface waters," *Geochimica et Cosmochimica Acta*, vol. 84, pp. 492–507, 2012.

[17] M. Ravichandran, "Interactions between mercury and dissolved organic matter—a review," *Chemosphere*, vol. 55, no. 3, pp. 319–331, 2004.

[18] Y. Zhang, X. Chen, Y. Yang, D. Wang, and X. Liu, "Effect of dissolved organic matter on mercury release from water body," *Journal of Environmental Sciences*, vol. 23, no. 6, pp. 912–917, 2011.

[19] W. Mao, R. G. Sun, D. Y. Wang, M. Ma, and C. Zhang, "Effects of nitrate ion on monomethylmercury photodegradation in water body," *Environmental Science*, vol. 34, no. 6, pp. 18–24, 2013.

[20] J. Chen, S. O. Pehkonen, and C.-J. Lin, "Degradation of monomethylmercury chloride by hydroxyl radicals in simulated natural waters," *Water Research*, vol. 37, no. 10, pp. 2496–2504, 2003.

[21] United States Environmental Protection Agency, *Method 1630: Methyl Mercury in Water by Distillation, Aqueous Ethylation, Purge and Trap, and Cold Vapor Atomic Fluorescence Spectrometry*, United States Environmental Protection Agency, Washington, DC, USA, 2001.

[22] C. R. Hammerschmidt and W. F. Fitzgerald, "Iron-mediated photochemical decomposition of methylmercury in an arctic Alaskan lake," *Environmental Science & Technology*, vol. 44, no. 16, pp. 6138–6143, 2010.

[23] M. Inoko, "Studies on the photochemical decomposition of organomercurials—methylmercury (II) chloride," *Environmental Pollution Series B, Chemical and Physical*, vol. 2, no. 1, pp. 3–10, 1981.

[24] R. G. Zepp, J. Hoigne, and H. Bader, "Nitrate-induced photooxidation of trace organic chemicals in water," *Environmental Science & Technology*, vol. 21, no. 5, pp. 443–450, 1987.